Title
Improved Single-Molecule Detection of Native Proteins Using Hydrogel-Backed Nanopores

Author
Nazarian, Reyhaneh

Publication Date
2021

Peer reviewed|Thesis/dissertation

UNIVERSITY OF CALIFORNIA

Los Angeles

Improved Single Molecule Detection of Native Proteins Using Hydrogel-Backed Nanopores

A dissertation submitted to the graduate school

of the University of California, Los Angeles

in partial fulfilment of the

requirements for the degree of

Doctor of Philosophy

By

Reyhaneh Nazarian

2021

ABSTRAT OF THE DISSERTATION

Improved Single-Molecule Detection of Native Proteins Using Hydrogel-Backed Nanopores

By

Reyhaneh Nazarian

Doctor of Philosophy in Bioengineering

University of California, Los Angeles, 2021

Professor Jacob Schmidt, Chair

Accurate identification and quantification of proteins in a solution using nanopores is technologically challenging in part because of the large fraction of missed translocation events due to short event times and limitations of conventional current amplifiers. Previously, we have shown that a nanopore interfaced with PEG(1000)-DMA hydrogel with an average mesh size of 3.1 nm significantly enhances protein residence time inside the nanopore, reducing the number of missed events. Following up on our previous work, here, we explored measurement limits, sensitivity, and further characterization capabilities of our proposed hydrogel-backed nanopore system. We demonstrated the ability of the hydrogel-backed nanopores to sense unlabeled proteins as small as 5.5 kD in size and 10 fM in concentration, without a major restriction on the nanopore size or the experimental setup. Also, we showed that the frequency of protein translocation events scales linearly with the bulk concentration over a wide range of concentrations, and an unknown protein concentration can be determined from an interpolation of the frequency-concentration calibration curve with less than 10% error. Further, we precisely determined protein volumes from

measurement data, and we employed an iterative method to determine a protein's volume when its diameter is comparable to nanopore diameter. We investigated possible mechanisms for detection enhancement enabled by the presence of the hydrogel; we found that the possible gap between the pore mouth and the hydrogel indicates the sensitivity of the hydrogel-backed nanopores.

Moreover, we demonstrated that hydrogel-backed nanopores can serve as an effective, reliable, ultra-sensitive, non-destructive, reproducible, and easy-to-operate substitute for commonly used UV-Vis detectors in fast protein liquid chromatography. The hydrogel-backed nanopores resolved protein fractions at much lower concentrations than the minimum concentration detectable by the standard UV-Vis detector. They also measured protein fractions with a higher selectivity and provided a more informative analysis of proteins' physical properties than the UV-Vis detector. Additionally, we integrated the nanopore with PDMS microchannels to create a fluidic circuit between a chromatographic column and the nanopore to facilitate the continuous and live measurement of column effluents.

Finally, we demonstrated that integrating lipid-bilayer coated nanopores with a hydrogel is a suitable platform for acquiring artifact-free and long protein translocation events to analyze a single protein translocation event accurately. Using hydrogel-backed lipid-bilayer coated nanopores, we determined the volumes of IgG, Ovalbumin, and gold nanoparticles (5 nm diameter) from individual single translocation events in agreement with reference values. Further, we observed that higher applied voltages increased the probability of IgG alignment. We determined the volume and the length-to-diameter ratio of IgG molecules at different applied voltages and noticed an expansion in the conformation of IgG molecules with an increase in the voltage; this is likely due to IgG's flexibility and an intense electric field's ability to expand the IgG hinges from one another.

The dissertation of Reyhaneh Nazarian is approved.

Committee Members:

Professor Jacob Schmidt (Chair)

Professor Gerard Wong

Professor Dino Di Carlo

Professor Harold Monbouquette

University of California, Los Angeles

2021

Table of Contents:

Acknowledgement

I would first like to thank and express my deepest appreciation for my thesis advisor, Professor Jacob Schmidt. His continuous support, generosity and kindness during the years of my PhD journey helped me stay on course. During my journey, his brilliance, consultation, and guidance has always lightened up my path and his open-ended questions and comments have challenged me to seek more and expand my own knowledge. His boundless support kept me confident and steady. He consistently allowed this dissertation to be my own work; however, whenever I was faced with a problem, he was there to steer me in the right direction with his thoughtful guidance. I deeply enjoyed all the moments we shared to discuss my work, and all the moments I worked in his lab. I cannot express my gratitude enough for his efforts and hard work to make this journey so enjoyable!

I would like to acknowledge Professor Gerard Wong for all his selfless guidance and support. During all these years, whenever I ran to his office, he was there with a warm greeting. I am gratefully indebted to his inspiration, encouragement, and support during my studies. If it wasn't for his assistance and support, I would not have been able to complete this dissertation on time and move on to the next level.

I also want to thank my other committee members such as Professor Dino Di Carlo and Professor Harold Monbouquette for serving on the committee, their time, and valuable comments and suggestions.

A very special gratitude goes out to my colleagues and friends Dr. Shiv Acharya, Eric Lee, Chance Kuo, Brian Siegel, Wilson Xie, and Ann Jiang for our time spent together. I was fortunate enough to work at the Schmidt lab with such brilliant scientists and gained lots of valuable knowledge.

I must express my profound gratitude to my parents because they taught me how to think for myself and always encouraged me to work hard to reach my goals. Without their unconditional love and support it would not be possible for me to succeed. I would also like to thank my brother, Hamed, for his unfailing support throughout my life.

I would also like to thank my husband, Behrang, who has supported me throughout the entire process. His support, patience and unwavering love were undeniably the base upon which my

passion has been built on. I would like to thank my two sons, Taha and Yaseen who shed light on my life and made it more meaningful and enjoyable with their presence.

I would like to thank all my friends, particularly Ms. Mothahara Basam, Ms. Akram Jourabchi, Dr. Christine Aidala, Dr. Zahra Vashaie , Dr. Maryam Ghajar, Dr. Golnaz Kamalinia, because without them I would not be as strong as I am today, and this accomplishment would not have been possible without them.

Reyhaneh Nazarian

Vita

Education:

- Ph.D., Bioengineering, Samueli School of Engineering, Department of Bioengineering, University of California, Los Angeles, Los Angeles, California, 2017-2021
  Thesis: Improved Single Molecule Detection of Native Proteins Using Hydrogel-Backed Nanopores
- M.Sc., Chemical Engineering, School of Engineering, University of Cincinnati, Cincinnati, Ohio, 2014-201**7**
  Thesis: Advanced Phosphate Removal in Dialysis Employing Lanthanum Activated Carbon column
- M.Sc. Applied Physics (Nano-Biotechnology), Sharif University of Technology, Tehran, Iran, 2005-2008
  Thesis: Synthesis of Highly Luminescent $Zn_2SiO_4:Mn^{2+}/SiO_2$ Nanostructures for Biological Labeling
- B.Sc. Applied Physics with honor, Sharif University of Technology, Tehran, Iran
  2001-2005

Selected Publications:

- **Nazarian R**.; Lee E.; Kuo C.; ; Khosh B.; Acharya S. , and Schmidt J., "Quantitative measurements of protein volume and concentration using hydrogel-backed nanopores", *ACS Sensors*, 2021, 6,3,722-726.
- **Nazarian R.**; Salem S.; Decsh R.; Thiel S.; "Kinetics and Equilibrium Adsorption of Phosphate on Lanthanum Oxide Supported on Activated Carbon", *Colloid & Surfaces A: Physiological and Engineering Aspects*, 2021, 624, 126813.
- Shiv Acharya**,** ,Ann Jiang, Chance Kuo, **Reyhaneh Nazarian**, Katharine Li, Anthony Ma, Brian Siegal, Christopher Toh, and Jacob J. Schmidt, "Improved measurement of proteins using a solid-state nanopore coupled with a hydrogel", *ACS Sensors*, 2020, 5, 370-376
- **Nazarian R**.; Acharya S.; Kuo C.; Lee E.; Khosh B.;, and Schmidt J.; "Protein Quantification Using Solid State Nanopore Coupled with a Hydrogel", 2020 Biophysical Society Annual Meeting (BPS), February 15-19, San Diego.
- **Nazarian R**.; Soltani M.; Sadatmousavi P.; Jafari M.; Chen P. "Self-Assembling Peptides: Potential Role in Tumor Targeting", Curr. Pharm. Biotechnol. 2011,12 (8), 1089-100.

- Sadatmousavi P.; Soltani M.; **Nazarian R.**; Mamo T.; Lu S.; Xu W.; Wang X.; Chen P. "Biomaterial Design", Comprehensive Biotechnology, Moo-Young, Murray, Ed.,Elsevier, 2010
- S. Fung, H.Yang, P. Sadatmousavi, Y. Sheng, T. Mamo, **R. Nazarian**, P.Chen, "Amino acid pairing for de novo design of self-assembling peptide and their drug delivery potential", Advanced Functional Materials, 21 (2011) 13, 2456-2464
- **Reyhaneh Nazarian**, Nima Taghavinia, Alireza Badieie, "Synthesis of highly luminescent Zn2SiO4:Mn2+/SiO2 nanostrusctures by impregnation method for biological labeling", International Conference on Nanotechnology, 6-8 June 2008, Kish, Iran.

Chapter 1: Background and Objectives

1.1. Introduction

Single-molecule proteomic, the precise single-molecule study of function, structure, and the absolute number of proteins in a biological system is crucial in understanding disease pathogenesis at the cellular level, developing disease protein biomarkers for early diagnosis, and improving therapeutic strategies. Among single-biomolecule detection techniques, nanopore biosensors have been extensively investigated for use as a highly precise, sensitive, rapid, and label-free platform. However, nanopore detection, identification, and quantification of proteins are limited due to their rapid transport through the nanopore, and consequently, a huge fraction of missed translocation events of proteins. Numerous efforts have been made to develop effective strategies to enhance protein detection. This chapter provides background information on the importance, basics, and challenges of nanopore sensing of proteins in their native conformations. It also summarizes all previous approaches to improve protein detection using solid-state nanopores, highlights their achievements, and discusses their challenges. Further, in this chapter, the motivation and significance of this dissertation are discussed.

1.2. Single-Molecule Detection of Proteins

Proteins regulate almost all biological functions in cells. They catalyze metabolic pathways, produce cellular motion, regulate signaling interactions and immune responses, assist with forming new biomolecules, and facilitate the transportation of molecules and ions across the cell membranes.[1] All protein functions are modulated by their 3D structures, conformational dynamics, interactions with other biomolecules, and abundance. [2–4] Proteins are the most diverse biomolecules in shape, structure, function, and concentration, and thus, they are the most difficult class of analytes to be investigated.

In proteomic studies and medicine, typically protein functions and structures are being investigated by advanced techniques, such as mass spectrometry, multi-dimensional gel electrophoresis, NMR, X-ray diffraction, Cryo-electron microscopy, and labeled-based screening technologies.[5,6] These techniques characterize the bulk property of proteins in a sample, measuring their ensemble behavior and their mean response, and consequently, missing rare behaviors, structural heterogeneity, or a broad distribution of biological states and properties. Also, these techniques cannot provide spatial and temporal information on the dynamics of protein conformational or quantitative changes in a solution.[7–9]

A complementary approach to study proteins in such a complex biological system is the single-molecule measurement of proteins. Single-molecule measurement approaches enable studying thousands of single molecules of proteins one-by-one, which provide rich information about their folding states, dynamics, interactions, functions, and heterogeneity. Moreover, with these approaches, single molecules of proteins can be visualized individually and be counted directly. Therefore, proteins can be resolved at extremely low abundance, their concentrations can be determined over a wide dynamic range, their ensemble structural and conformational heterogeneity can be identified, and time-resolved spatial dynamics information can be obtained.[7,9,10]

Recently, various single-molecule approaches have been developed and employed as complementary methods to study static and dynamic biological properties of proteins. Single-molecule force spectroscopies can probe the mechanical properties of immobilized proteins on the surface, and single-molecule fluorescence imaging methods can investigate temporal and spatial information on labeled single protein primary structures, folded conformations, and protein-protein interactions.[6,11–17] In addition, inspired by impressive advances in nucleic acid

identification and sequencing using nanopores, electrical nanopore detection has attracted much attention in the real-time identification of native proteins in a solution and characterizations of their primary amino acid sequences, dynamic folding conformations, and physical properties.[18–30] During this work, we mainly focus on the nanopore detection of native proteins in a solution and improving current techniques for native protein detection, identification, and characterization.

1.3. Measurement of Native Proteins Using Solid-State Nanopores

Nanopore biosensors have been extensively investigated for use as a highly precise and sensitive biosensor for single-biomolecule sensing in aqueous solutions. In this technique, a single nanoscale pore is embedded in an insulating membrane, which separates two compartments of electrolytes. Upon applying the electric voltage between the two electrodes immersed in electrolyte compartments, an ion current flows through the nanopore, creating an electric field in the vicinity of a nanopore. The created electric field electrokinetically drives the charged biomolecules in the electrolyte solution toward and eventually through the nanopore. The transition of a biomolecule through the nanopore blocks the ways of ionic current, increases the nanopore resistance, and results in a measurable temporal drop in the nanopore ionic current, which is called a translocation event.[31] Each translocation event is characterized by two quantities: its amplitude and its dwell time.

The amplitude of an event i.e. the magnitude of ionic current drop, depends on the volume, shape, and the orientation of a passing biomolecule to the electric field, and it is expressed as follows:[32–34]

$$\Delta I = \frac{\Lambda V_A \gamma}{\rho\left(l_p + 0.8 d_{pore}\right)^2} S\left(d_{particle}, d_{pore}\right) \tag{1.1}$$

where V_A is the applied voltage, γ is the protein's shape factor, ρ is the resistivity of the measurement buffer, and l_p is the nanopore length, d_{pore} is the nanopore diameter, and S $\left(d_{particle}, d_{pore}\right)$ is a correction factor that is a function of the ratio of particle to the nanopore diameter.

The dwell time shows the residence time of a biomolecule inside the nanopore which depends on its diffusion, net charge, and electrophoretic mobility. Probability distribution of measured dwell times, F(t), is described by the solution of the Fokker-Plan equation and is given by:[35]

$$F(t) = \frac{l_p}{\sqrt{4\pi D t^3}} e^{-(l_p - vt)^2/4Dt} \quad (1.2)$$

where l_p is the nanopore length, D and v are the diffusivity and electrophoretic drift velocity of a biomolecule.

Analyzing the amplitudes and dwell times of a population of translocation events provides rich physical and structural information about the proteins.

Solid-state nanopores have been used repeatedly to probe native proteins for different purposes in previous studies. Solid-state nanopores have been used to explore structural and physical conformations of native proteins or protein complexes.[36–43] For example, Yusko and coworkers[41] measured and classified the kinetic heterogeneity in size and conformation of individual aggregates of amyloid-β oligomers in solution using lipid-coated nanopores; they determined three classes of spherical oligomers, protofibrils, and mature fibers among aggregates.

In addition, solid-state nanopores have been employed to study the interactions of proteins with other biomolecules, antibodies, or substrates.[44–50] For instance, a chemically modified solid-

state nanopore with nitrilotriacetic acid (NTA) headgroups was used to quantitatively evaluate the strength of the interaction of his-tagged proteins with NTA headgroups, and their binding dissociation rates were estimated from dwell time distributions of binding events as a function of applied voltages.[49] In another work, using low noise solid-state nanopores, the interaction of anticancer therapeutic p53 transactivation domain to form complexes of (p53TAD)/ MDM2 was investigated in the absence and presence of an inhibitor.[45]

Furthermore, solid-state nanopores have allowed real-time monitoring of the conformational dynamics of proteins. Freedman and coworkers[51] monitored the gradual stretching and unfolding of proteins inside solid-state nanopores by applying electric fields greater than 10^6 V/m. In another work, the real-time increase in magnitudes of current blockades of calmodulin translocation events indicated its conformational changes in response to calcium binding.[52] Also, using solid-state nanopores, the dynamics of folding-unfolding states of *apo* and *holo* human serum transferrin (hSTF) protein were investigated as a function of applied voltages and solution pH.[53] In addition, solid-state nanopores have been utilized to investigate the primary amino acid structures of labeled peptides.[54]

The studies previously mentioned illustrated the promising potential of solid-state nanopores in single-molecule proteomic studies; however, nanopore identification and characterization of native proteins are challenging mainly due to the finite temporal resolution of conventional amplifiers. In the next section, we address this issue in more depth.

1.4. Insufficient Temporal Resolution of Recording Systems for Measurement of Native Proteins

Protein measurements using solid-state nanopores reveal extremely low resolvable event rates, which are orders of magnitudes smaller than theoretical estimates based on the electro-diffusion capture rate model; this model assumes a hemispherical capture zone at the nanopore entrance where the protein motion transitions from diffusion-free to electrophoretic drift. Also, this model assumes that the event rate is dominated by diffusion of proteins to the capture zone. The event rate at which biomolecules arrive at the capture radius based on the electro-diffusion capture rate model is described by the Smoluchowski equation:

$$J = 2\pi cDr_p \tag{1.3}$$

where J is the event rate (Hz), D (nm^2/s) is the biomolecule diffusivity, c ($\#/nm^3$) is the bulk concentration of biomolecules, and r_p (nm) is the nanopore radius.

Plesa and colleagues performed systematic experimental observations on the event rates of 12 translocating proteins ranging in size from 6 to 660 kD.[55] They observed much lower event rates for all the protein measured, 3 or 4-fold less than theoretically predicted by Equation 1.3. Also, their findings indicated that the observed event rates deviated more significantly from theoretical estimates for smaller proteins, which are expected to move faster and have a lower signal-to-noise ratio. They attributed this issue to (1) the limited temporal resolution of conventional recording systems to resolve the swift transition of proteins through solid-state nanopores and (2) attenuation effect of filtering on low signal-to-noise ratio of protein translocation events (Figure 1.1).

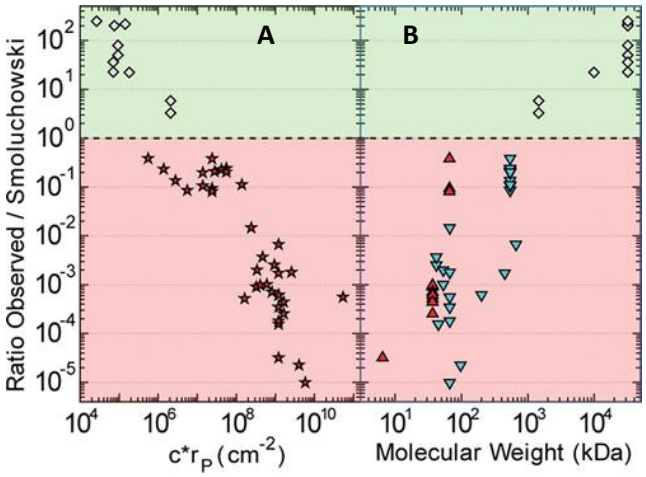

Figure 1.1. Comparison of the observed to the theoretically predicted event rates using Equation 1.1. The plot shows the ratio of the observed to the theoretically predicted event rates A) for dsDNA (white diamonds) and proteins (red stars) as a function of concentration x nanopore radius B) for dsDNA (white diamonds), positively charged proteins (red triangles), and negatively charged proteins (blue triangles) as a function of their molecular weight.[55]Copyright 2013 American Chemical Society.

The commonly used Axopatch 200B amplifier has a bandwidth of around 50 kHz, enabling a maximum data acquisition rate of 100 kHz with a temporal resolution of 20 µs. However, looking over the residence time distributions of different proteins inside the nanopore (Equation 1.2) reveals that most proteins spend much less than 20 µs transiting through a 20 nm thick nanopore (Figure 1.2A) which may explain the huge number of undetected proteins. So, the observed events are longer than 20 µs and either belong to the tail of the residence time distributions or from the proteins that reside longer inside the nanopore due to protein-pore interactions. Figure 1.2A also shows that residence time distributions of smaller proteins have the smaller most probable dwell time inside a nanopore; however, they have a larger tail distribution (illustrated in panel of the Figure 1.2A), suggesting greater numbers of smaller proteins should be resolved by recording systems, which is in contrast with the experimental observations.

A B

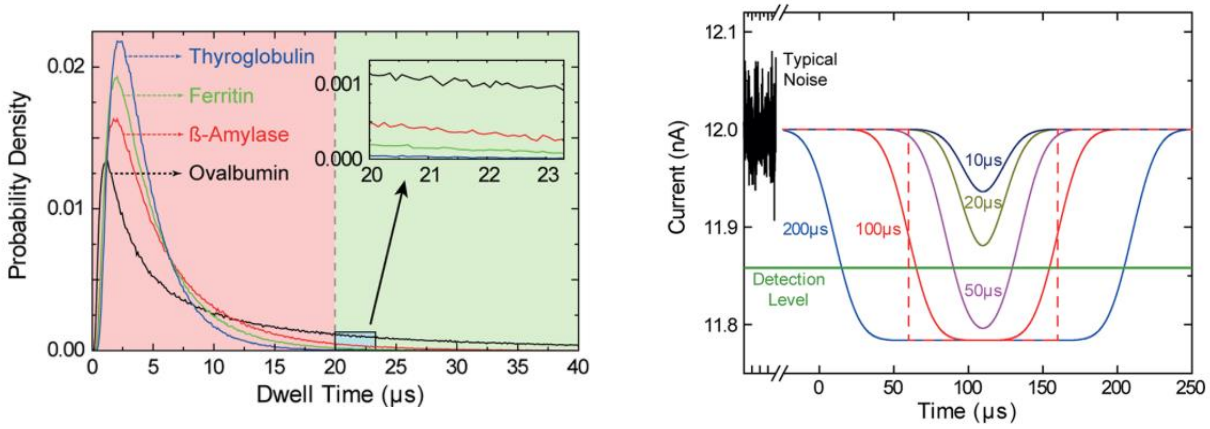

Figure 1.2. A) simulated residence time distributions of four proteins having different sizes and charges B) Attenuation effect of 10 kHz low-pass Gaussian filtering on a 200 pA resistive pulse signal with duration of 10-200 µs. Copyright 2013 American Chemical Society.

The observed decrease in translocation events of smaller proteins was assigned to the low signal-to-noise ratio of translocation events. Typically, recorded traces of nanopore measurements are low-pass filtered to extract the translocation events from the intrinsic capacitive noise of the system. Filtration has been shown to distort the shape of the translocation events, which are shorter than twice the rise time of the filter used (66 µs for 10kHz low-pass Gaussian filter) and attenuate their current blockade amplitudes. As an example, Figure 1.2B shows the attenuation effect of 10 kHz low-pass Gaussian filter on translocation events with a duration of 10-200 µs and blockade amplitude of 200 pA. As shown from the figure, the extent of amplitude attenuation after filtration depends on the duration of the events, with shorter events dropping more. When the duration of an event is sufficiently below twice the rise time of a filter, its amplitude drops below the detection threshold of the system and cannot be detected. Smaller proteins have smaller blockade

amplitudes, and their translocation events are more prone to being diminished and lost within the system noise after filtering.

The limited temporal resolution of amplifiers to enhance the protein detection can be addressed based on two main strategies: (1) improving the electronics by increasing the bandwidth of amplifiers and decreasing the inherent noise of the system, and (2) slowing down the speed of biomolecules. In the following section we will review these approaches.

1.5. Improvement of Nanopore Systems for Enhanced Protein Detection

As discussed, Improving the temporal resolution of amplifiers alongside using low-noise nanopores and slowing down the transition speed of proteins are the two main strategies that are utilized to enhance protein detection and identification using solid-state nanopores.

1.5.1. High Bandwidth Measurements of Proteins

The translocation process of proteins is usually studied by using a conventional Axopatch 200B amplifier. The temporal resolution of this amplifier is 20 μs, determined by the inverse of its maximum bandwidth (100 kHz) (as discussed in previous section). However, the maximum 100 kHz bandwidth of this amplifier is limited by the required signal-to-noise ratio of the measurements and cannot easily be improved.[56] Signal-to-noise ratio (SNR) is defined as the ratio of the event amplitude to the root-mean-square (RMS) current noise of the system (SNR $=\Delta I_{pore}/I_{noise}$). ΔI_{pore} is controlled by the applied voltage across the membrane and the conductance of the nanopore. In addition, the conductance of a nanopore is determined by its size (i.e. length and diameter) and the electrolyte conductivity. However, I_{noise} is inherently present in the system, originating from the intrinsic noises of the headstage, the amplifier, the pore, the substrate material, and the digitizer, and its magnitude depends on the frequency of signal bandwidth (f).[57]

Figure 1.3A qualitatively illustrates the four frequency regimes of the current noise spectrum for a recording system. In the low frequency regime, current noise linearly scales with 1/f; at medium frequencies, the current noise is independent of frequency (white frequency regime); a linearly dependent f regime follows white frequency regime over a short interval of frequencies, and at high frequencies (> 100 kHz) the current noise increases as f^2. A significant increase in the current noise at high bandwidth frequencies (> 100 kHz) is the main obstacle to achieve a higher bandwidth and temporal resolution in nanopore measurements; this necessitates a significant improvement in the measurement electronics.[56] For example, it was shown that using tightly integrating measurement electronics fabricated in complementary metal oxide semiconductors (CMOS) with solid-state nanopores can reduce wiring capacitance and current noise, pushing the maximum achievable bandwidths from 100 kHz to MHz ranges (Figure 1.3B).[58]

A B

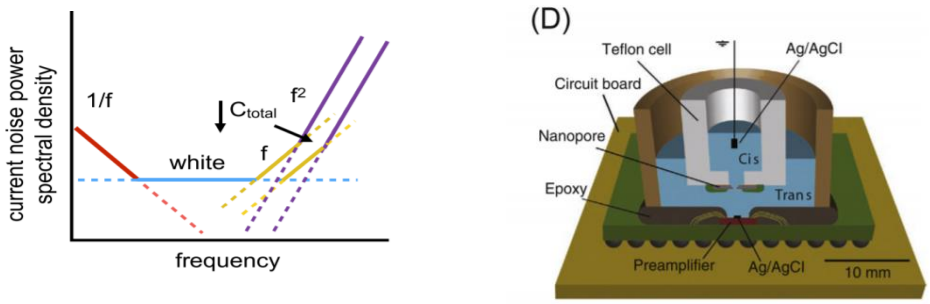

Figure1.3. A) qualitative plot of current noise power spectral density as a function of frequency. B) high bandwidth protein measurement set up: tightly integration of a custom designed amplifier with nanopore sensing fluidic.[56] Copyright 2019 Elsevier.

Using the CMOS based electronic in the experimental setup (shown in Figure 1.3B) in a combination of (1) a 250 kHz high bandwidth amplifier (temporal resolution of 2.5 μs), (2) tightly integrated CMOS measurement circuit, (3) small nanopores with diameters only 1 nm larger than

the diameter of a target protein to enhance nanopore-protein interactions, and (4) low-noise ultrathin membranes (<10 nm) to increase the signal-to-noise ratio of translocation events, Larkin and colleagues sensed two sub-30 kD proteins with high resolution at μM concentrations. The dwell-time distributions of the observed protein events were fitted to the 1D first-passage time distribution model to estimate the diffusion constants and electrophoretic mobilities of the two measured proteins The estimated best-fit values of diffusion constants and electromobilities were smaller than their bulk values by one or two orders of magnitude.[59]

The development of high bandwidth amplifiers alongside the strategies to reduce inherent capacitive noises of measurement systems is a powerful approach to address short residence times of proteins inside the nanopores; however, these experimental setups are extremely complicated, expensive, and not easily accessible and commercializable. Also, protein detection rates using the mentioned high bandwidth apparatus deviate from theoretical predictions by one to two order of magnitudes. The much lower estimated values for protein diffusivities and electrophoretic mobilities as well as high protein concentrations consumed in Larkin's experiments, might confirm the insufficient temporal resolution of their apparatus. Also, using tuned size nanopores requires prior knowledge about the target proteins, and it is an impeding factor to measure an unknown protein or a mixture of proteins.

In another study, using a low-noise silicon nitride nanopore in combination with a high bandwidth recording system, Houghtaling and coworkers[60] estimated the shape, volume, and dipole moments of individual proteins that were freely translocating through a nanopore. Their low-noise nanopores were fabricated in 3 mm x 3mm frame and mounted between two layers of PDMS; Consequently, the current noise reduced by 40% and the signal-to-noise ratio of the

measurement increased at the amplifier bandwidth of 50 kHz. The high signal-to-noise ratio in the experimental setup allowed them to digitally low-pass filter the recorded traces at 50 kHz compared to commonly used 10 or 15 kHz filtering cut-off frequency. The higher cut-off frequency of the filter used in this study resolved the high-frequency rotations of proteins more accurately to estimate their shapes, volumes, and dipole moments from long translocation events greater than 150 μs. However, events longer than 150 μs are less than 1% of the total number of translocation events sensed in the measurement. This problem limits the achievable minimum detectable concentration and size of proteins and restricts the resolution in detecting various types of proteins.

1.5.2. Slowing down The Translocation of Proteins

An alternative to improving the bandwidth of recording systems is slowing down the transient speed of proteins to reside longer in the nanopore. This strategy is so desirable, because: (1) it can reduce the fraction of undetected proteins and make it possible to study proteins at extremely low concentrations and sizes (2) it enhances the measurement resolution, providing a better chance to visualize free rotations and movements of individual proteins to time-resolve their conformational dynamics (3) it can significantly compromise the limited bandwidth of amplifiers without additional technical difficulties involved in the development of high bandwidth recording systems, and (4) it is less expensive and gives more experimental freedom to select the convenient method. A wide variety of techniques have been employed to slow down the proteins in previous studies, and here we summarize them.

1.5.2.1. Altering Buffer Properties

Maybe the most trivial approach to slow down the proteins is the modification of their surroundings. Altering buffer properties such as viscosity and temperature makes it possible to slow down the transition of proteins through solid-state nanopores; however, these approaches reduce the conductivity of solutions and, consequently, the amplitude of protein translocation events.[61] Reducing the pH of the buffer solution to be close to the isoelectric point of the protein can also reduce the electrophoretic force in a solution to slow down the transition velocity of proteins;[38] however, it will enhance the chance of clogging the nanopore, and it will require the prior knowledge about the PI of the target proteins.

1.5.2.2. Tethering Proteins to Lipid Coatings on The Surface of Nanopores

In another study to slow down the transient velocity of proteins through the nanopore, Yusko and colleagues[34,62] demonstrated the bio-inspired technique of coating a nanopore with a fluidic lipid bilayer and tethering the target proteins to the bilayer (Figure 1.4). They have shown that the translocation velocities of the tethered proteins were dominated by the in-plane diffusion constant of the lipids and reduced by two orders of magnitudes. In the follow-up work, Yusko and colleagues[34] have shown that the slow speed of proteins inside the nanopore, along with the elimination of non-specific interactions between proteins and the lipid-coated nanopore wall, resulted in resolved time-dependent ionic current blockades, and enabled quantitative determination of shape, volume, dipole moment, charge, and rotational diffusion constant of proteins. However, using this approach, the target proteins have to be attached to a lipid anchor ligand embedded in a bilayer, which requires prior knowledge about the specific molecular linkage and the target proteins. Also, it cannot be used for an unknown protein population.

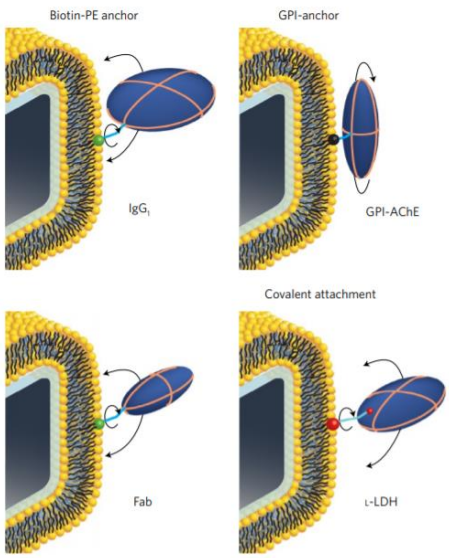

Figure 1.4. four classes of highly flexible crosslinkers, embedded in the lipid-bilayer coating, to anchor a target protein to the fluidic lipid-bilayer on the surface of a nanopore[34]. Copyright 2016 Springer Nature.

1.5.2.3. Macromolecular Crowding

It was shown that the interfacing of a nanopore with a crowded macromolecular electrolyte bath on either side of a membrane slowed down the translocation of biomolecules out of a nanopore and enhanced DNA and protein detection.[63,64] It is not fully clear that how the presence of giant macromolecules around a nanopore may slow down the biomolecules, but in one hypothesis, the slowing-down mechanism in the presence of crowding agents is attributed to the enhanced entropic interactions between the nanopore and a target biomolecule. Big macromolecules of crowding agents occupy and limit the space for DNA or protein molecules inside the solution, entropically drive depletion attraction between a target biomolecule and the nanopore. The stronger biomolecule-nanopore interaction decreases the transient velocity of a biomolecule, allowing it to stay longer inside a nanopore. For instance, in a recent study, Chau and collegueas[64] found that the presence of highly concentrated PEG 8000 macromolecules on the *trans* side of a nanopore at

low PBS buffer concentration changed the dynamics of β-galactosidase protein (466 kD) translocation and increased its residence time inside a nanopore. In addition to the entropic effect, they explained the mechanism of protein detection enhancement as a result of modified electroosmotic flow in the presence of PEG 8000 macromolecules.

Although this technique is quite simple, it is effective in enhancing the detection of DNA and larger proteins; however, it may not be useful for detecting smaller proteins and polypeptides that cannot sense the presence of the bulky macromolecules in their environment.

1.5.2.4. Coupling of a Solid-Sate Nanopore with a Hydrogel

As reviewed above, enormous efforts have been made toward improving nanopore-based protein biosensors; however, the promise to design a sensitive and accurate nanopore biosensor for native and non-modified protein detection and characterization in a wide range of sizes and concentrations is unfulfilled. Also, the current existing platforms are not suitable to study a heterogeneous mixture of proteins and cannot discriminate between different proteins in a solution. In response to all these challenges, recently, our group has engineered a hydrogel-backed nanopore platform to extend protein residence time inside the nanopore, improve protein capture rates, and enhance the measurement resolution.[65] We interfaced the hydrogel at the distal side of a nanopore to prevent fast electrophoretic passage of proteins. Theoretically, we hypothesized that the hydrogel on the distal side of the nanopore acts as a physical barrier and inhibits electrophoretic translocation of proteins. So, the proteins reaching the hydrogel (1) may diffuse back against the electric field and escape to the *cis* compartment of the nanopore, (2) may leave the nanopore through the open mesh of the hydrogel, or (3) may escape a nanopore through a possible gap between the pore mouth and the surface of the hydrogel. In each of these scenarios, proteins have

a longer residence time inside the nanopore, enhancing their chance to be resolved. Figure 1.5 schematically shows the hypothesized escaping mechanisms of proteins through a hydrogel-backed nanopore.

Experimentally, we have also demonstrated the enhancement in protein detection in the presence of the hydrogel. Using a 24 nm diameter nanopore, the measurement of 10 nM IgG showed the detection frequency of 0.49 Hz and the most probable maximum event amplitude of 538 ± 120 pA, in consistent with other studies using solid-state nanopores to detect proteins. However, repeating the measurement with the same nanopore, but in the presence of the hydrogel at the *trans* side of the support membrane, revealed an elevated detection frequency of 490 Hz with the most probable maximum event amplitude of 963± 470 pA (Figure 1.7A). Much higher frequency of events observed in the second experiment given the same concentration of IgG indicated significant reduction in the fraction of missed translocation events, confirming the extended residence time of proteins inside the nanopore in the presence of the hydrogel. In addition, the more extended residence time of proteins inside the hydrogel-backed nanopores enables precise determination of the shape and the volume of the proteins.

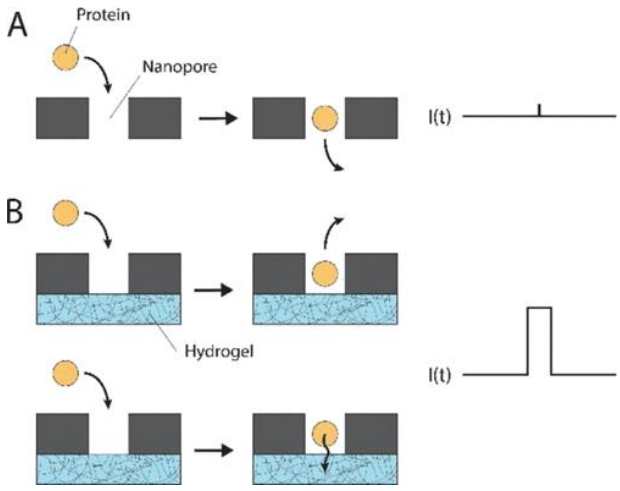

Figure 1.5. A) Fast translocation of proteins in a regular nanopore system B) Hydrogel acts a physical barrier to prevent full translocation of proteins: they may diffuse back to the *cis* side of the membrane or find their way to exit the nanopore through the open mesh of the hydrogel or the possible gap between the nanopore and the hydrogel.[65] Copyright 2020 American Chemical Society.

The protein shapes and volumes can be determined by a distribution of the maximum amplitudes of a population of protein translocation events based on the theory of rotating particles inside the uniform electric field of the nanopore developed by Yusko and coworkers.[34] Based on this theory, the distribution of maximum amplitudes is an asymmetric bimodal distribution for the charged spheroid proteins and is a unimodal Normal distribution for the spherical proteins. In either case, protein volumes can be determined by the value of the peak maxima of the maximum amplitude distribution. The precise estimate of protein shapes and volumes by this method relies on the accurate measurement of the event blockade amplitudes. However, when the transient speed of a protein is faster than the resolution of the amplifier, the recording of the blockade amplitude may be "clipped" or slip-up on translocation events that occur between two acquired data points, and the recorded blockade amplitude may not be precise and error-free.[57]Consequenctly, the protein shape and volume cannot be determined accurately. Therefore, the bandwidth of the

measurement i.e., the protein residence time inside a nanopore is a critical factor for recording accurate blockade amplitudes and precisely estimating the protein shape and volume.

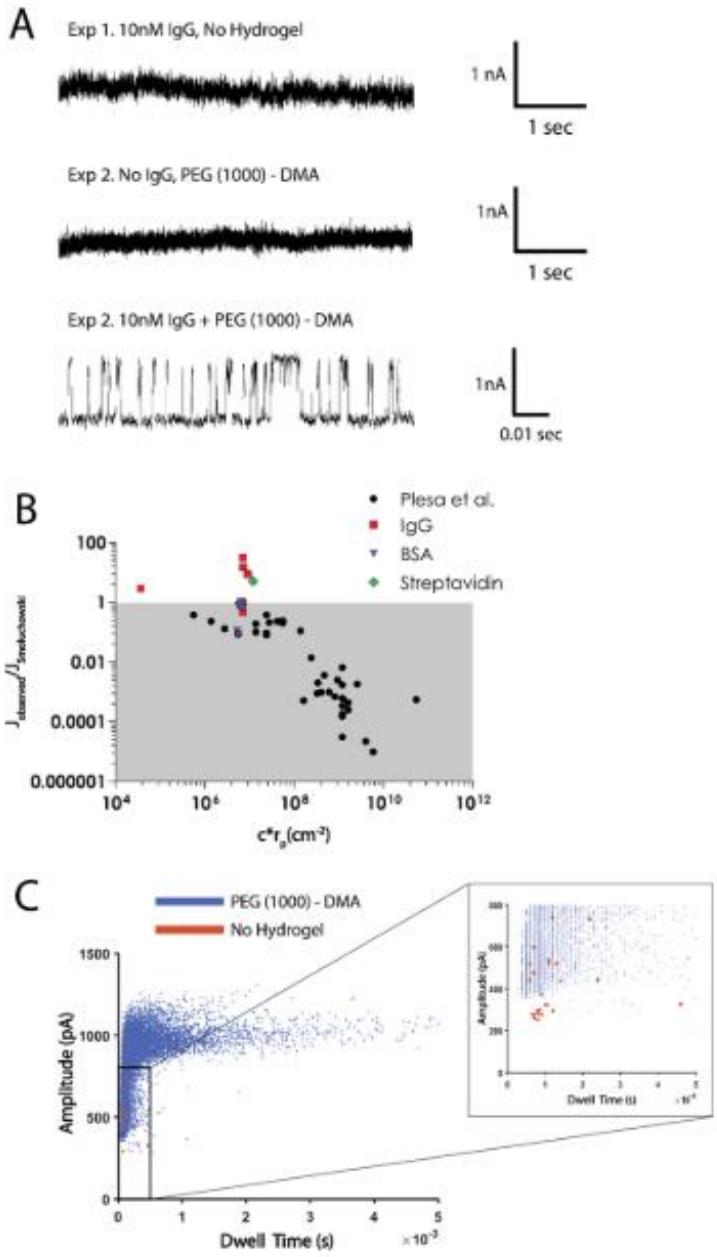

Figure 1.6. A) IgG detection at 10 nM using a 24 nm diameter nanopore with and without hydrogel. B) Enhanced protein detection of BSA and streptavidin enabled by the hydrogel-facilitated nanopore platform compared to previous studies C) Enhanced detection rate and blockade amplitude resolution in IgG measurements using a hydrogel-backed nanopore.[65]Copyrght 2020 American Chemical Society.

As mentioned earlier, the longer residence time of proteins inside the nanopore enabled by the presence of the hydrogel enhances the resolution in amplitude measurement, enabling shape and volume determination, and simultaneous measurements of two proteins. Figure 1.7 demonstrates the maximum amplitude histograms of A) spherical 10 nm gold nanoparticles and B) oval shape IgG protein translocation events measured using a hydrogel-facilitated nanopore. A unimodal, Gaussian, and symmetric shape of Figure 1.7A confirms the spherical shape of the 10 nm gold particles, and the bimodal and non-symmetric distribution of Figure 1.7B reveals the oval shape of a molecule of IgG protein with two main orientations along its main axis.

Moreover, using hydrogel-backed nanopores, IgG and BSA were simultaneously detected in a binary mixture solution. Figure 1.8 illustrates the series of nanopore measurements to sense IgG, BSA, and a solution containing a mixture of both IgG and BSA. The observed translocation events of the mixture of IgG and BSA (the green data cluster in Figure 1.8A and the green histogram in Figure 1.8B) indicate two distinguishable regimes, overlapping with distributions of BSA and IgG translocation events obtained from individually purified protein measurements. This result confirms a distinguishable identification of two species of proteins in a mixture solution as a result of accurately measured blockade amplitudes of protein events with higher dwell time in the presence of the hydrogel.

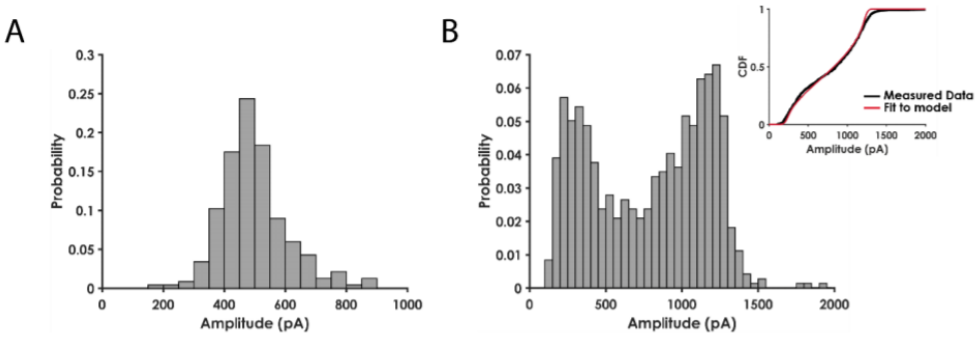

Figure 1.7. Molecule conformation determination using hydrogel-backed nanopores A) 10 nm gold nanoparticles B) IgG protein.[65] Copyright 2020 American Chemical Society.

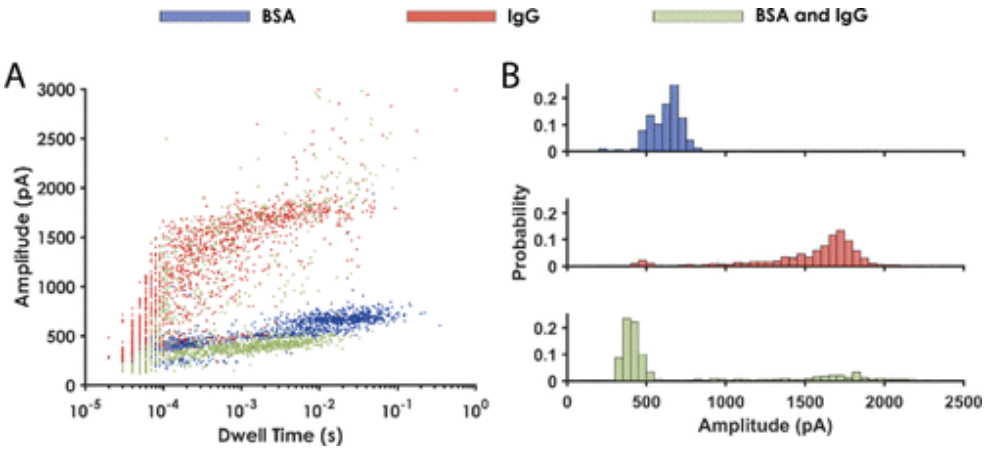

Figure 1.8. Simultaneous measurements of a mixture of two proteins A) The results of the simultaneous measurements of a solution containing a mixture of IgG and BSA using a hydrogel-backed 22 nm diameter nanopore illustrated two distinguishable data clusters on the 2D amplitude-dwell time plot (green dots). Each cluster overlaps with the results of the measurement of each individual, purified protein. B) Amplitude blockade histograms of purified BSA (blue), IgG (red), a mixture of IgG and BSA (green).[65] Copyright 2020 American Chemical Society.

1.6. Research Motivation and Objectives

All of our group's previous work has shown that introducing hydrogel on the *cis* side of the silicon nitride nanopore effectively improves protein detection by sterically hindering the passage of proteins from the *trans* side, leading to significantly enhanced protein residence time within the nanopore sensing zone, and resulting in a significant reduction in missed translocation events. In addition, our group has shown that the longer residence time of proteins inside a nanopore effectively improves the resolution of protein measurements, enabling the simultaneous measurement of two proteins.

What remains unclear is exploring the measurement limitations of the proposed platform and how to improve it for various proteomic applications. The main goal of the following research is exploring and improving hydrogel-backed nanopore biosensors for ultrasensitive protein detection. Three objectives summarize the primary goal of this research:

First, exploring further capabilities and the extent to which the proposed hydrogel-backed nanopore biosensor can resolve and characterize various proteins spanning a range of sizes and concentrations.

Second, the investigation, adaptation , and improvement of a hydrogel-backed nanopore biosensor as an ultra-sensitive protein detector for liquid chromatography.

Third, the surface coating of a hydrogel-backed nanopore with the antifouling ligands for advanced protein detection and characterization.

The organization of this dissertation is as follows:

Chapter 1: Background and Introduction

Provides background information on nanopore sensing measurements of single-molecule proteins in their native conformation, the technological challenges, and previous approaches to

improve nanopore sensing platforms for enhanced single-molecule protein detection, identification, and quantification.

Chapter 2: Quantitative Measurement of Protein Volume and Concentration Using Hydrogel-backed Nanopores

The minimum achievable detection limits of proteins in terms of size and concentration is explored using hydrogel-facilitated nanopore sensing. Also, the algorithms are developed to quantify an unknown protein volume and concentration. Further, the possible competing mechanism of enhanced protein detection in the presence of the hydrogel is investigated.

Chapter 3: Hydrogel-backed Nanopore as an Ultrasensitive Protein Detector for Liquid Chromatography

Hydrogel-facilitated nanopore sensors are introduced as an effective alternative for the typical UV-Vis detectors with promising applications in proteomic studies. Further, the hydrogel-backed nanopore is integrated with microfluidic channels to facilitate the nanopore measurement of a managed flow of protein fractions emerging from a chromatographic column.

Chapter 4: Hydrogel-backed Lipid Coated Nanopore

The integration of lipid-bilayer coated nanopores with a hydrogel is explored for accurate and ultra-sensitive intra-event ionic current analysis of single protein translocation events in the absence of non-specific interactions between nanopore and protein molecules.

Chapter 5: Conclusion and Recommendation for Future Works

1.7.References:

(1) Berg, J. M.; Tymoczko, J. L.; Stryer, L. *Biochemistry*, 5th ed.; W.H. Freeman & Co., 2002.

(2) Beck, M.; Schmidt, A.; Malmstroem, J.; Claassen, M.; Ori, A.; Szymborska, A.; Herzog, F.; Rinner, O.; Ellenberg, J.; Aebersold, R. The Quantitative Proteome of a Human Cell Line. *Mol. Syst. Biol.* **2011**, *7* (549), 1–8. https://doi.org/10.1038/msb.2011.82.

(3) Chandramouli, K.; Qian, P.-Y. Proteomics: Challenges, Techniques and Possibilities to Overcome Biological Sample Complexity. *Hum. Genomics Proteomics* **2009**, *1* (1). https://doi.org/10.4061/2009/239204.

(4) Sam Hanash. Disease Proteomics. *Nature* **2003**, *422* (March), 226–232.

(5) Kavallaris, M.; Marshall, G. M. Proteomics and Disease: Opportunities and Challenges. *Med. J. Aust.* **2005**, *182* (11), 575–579. https://doi.org/10.5694/j.1326-5377.2005.tb06817.x.

(6) Schuler, B.; Soranno, A.; Hofmann, H.; Nettels, D. Single-Molecule FRET Spectroscopy and the Polymer Physics of Unfolded and Intrinsically Disordered Proteins. *Annu. Rev. Biophys.* **2016**, *45*, 207–231. https://doi.org/10.1146/annurev-biophys-062215-010915.

(7) Gooding, J. J.; Gaus, K. Single-Molecule Sensors: Challenges and Opportunities for Quantitative Analysis. *Angew. Chemie - Int. Ed.* **2016**, *55* (38), 11354–11366. https://doi.org/10.1002/anie.201600495.

(8) Dhakal, D.; Winterhalter, M. Current Measurement and Noise Modeling in Solid State Nanopores. **2010**, No. December.

(9) Restrepo-Pérez, L.; Joo, C.; Dekker, C. Paving the Way to Single-Molecule Protein Sequencing. *Nat. Nanotechnol.* **2018**, *13* (9), 786–796. https://doi.org/10.1038/s41565-018-0236-6.

(10) Schmid, S.; Dekker, C. Nanopores – A Versatile Tool to Study Protein Dynamics. *arXiv* **2020**, No. November, 1–15. https://doi.org/10.1042/ebc20200020.

(11) Moore, S. W.; Roca-Cusachs, P.; Sheetz, M. P. Stretchy Proteins on Stretchy Substrates: The Important Elements of Integrin-Mediated Rigidity Sensing. *Dev. Cell* **2010**, *19* (2), 194–206. https://doi.org/10.1016/j.devcel.2010.07.018.

(12) Eggeling, C.; Ringemann, C.; Medda, R.; Schwarzmann, G.; Sandhoff, K.; Polyakova, S.;

Belov, V. N.; Hein, B.; Von Middendorff, C.; Schönle, A.; Hell, S. W. Direct Observation of the Nanoscale Dynamics of Membrane Lipids in a Living Cell. *Nature* **2009**, *457* (7233), 1159–1162. https://doi.org/10.1038/nature07596.

(13) Schuler, B.; Eaton, W. A. Protein Folding Studied by Single-Molecule FRET. *Curr. Opin. Struct. Biol.* **2008**, *18* (1), 16–26. https://doi.org/10.1016/j.sbi.2007.12.003.

(14) Deniz, A. A.; Laurence, T. A.; Beligere, G. S.; Dahan, M.; Martin, A. B.; Chemla, D. S.; Dawson, P. E.; Schultz, P. G.; Weiss, S. Single-Molecule Protein Folding: Diffusion Fluorescence Resonance Energy Transfer Studies of the Denaturation of Chymotrypsin Inhibitor 2. *Proc. Natl. Acad. Sci. U. S. A.* **2000**, *97* (10), 5179–5184. https://doi.org/10.1073/pnas.090104997.

(15) Afrin, R.; Alam, M. T.; Ikai, A. Pretransition and Progressive Softening of Bovine Carbonic Anhydrase II as Probed by Single Molecule Atomic Force Microscopy. *Protein Sci.* **2009**, *14* (6), 1447–1457. https://doi.org/10.1110/ps.041282305.

(16) Yang, H.; Luo, G.; Karnchanaphanurach, P.; Louie, T. M.; Rech, I.; Cova, S.; Xun, L.; Xie, X. S. Protein Conformational Dynamics Probed by Single-Molecule Electron Transfer. *Science (80-.).* **2003**, *302* (5643), 262–266. https://doi.org/10.1126/science.1086911.

(17) Merchant, K. A.; Best, R. B.; Louis, J. M.; Gopich, I. V.; Eaton, W. A. Characterizing the Unfolded States of Proteins Using Single-Molecule FRET Spectroscopy Any Molecular Simulations. *Proc. Natl. Acad. Sci. U. S. A.* **2007**, *104* (5), 1528–1533. https://doi.org/10.1073/pnas.0607097104.

(18) Ananth, A.; Genua, M.; Aissaoui, N.; Díaz, L.; Eisele, N. B.; Frey, S.; Dekker, C.; Richter, R. P.; Görlich, D. Reversible Immobilization of Proteins in Sensors and Solid-State Nanopores. *Small* **2018**, *14* (18). https://doi.org/10.1002/smll.201703357.

(19) LIU, Y.; YAO, X. F.; WANG, H. Y. Protein Detection Through Single Molecule Nanopore. *Chinese J. Anal. Chem.* **2018**, *46* (6), e1838–e1846. https://doi.org/10.1016/S1872-2040(18)61093-X.

(20) Plesa, C.; Ruitenberg, J. W.; Witteveen, M. J.; Dekker, C. Detection of Individual Proteins Bound along DNA Using Solid-State Nanopores. *Nano Lett.* **2015**, *15* (5). https://doi.org/10.1021/acs.nanolett.5b00249.

(21) Charron, M.; Briggs, K.; King, S.; Waugh, M.; Tabard-cossa, V. Precise DNA Concentration Measurements with Nanopores by Controlled Counting. *Anal. Chem.* **2019**, *91*, 12228–12237. https://doi.org/10.1021/acs.analchem.9b01900.

(22) Freedman, K. J.; Edel, J. B.; Haq, S. R.; Jemth, P.; Fletcher, M. R.; Foley, J. P.; Kim, M. J. Nonequilibrium Capture Rates Induce Protein Accumulation and Enhanced Adsorption to Solid-State Nanopores. *ACS Nano* **2014**, *8* (12), 12238–12249. https://doi.org/10.1021/nn5062645.

(23) Soni, G. V.; Dekker, C. Detection of Nucleosomal Substructures Using Solid-State Nanopores. *Nano Lett.* **2012**, *12* (6), 3180–3186. https://doi.org/10.1021/nl301163m.

(24) Ivankin, A.; Toscano, M. L.; Henley, R. Y.; Wanunu, M.; Carson, S.; Larkin, J. Label-Free Optical Detection of Biomolecular Translocation through Nanopore Arrays. *ACS Nano* **2014**, *8* (10), 10774–10781. https://doi.org/10.1021/nn504551d.

(25) Ivankin, A.; Carson, S.; Kinney, S. R. M.; Wanunu, M. Fast, Label-Free Force Spectroscopy of Histone − DNA Interactions in Individual Nucleosomes Using Nanopores. **2013**, 15350–15352. https://doi.org/10.1021/ja408354s.

(26) Freedman, K. J.; Otto, L. M.; Ivanov, A. P.; Barik, A.; Oh, S. H.; Edel, J. B. Nanopore Sensing at Ultra-Low Concentrations Using Single-Molecule Dielectrophoretic Trapping. *Nat. Commun.* **2016**, *7*, 1–9. https://doi.org/10.1038/ncomms10217.

(27) Zhang, H.; Hiratani, M.; Nagaoka, K.; Kawano, R. MicroRNA Detection at Femtomolar Concentrations with Isothermal Amplification and a Biological Nanopore. *Nanoscale* **2017**, *9* (42), 16124–16127. https://doi.org/10.1039/c7nr04215a.

(28) Galenkamp, N. S.; Soskine, M.; Hermans, J.; Wloka, C.; Maglia, G. Direct Electrical Quantification of Glucose and Asparagine from Bodily Fluids Using Nanopores. *Nat. Commun.* **2018**, *9* (1). https://doi.org/10.1038/s41467-018-06534-1.

(29) Fologea, D.; Ledden, B.; McNabb, D. S.; Li, J. Electrical Characterization of Protein Molecules by a Solid-State Nanopore. *Appl. Phys. Lett.* **2007**, *91* (5), 1–4. https://doi.org/10.1063/1.2767206.

(30) Chuah, K.; Wu, Y.; Vivekchand, S. R. C.; Gaus, K.; Reece, P. J.; Micolich, A. P.; Gooding, J. J. Nanopore Blockade Sensors for Ultrasensitive Detection of Proteins in Complex Biological Samples. *Nat. Commun.* **2019**, *10* (1), 1–9. https://doi.org/10.1038/s41467-019-10147-7.

(31) Kowalczyk, S. W.; Grosberg, A. Y.; Rabin, Y.; Dekker, C. Modeling the Conductance and DNA Blockade of Solid-State Nanopores. *Nanotechnology* **2011**, *22* (31), 1–5. https://doi.org/10.1088/0957-4484/22/31/315101.

(32) DeBlois, R. W.; Bean, C. P. Counting and Sizing of Submicron Particles by the Resistive Pulse Technique. *Rev. Sci. Instrum.* **1970**, *41* (7), 909–916.

https://doi.org/10.1063/1.1684724.

(33) DeBlois, R. W.; Bean, C. P.; Wesley, R. K. A. Electrokinetic Measurements with Submicron Particles and Pores by the Resistive Pulse Technique. *J. Colloid Interface Sci.* **1977**, *61* (2), 323–335. https://doi.org/10.1016/0021-9797(77)90395-2.

(34) Yusko, E. C.; Bruhn, B. R.; Eggenberger, O. M.; Houghtaling, J.; Rollings, R. C.; Walsh, N. C.; Nandivada, S.; Pindrus, M.; Hall, A. R.; Sept, D.; Li, J.; Kalonia, D. S.; Mayer, M. Real-Time Shape Approximation and Fingerprinting of Single Proteins Using a Nanopore. *Nat. Nanotechnol.* **2017**, *12* (4), 360–367. https://doi.org/10.1038/nnano.2016.267.

(35) Ling, D.; Ling, X. On the Distribution of DNA Translocation Times in Solid-State Nanopores: An Analysis Using Schrödinger's First-Passage-Time Theory. *J. Phys. Condens. Matter Condens. Matter* **2013**, *25* (37). https://doi.org/10.1088/0953-8984/25/37/375102.On.

(36) Li, W.; Bell, N. A. W.; Hernández-Ainsa, S.; Thacker, V. V.; Thackray, A. M.; Bujdoso, R.; Keyser, U. F. Single Protein Molecule Detection by Glass Nanopores. *ACS Nano* **2013**, *7* (5), 4129–4134. https://doi.org/10.1021/nn4004567.

(37) Rivas, F.; Zahid, O. K.; Reesink, H. L.; Peal, B. T.; Nixon, A. J.; DeAngelis, P. L.; Skardal, A.; Rahbar, E.; Hall, A. R. Label-Free Analysis of Physiological Hyaluronan Size Distribution with a Solid-State Nanopore Sensor. *Nat. Commun.* **2018**, *9* (1), 1–9. https://doi.org/10.1038/s41467-018-03439-x.

(38) Han, A.; Schürmann, G.; Linder, V.; De Rooij, N. F.; Staufer, U.; Creus, M.; Ward, T. R. Label-Free Detection of Single Protein Molecules and Protein-Protein Interactions Using Synthetic Nanopores. *Anal. Chem.* **2008**, *80* (12), 4651–4658. https://doi.org/10.1021/ac7025207.

(39) Wloka, C.; Van Meervelt, V.; Van Gelder, D.; Danda, N.; Jager, N.; Williams, C. P.; Maglia, G. Label-Free and Real-Time Detection of Protein Ubiquitination with a Biological Nanopore. *ACS Nano* **2017**, *11* (5), 4387–4394. https://doi.org/10.1021/acsnano.6b07760.

(40) Tang, Z.; Zhang, D.; Cui, W.; Zhang, H.; Pang, W.; Duan, X. Fabrications, Applications and Challenges of Solid-State Nanopores: A Mini Review. *Nanomater. Nanotechnol.* **2016**, *6*, 35. https://doi.org/10.5772/64015.

(41) Yusko, E. C.; Prangkio, P.; Sept, D.; Rollings, R. C.; Li, J.; Mayer, M. Single-Particle Characterization of Aβ Oligomers in Solution. *ACS Nano* **2012**, *6* (7), 5909–5919. https://doi.org/10.1021/nn300542q.

(42) Li, X.; Tong, X.; Lu, W.; Yu, D.; Diao, J.; Zhao, Q. Label-Free Detection of Early Oligomerization of α-Synuclein and Its Mutants A30P/E46K through Solid-State Nanopores. **2019**, 6480–6488. https://doi.org/10.1039/c9nr00023b.

(43) Talaga, D. S.; Li, J. Single-Molecule Protein Unfolding in Solid State Nanopores. *J. Am. Chem. Soc.* **2009**, *131* (26), 9287–9297. https://doi.org/10.1021/ja901088b.

(44) Ivankin, A.; Carson, S.; Kinney, S. R. M.; Wanunu, M. Fast, Label-Free Force Spectroscopy of Histone-DNA Interactions in Individual Nucleosomes Using Nanopores. *J. Am. Chem. Soc.* **2013**, *135* (41), 15350–15352. https://doi.org/10.1021/ja408354s.

(45) Kwak, D. K.; Chae, H.; Lee, M. K.; Ha, J. H.; Goyal, G.; Kim, M. J.; Kim, K. B.; Chi, S. W. Probing the Small-Molecule Inhibition of an Anticancer Therapeutic Protein-Protein Interaction Using a Solid-State Nanopore. *Angew. Chemie - Int. Ed.* **2016**, *55* (19), 5713–5717. https://doi.org/10.1002/anie.201511601.

(46) Soni, G. V.; Dekker, C. Detection of Nucleosomal Substructures Using Solid-State Nanopores. *Nano Lett.* **2012**, *12* (6), 3180–3186. https://doi.org/10.1021/nl301163m.

(47) Hu, R.; Rodrigues, J. V.; Waduge, P.; Yamazaki, H.; Cressiot, B.; Chishti, Y.; Makowski, L.; Yu, D.; Shakhnovich, E.; Zhao, Q.; Wanunu, M. Differential Enzyme Flexibility Probed Using Solid-State Nanopores. *ACS Nano* **2018**, *12* (5), 4494–4502. https://doi.org/10.1021/acsnano.8b00734.

(48) Ananth, A.; Genua, M.; Aissaoui, N.; Díaz, L.; Eisele, N. B.; Frey, S.; Dekker, C.; Richter, R. P.; Görlich, D. Reversible Immobilization of Proteins in Sensors and Solid-State Nanopores. *Small* **2018**, *14* (18), 1–11. https://doi.org/10.1002/smll.201703357.

(49) Rant, U. Stochastic Sensing of Proteins with Receptor-Modified Solid-State Nanopores ´ 2 *. **2012**, *7* (April), 257–263. https://doi.org/10.1038/nnano.2012.24.

(50) Sexton, L. T.; Horne, L. P.; Sherrill, S. A.; Bishop, G. W.; Baker, L. A.; Martin, C. R. Resistive-Pulse Studies of Proteins and Protein/Antibody Complexes Using a Conical Nanotube Sensor. *J. Am. Chem. Soc.* **2007**, *129* (43), 13144–13152. https://doi.org/10.1021/ja0739943.

(51) Freedman, K. J.; Haq, S. R.; Edel, J. B.; Jemth, P.; Kim, M. J. Single Molecule Unfolding and Stretching of Protein Domains inside a Solid-State Nanopore by Electric Field. *Sci. Rep.* **2013**, *3*, 1–8. https://doi.org/10.1038/srep01638.

(52) Waduge, P.; Hu, R.; Bandarkar, P.; Yamazaki, H.; Cressiot, B.; Zhao, Q.; Whitford, P. C.; Wanunu, M. Nanopore-Based Measurements of Protein Size, Fluctuations, and Conformational Changes. *ACS Nano* **2017**, *11* (6).

https://doi.org/10.1021/acsnano.7b01212.

(53) Saharia, J.; Bandara, Y. M. N. D. Y.; Goyal, G.; Lee, J. S.; Karawdeniya, B. I.; Kim, M. J. Molecular-Level Profiling of Human Serum Transferrin Protein through Assessment of Nanopore-Based Electrical and Chemical Responsiveness. *ACS Nano* **2019**, *13* (4), 4246–4254. https://doi.org/10.1021/acsnano.8b09293.

(54) Kong, J.; Bell, N. A. W.; Keyser, U. F. Quantifying Nanomolar Protein Concentrations Using Designed DNA Carriers and Solid-State Nanopores. *Nano Lett.* **2016**, *16* (6), 3557–3562. https://doi.org/10.1021/acs.nanolett.6b00627.

(55) Plesa, C.; Kowalczyk, S. W.; Zinsmeester, R.; Grosberg, A. Y.; Rabin, Y.; Dekker, C. Fast Translocation of Proteins through Solid State Nanopores-Supporting Information. *Nano Lett.* **2013**, *13* (2), 658–663. https://doi.org/10.1021/nl3042678.

(56) Hartel, A. J. W.; Shekar, S.; Ong, P.; Schroeder, I.; Thiel, G.; Shepard, K. L. High Bandwidth Approaches in Nanopore and Ion Channel Recordings - A Tutorial Review. *Anal. Chim. Acta* **2019**, *1061*, 13–27. https://doi.org/10.1016/j.aca.2019.01.034.

(57) Uram, J. D.; Ke, K.; Mayer, M. Noise and Bandwidth of Current Recordings from Submicrometer Pores and Nanopores. *ACS Nano* **2008**, *2* (5), 857–872. https://doi.org/10.1021/nn700322m.

(58) Rosenstein, J. K.; Wanunu, M.; Merchant, C. A.; Drndic, M.; Shepard, K. L. Integrated Nanopore Sensing Platform with Sub-Microsecond Temporal Resolution. *Nat. Methods* **2012**, *9* (5), 487–492. https://doi.org/10.1038/nmeth.1932.

(59) Larkin, J.; Henley, R. Y.; Muthukumar, M.; Rosenstein, J. K.; Wanunu, M. High-Bandwidth Protein Analysis Using Solid-State Nanopores. *Biophys. J.* **2014**, *106* (3), 696–704. https://doi.org/10.1016/j.bpj.2013.12.025.

(60) Houghtaling, J.; Ying, C.; Eggenberger, O. M.; Fennouri, A.; Nandivada, S.; Acharjee, M.; Li, J.; Hall, A. R.; Mayer, M. Estimation of Shape, Volume, and Dipole Moment of Individual Proteins Freely Transiting a Synthetic Nanopore. *ACS Nano* **2019**, *13* (5), 5231–5242. https://doi.org/10.1021/acsnano.8b09555.

(61) Fologea, D.; Uplinger, J.; Thomas, B.; Mcnabb, D. S. Slowing DNA Translocation in a Solid-State Nanopore. **2005**, 20–23. https://doi.org/10.1021/nl051063o.

(62) Yusko, E. C.; Johnson, J. M.; Majd, S.; Prangkio, P.; Rollings, R. C.; Li, J.; Yang, J.; Mayer, M. Controlling Protein Translocation through Nanopores with Bio-Inspired Fluid Walls. *Nat. Nanotechnol.* **2011**, *6* (253–260). https://doi.org/10.1038/nnano.2011.12.

(63) Yao, F.; Peng, X.; Su, Z.; Tian, L.; Guo, Y.; Kang, X. F. Crowding-Induced DNA Translocation through a Protein Nanopore. *Anal. Chem.* **2020**, *92* (5), 3827–3833. https://doi.org/10.1021/acs.analchem.9b05249.

(64) Chau, C. C.; Radford, S. E.; Hewitt, E. W.; Actis, P. Macromolecular Crowding Enhances the Detection of DNA and Proteins by a Solid-State Nanopore. *Nano Lett.* **2020**, *20* (7), 5553–5561. https://doi.org/10.1021/acs.nanolett.0c02246.

(65) Acharya, S.; Jiang, A.; Kuo, C.; Nazarian, R.; Li, K.; Ma, A.; Siegal, B.; Toh, C.; Schmidt, J. J. Improved Measurement of Proteins Using a Solid-State Nanopore Coupled with a Hydrogel. *ACS Sensors* **2020**, *5*, 370–376. https://doi.org/10.1021/acssensors.9b01928.

Chapter 2: Quantitative Measurements of Protein Volumes and Concentrations Using Hydrogel-Backed Nanopores

2.1. Introduction:

Nanopore biosensors have been extensively investigated for use as a highly precise, sensitive, rapid, and label-free platform for single-biomolecule sensing in aqueous solution solutions.[1–14] Real-time single molecule detection and quantification of protein biomarkers at the single-molecule level may enable the next generation of diagnostics tools and treatment strategies. However, detection, identification, and quantification of proteins has been shown to be limited as a result of their rapid transport through the nanopore.[15,16] Their wide range of sizes and concentrations make proteins particularly a difficult analyte to sense.

Measurement of small proteins (below 10 kD) typically requires: custom low-noise nanopores which are only slightly larger (sometimes only 1 nm larger) than the hydrodynamic diameter of the target protein to enhance the protein-pore interaction; low-noise, high bandwidth amplifiers; and tailoring the measurement pH of the electrolyte to enhance surface interactions by reducing protein surface charge.[17–20] Although there are some reports of protein detection at low concentrations and quantitation of protein concentration, these approaches are characterized by protein binding to modified nanopore surfaces, or other specific labeling strategies.[21–23] Furthermore, target proteins were typically measured at μM or greater concentrations, and experimental durations extended to hours or longer to overcome the larger number of missed events described above. Most approaches for measurement of small proteins and low concentrations require prior knowledge of the target protein and corresponding modification of the nanopore or protein, precluding the measurement of an unknown protein or a mixture of proteins.

Recently, we described an approach to improving nanopore sensitivity by polymerizing a hydrogel on one side of the nanopore.[24] The presence of the hydrogel extended the analyte residence time within the nanopore, increasing the detection rate by several orders of magnitude

for a given analyte concentration while using a standard amplifier and requiring no significant noise on nanopore size. The increased residence time within the nanopore reduced the measurement bandwidth required, increasing the signal to noise ratio, improving measurement resolution, and enabling discrimination of two proteins in a mixture. The increased resolution also enables detection of smaller proteins, and the large reduction of missed events enables detection of proteins at lower concentrations. Here, we describe experiments showing the limits of detection achievable with this approach with respect to concentrations (10 fM) and protein size (≤5.5 kD). We also explored using the event rate to quantitatively determine protein concentration, finding that the unknown concentrations could be determined to within 10%, following nanopore calibration. We find that variations in the event rate for similar size nanopores may be related to the proximity of the hydrogel to the surface of the nanopore, which affects the efficacy of the hydrogel to enhance protein detection. We developed an iterative algorithm to determine correction factors and volumes of unknown proteins from nanopore data. Determination of protein volumes from measurements made with this system also agreed with previous literature reports and show an increase in protein volume with increasing pH for IgG and myoglobin.

2.2. Results and Discussion:

We measured immunoglobulin G1 (IgG) in its native state using nanopores 23-31 nm in diameter and 15 nm long, backed with the PEG-DMA hydrogel of average mesh size ~ 3.1 nm, as described previously (Figure 2.1).

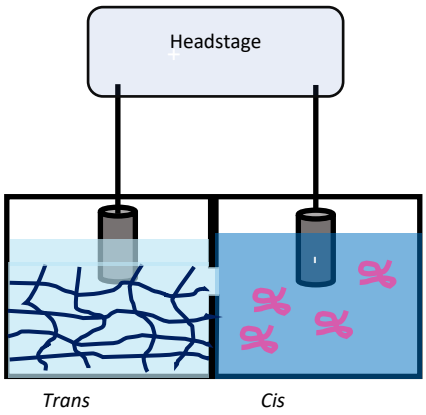

Figure 2.1. Schematic diagram of measurement apparatus. The nanopore chip separates the hydrogel-containing *trans* chamber from the protein containing *cis* chamber.

To determine the average event frequency (f), we divided the number of single-molecule translocation events (N) by the duration of observation (Δt): $f = N / \Delta t$.[25,26] We applied -50 mV to the nanopore and found that the event frequency rapidly increased following protein addition and plateaued after 5 to 9 minutes (Figure 2.2), indicating the amount of time for protein monomers to homogenously disperse throughout the measurement chamber. The plateau after the first 9 minutes indicates a quasi-equilibrium capture mechanism with no net protein accumulation nor adsorption near the nanopore. For consistency, we analyzed minute-long stretches of data at minutes 9 and 11 (we reserved minute 10 for applying a positive voltage in case the nanopore clogged.)

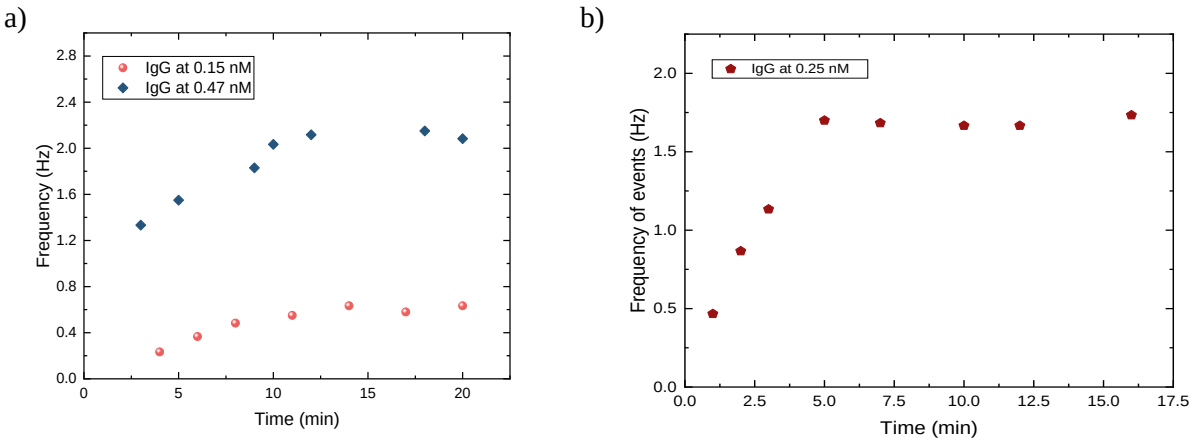

Figure 2.2. a) Measured event frequencies versus time of IgG at 0.15 and 0.47 nM after injection into the flow cell; 21 nm diameter nanopore. b) Measured event frequency of 0.25 nM IgG vs. time; 24 nm diameter nanopore. Data from both panels obtained with -50 mV applied potential.

2.2.1. Protein Concentration Determination

We measured event frequencies of 0.01-43 Hz for IgG concentrations at 10 pM-10 nM (Figure 2.3). The observed frequency for 10 pM was 0.01 Hz, equivalent of 2 events every 3 minutes; We expected that lower concentrations would be detectable if the measurement duration were increased to several hours and beyond. Plots of event frequency versus IgG bulk concentrations show a linear relationship, although the slope changed when different nanopores were used. We repeated the measurement with Ovalbumin, a globular 44 kD protein, again finding a linear relationship between event frequency and protein concentration (Figure 2.3). The linear dependance of event frequency versus protein bulk concentrations has been described in previous studies,[27–30] which assumes a hemispherical capture zone at the nanopore entrance when the protein motion transitions from non-biased diffusion to electrophoretic drift.

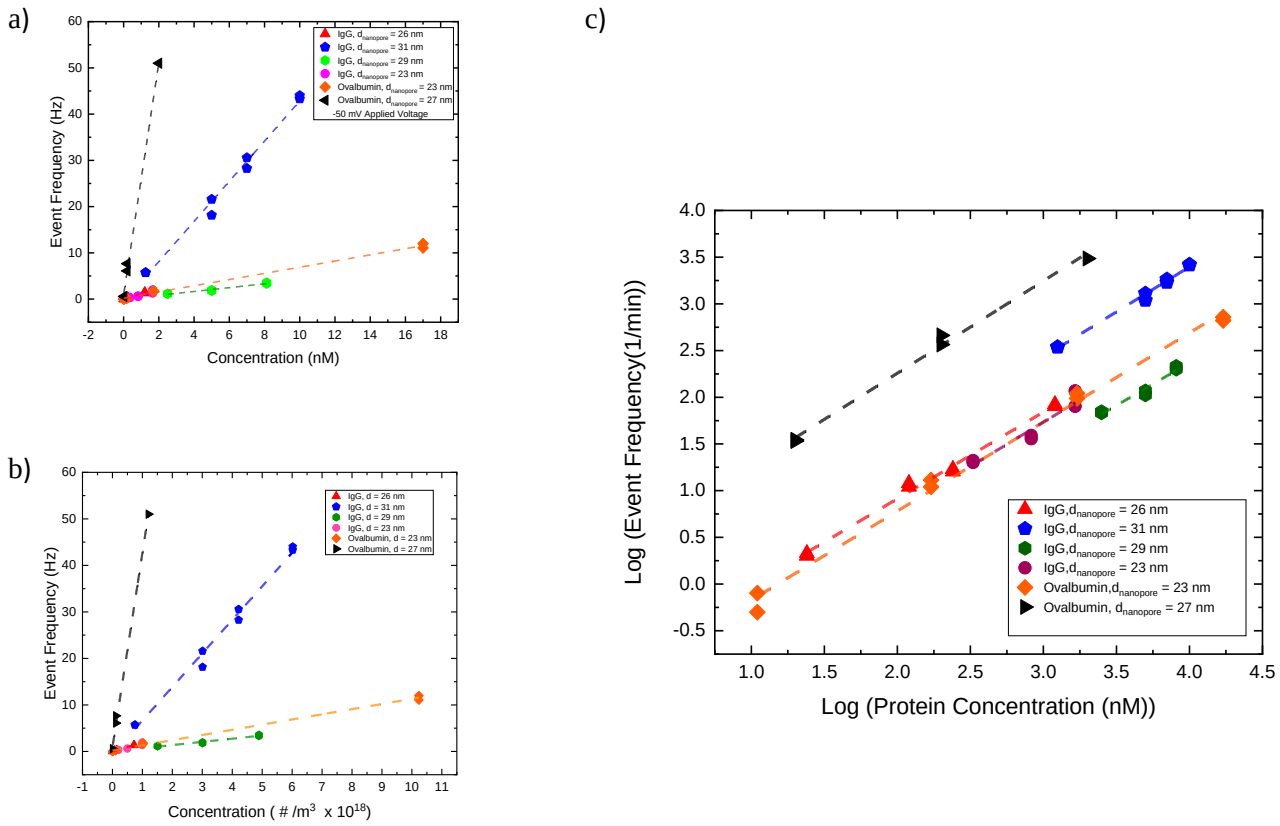

Figure 2.3. Linear relation of event frequency vs. protein bulk concentration. a) Event frequency (Hz) vs. concentration (nM); b) event frequency (Hz) vs. concentration (# / m^3 x 10^{18}); c) log (event frequency (Hz)) vs. log (concentration (concentration (nM))

Figure 2.3 also shows a large variation in event frequencies for nanopore that are similar in size. We hypothesize that this arises from variations in the gap between the hydrogel and nanopore surface in different experiments, with larger gap less effective in inhibiting protein transport through the nanopore. We explored this hypothesis by functionalizing the trans surface of the SiN chip with 3-(Trimethoxy silyl)propyl methacrylate and cured the hydrogel to this surface to eliminate the gap between the hydrogel and chip. IgG measured with this system exhibited high event frequency, long event dwell times, and dwell time that increased with increasing voltage, all in contrast with non-bonded hydrogel measurement (Figure 2.4a).

a b

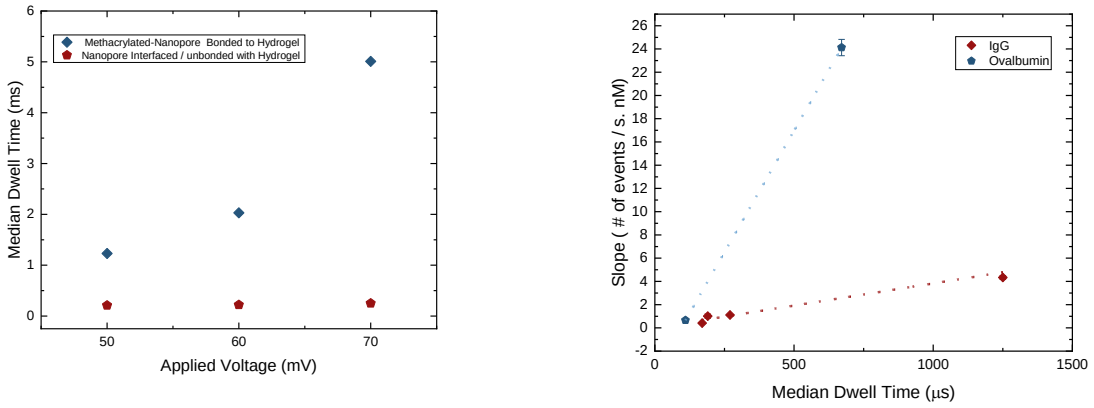

Figure 2.4. The median dwell times were obtained from data sets recorded for three voltages on nanopores with hydrogel bonded and unbonded to the *trans* side of the chip.

The increasing dwell time with increasing voltage for the bonded hydrogel suggests that protein may escape by diffusing against the electric field to escape from the pore on the *cis* side. Assuming that the hydrogel is a perfectly reflecting barrier, and the *cis* entrance is an absorbing barrier (corresponding to particle escape) the first passage time is given by:[31]

$$t = 2\left(\frac{l^2}{2D}\right)\left(\frac{kT}{qV}\right)^2\left\{e^{\frac{qV}{kT}} - 1 - \frac{qV}{kT}\right\} \qquad 2.1$$

where D is the protein diffusion constant, l is the pore length, k is Boltzmann's constant, T is the temperature, q is the protein charge, and V is the applied voltage.

On the other hand, if the particle escaped the nanopore on the trans side by going into the hydrogel or into the gap between the hydrogel and the nanopore chip, we may expect that the dwell time would decrease with increasing voltage. The large change in results following the bonding to the chip may indicate that the hydrogel-chip gap escape mechanism is being minimized. Variations

in hydrogel-chip gaps may also explain how nanopores of similar diameter can show significantly different event rates, as seen in Figure 2.3. In support of this hypothesis, we plotted the slope of frequency versus concentration for the data sets in Figure 2.3 versus the median dwell times of the same data (Figure 2.4b) and found that increasing dwell times were strongly correlated with high nanopore sensitivity (higher event rate per concentration).

To determine an unknown concentration of proteins, we explored weather the event frequency versus concentration can be calibrated for each nanopore and the unknown concentration indicated by interpolation of the observed event frequency on the nanopore calibration curve. To assess this capability, we calibrated each nanopore using the obtained data sets shown in Figure 2.3 but leaving out the last data point. The last data point was treated as the unknown concentration, which was estimated by interpolation of the nanopore calibration curve using the observed event frequency. Table 2.1 shows the results of prediction the unknown protein concentration based on two or three-point calibration curves. When using three calibration points, the unknown protein concentration was determined to within less than 10% error.

Table 2.1. Determination of unknown protein concentrations using hydrogel-backed nanopores.

Nanopore Diam. (nm)	**Protein**	**# of Cal. Pts**	**Concentration (nM)**		**Confidence Interval**		**Error**
			Actual	Predicted	Lower (nM)	Upper (nM)	
29	IgG	2	8.12	11.22	5.88	21.37	38%
23	IgG	2	1.64	2.15	1.34	4.36	31%
27	Ovalbumin	2	2.00	1.28	0.58	2.75	36%
26	IgG	3	1.20	1.12	0.57	2.29	7%
31	IgG	3	10.00	10.71	8.05	14.12	7%
23	Ovalbumin	3	17.00	15.48	5.37	25.70	9%

2.2.2. Protein Detection at Ultimately Low Concentrations

Previous studies have shown that electrostatic focusing by creation of a salt gradient across the membrane significantly increases capture rate.[32,33] To investigate whether this would allow

our system to achieve lower concentration limits of detection, we measured the IgG translocation rate with a 29 nm diameter nanopore (with hydrogel on the *trans* side) under symmetric and asymmetric salt conditions. In the first experiment, the electrolyte on both sides of the nanopore was 2 M KCl. Event rate for 10 pM IgG were 0.02 Hz at -50 mV applied voltage. In the second experiment, the same nanopore was used but the electrolyte concentration on the cis side was changed to 0.2 M KCl. An approximately order-of-magnitude increase in event frequency was observed. This change in *cis* solution composition also reduced the solution conductivity and the signal-to-noise ratio. The nanopore open current decreased from ~14 to ~7 nA, and the amplitude of IgG events decreased from ~660 to ~390 pA (Figure 2.5 a and b). We repeated the experiment with a 36 nm diameter nanopore using -70 mV applied potential and observed a detectable event rate for IgG at 100 fM and 10 fM (Figure 2.6). To our knowledge, this is the lowest concentration reported for single molecule detection of an unlabeled native protein. The collected event amplitude at 100 fM were statistically analyzed (Figure 2.6 b and c), showing the effects of non-spherical protein shape as we and others have previously reported[24,34] and with strong similarity to those of 100 pM data taken under symmetric electrolyte.

a) b)

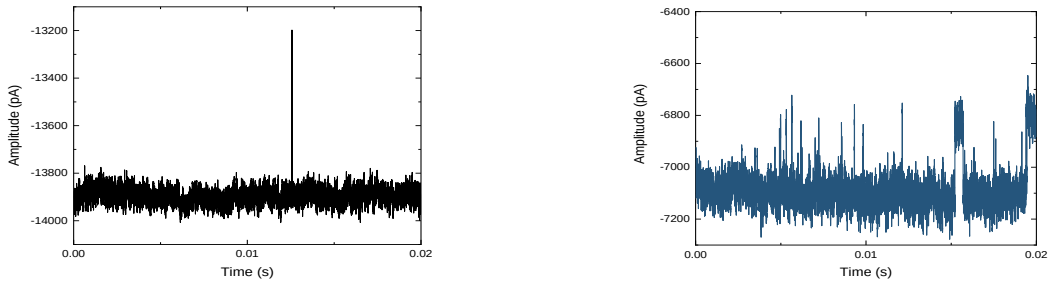

Figure 2.5. Measurement of IgG under symmetric and asymmetric salt concentration: a) Measurement of 10 pM IgG under symmetric 2 M/2 M KCl with a 29 nm diameter nanopore with hydrogel on *trans* side. b) Measurement of 10 pM IgG with same nanopore but with 0.2 M KCL on the *cis* side.

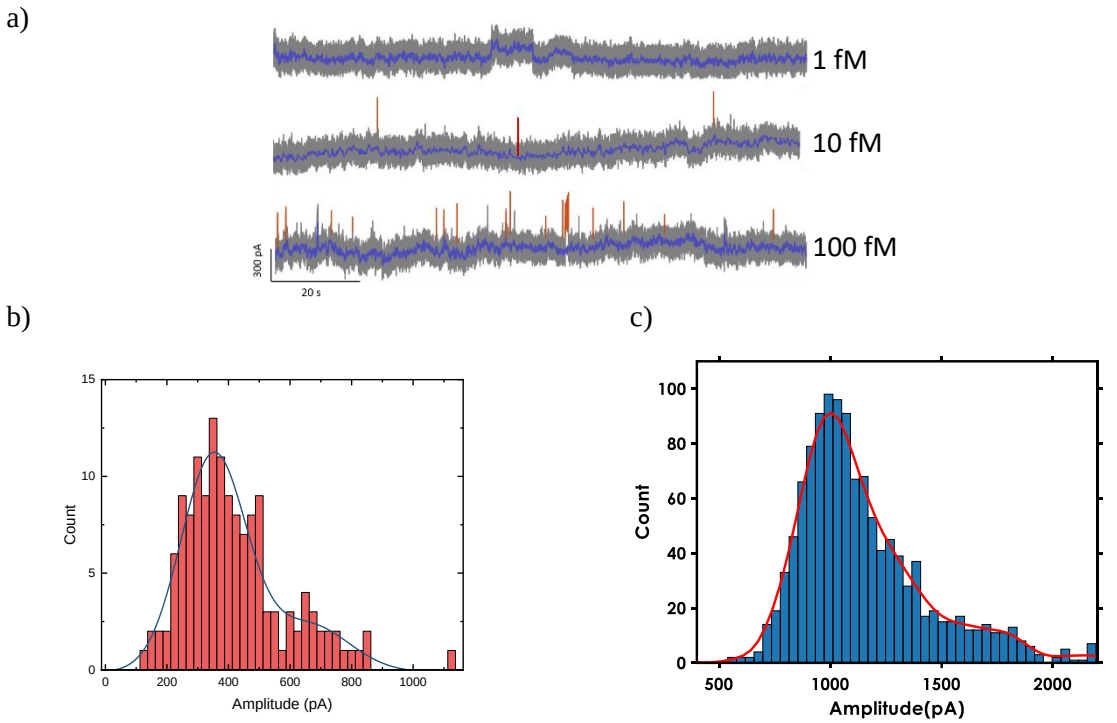

Figure 2.6. Measurements of 1, 10, and 100 fM IgG in 0.2 M/2 M KCl using a 36 nm diameter hydrogel-backed nanopore at -70 mV applied voltage. A) Short ionic current traces of each measurement: Identified events are highlighted in red. b and c: Amplitude histograms of the captured IgG events at (b) 100 fM under asymmetric salt gradient 0.2 M /2 M KCl (c) 100 pM under symmetric salt gradient.

2.2.3. Protein Volume Determination

2.2.3.1. Theory

The blockage current measured from a protein with the excluded volume Λ is derived from Maxwell's calculations on the resistivity of an insulating particle in the presence of an electromagnetic field.[34,35] In the presence of an insulating particle inside an electrolyte-filled nanopore, the uniform electric field inside a cylindrical nanopore distorts slightly around the particle and changes the nanopore resistivity. The change in the resistivity of a nanopore depends both on the volume and orientation of the particle. For particles with volume much smaller than the volume of the cylindrical pore, Maxwell's expression simplifies to:

$$\frac{\Delta R}{R} = \gamma \frac{\Delta v}{V} \qquad 2.2$$

where R is the pore resistance, ΔR is the change in pore resistance due to the presence of the particle, γ is the particle's electric shape factor (a function of the particle shape and orientation relative to the pore axis), Δv is the particle volume, and V is the pore volume.

For a sphere, γ is 3/2, and for ellipsoidal particles the extremes of γ are related to demagnetization factors:[35]

$$\gamma_{\parallel} = \frac{1}{1 - n_{\parallel}}$$

$$\gamma_{\perp} = \frac{1}{1 - n_{\perp}} \qquad 2.3$$

$$n_{\parallel} + 2n_{\perp} = 1$$

where $\gamma_{\parallel}$ and $n_{\parallel}$ are the electric shape and demagnetization factors when the electric field is oriented in the same direction of the axis of revolution of the spheroid, and $\gamma_{\perp}$ and $n_{\perp}$ are the electric shape and demagnetization factors for the perpendicular orientation.

Parallel and perpendicular demagnetization factors are determined by the geometry of the spheroid and are proportional to m, the ratio of diameter "a" to thickness "b" of a spheroid (m = a / b). In the case of oblate (m < 1) and prolate (m > 1) spheroids, demagnetization factors are calculated from Equation 2.4 and 2.5:[36]

For oblate with m < 1:

$$n_{\parallel} = \frac{1}{1 - m^2}\left[1 - \frac{m}{\sqrt{1 - m^2}} cos^{-1} m\right] \qquad 2.4$$

For prolate with m > 1:

$$n_{\perp} = \frac{1}{m^2 - 1}\left[\frac{m}{\sqrt{m^2 - 1}} cosh^{-1} m - 1\right] \quad 2.5$$

However, Equation 2.2 is only valid in the limit of very small insulating particles in comparison with the diameter of the nanopore. In that case, the distortion of the electric field restricts just to the surrounding of the particle. For a bigger particle, the electric field deformation around the particle expands toward the nanopore wall and this effect increases the measured blockage current beyond the linear dependence on the particle volume. Extensive theoretical and experimental studies have been conducted to determine the measured blockage amplitude with respect to the ratio of a particle to a nanopore diameters,[37–39] and different correction coefficients were introduced into Equation 2.2 to account for the extra increase in nanopore resistance due to the presence of large particles. DeBlois and Bean[38] derived and tabulated values of the correction factor for large spherical particles with $\left(\frac{d_{particle}}{d_{pore}}\right)^3 > 0.1$, presented in Table 2.2:

Table 2.2. Correction factors derived by DeBlois and Bean.

$\left(\frac{d_{particle}}{d_{pore}}\right)^3$	S	$\left(\frac{d_{particle}}{d_{pore}}\right)^3$	S
0	1.0	0.5	2.31
0.1	1.14	0.6	2.99
0.2	1.32	0.7	4.15
0.3	1.55	0.8	6.50
0.4	1.87	0.9	13.7

Introducing this correction factor into Equation 2.2 to correct Maxwell's first order approximation, and further substitution of open nanopore current ($I = \frac{V_{applied\ voltage}}{R_{\ nanopore} + R_{access\ resistance}}$) with nanopore resistance R, and the blockage current ΔI with the change in the resistance ΔR yields Equation 2.6:[34]

$$\Delta I = \frac{\Lambda V_A \gamma}{\rho\left(l_p + 0.8 d_{pore}\right)^2} S \left(\frac{d_{particle}}{d_{pore}}\right)^3 \quad 2.6$$

where V_A is the applied voltage, γ is the protein's shape factor, ρ is the resistivity of the measurement buffer, and l_p is the nanopore length.

For a globular protein, we approximate γ = 3/2, and Equation 2.6 becomes:

$$\Delta I_{globular} = \frac{\frac{3}{2}\Lambda V_A}{\rho\left(l_p + 0.8 d_p\right)^2} S \left(\frac{d_{particle}}{d_{pore}}\right)^3 \quad 2.7$$

For ellipsoidal proteins, the blockage current depends on the orientation of the protein within the nanopore. For oblate proteins, the blockage current is minimized when the protein axis is parallel to the nanopore axis and maximized when it is perpendicular. Rewriting Equation 2.6 yields:[34]

$$\Delta I_{ell_{min}} = \frac{\Lambda V_A \gamma_\perp}{\rho\left(l_p + 0.8 d_p\right)^2} S \left(\frac{d_{particle}}{d_{pore}}\right)^3$$

$$\Delta I_{ell_{max}} = \frac{\Lambda V_A \gamma_\parallel}{\rho\left(l_p + 0.8 d_p\right)^2} S \left(\frac{d_{particle}}{d_{pore}}\right)^3 \quad 2.8$$

To calculate the protein volumes, we assume no prior knowledge about the size of the measured proteins, and consequently the ratio of protein to nanopore diameter for selection of an appropriate correction factor. We used the following iteration method to determine protein diameter and volumes. We start by the assumption that the protein diameter is much smaller than the nanopore diameter, and S = 1. Protein volume and hydrodynamic radius are calculated, and the ratio of protein to nanopore diameter is determined. This first approximation of the ratio of protein

to nanopore diameter determines the next value of "S" read from Table 2.2. Then we use this new "S" to find the protein volume, hydrodynamic radius, and a new ratio of protein to nanopore diameter. This is repeated until the calculated ratio is the same as the ratio from the previous step. The protein volume and hydrodynamic radius is determined from this final value of "S". For the proteins described in this work, this algorithm was convergent. Figure 2.7 summarizes this algorithm.

2.2.3.2. Experimental Measurement

The extended dwell time also allows detection of smaller signals and smaller proteins as a result of a decrease in measurement bandwidth required. Although detection of small protein have been previously described,[17] the size of the nanopore constrained to be slightly larger than the of the protein, limiting the range of protein sizes detectable in a single experiment. We used an 18 nm diameter hydrogel-backed nanopore (pore A) to sense Myoglobin (18 kD), Ovalbumin (44 kD), and IgG (160 kD) (Figure 2.8). The excluded volumes of all three proteins were estimated using Equation 2.7 for Ovalbumin (253 nm^3) and Myoglobin (100 nm^3), and Equation 2.8 for ellipsoidal IgG (361 nm^3) as others have done previously;[34,40,41] these are presented in Table 2.3. Correction factors from Equation 2.7 and 2.8 were utilized to account for an additional increase in nanopore resistance when the particle diameter is comparable with to the nanopore diameter.[35,37,38,42,43] The correction factors are non-linear functions of the ratio of protein to nanopore diameter. To estimate the correction factors, we used the iterative described above without any prior knowledge of the measured protein.

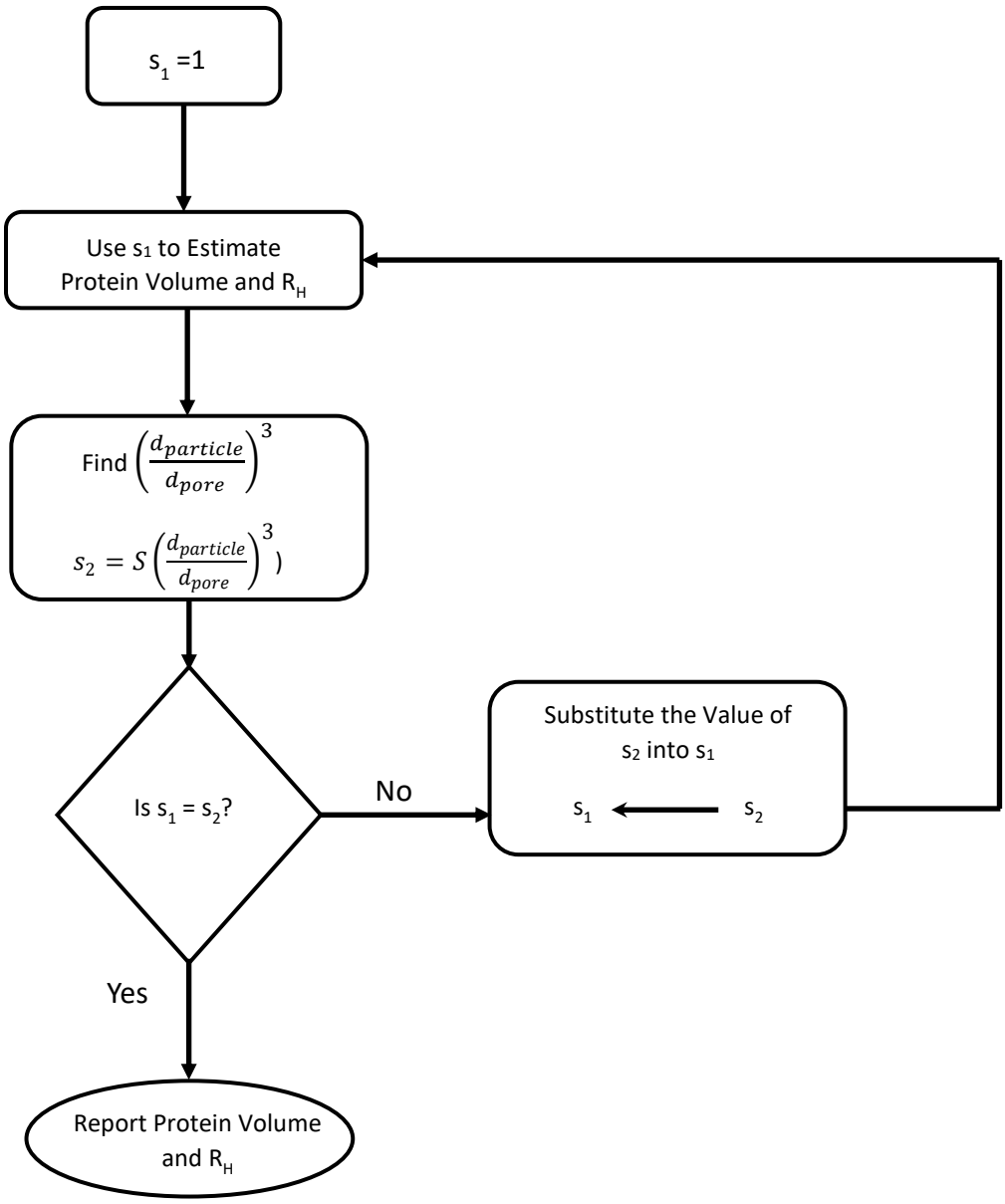

Figure 2.7. The iterative algorithm to find the protein volume and hydrodynamic radius R_H.

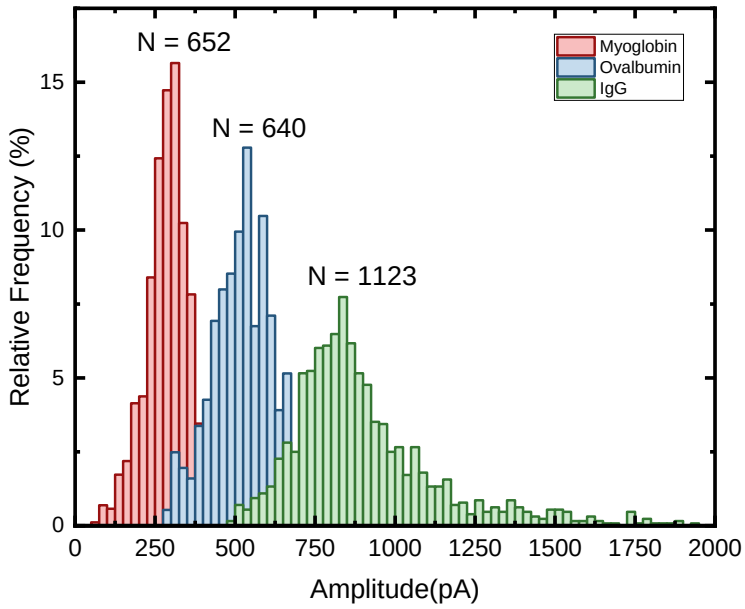

Figure 2.8. Measurement of Myoglobin (18 kD), Ovalbumin (44 kD), and IgG (160 kD) (concentrations 1-5 nM) using the same hydrogel-backed 18 nm diameter nanopore ("Pore A") for 7, 5, and 10 minutes, respectively. Each protein was measured separately with the solutions exchanged between measurements, at -60 mV applied voltage.

For comparison, alongside these numbers we provide literature values of the hydrodynamic radii for these proteins measured using Dynamic Light Scattering (DLS) (at pH 7-8) and the volume estimated from them.

As can be seen from Table 2.3, the volumes obtained from our nanopore measurements at pH 10 are all greater than the literature values obtained at pH 7-8. Factors contributing to this include protein adsorption to the pore wall, which can increase the measured blockade amplitudes due to off-axis effect by up to 18%, as well as an extended hydration shell around the proteins or structural changes at pH 10, due to enhanced negative surface charge of the proteins at higher pH.

Table 2.3. Comparison of protein volumes measured using nanopores and dynamic light scattering for IgG, Ovalbumin, and Myoglobin

	Nanopore	Dynamic Light Scattering	
Protein	Excluded vol. (nm^3)	Hydrodynamic radius (nm)	Calculated vol. (nm^3)
IgG (pore A) IgG (pore B) IgG (pore B)	361 (pH 10) 376 (pH 10) 252 (pH 8)	5.5 (pH 7.4)[44]	258
Oval. (pore A) Oval. (pore C) Oval. (pore C)	235 (pH 10) 224 (pH 10) 197 (pH 8)	3.3 (pH 7.5)[15]	150
Myo. (pore A)	100 (pH 10)	2.4 (pH 7.4)[45,46]	58

To investigate effects of pH on current blockade amplitudes and volumes derived from them, we repeated the IgG measurements at pH 8 and pH 10 using "Pore B" (23 nm diameter), and compared them with Ovalbumin, measured at pH 8 and pH 10 with "Pore C" (12 nm diameter). Amplitude histograms for these experiments are shown in Figure 2.9.

We observed a significant reduction in the measured currents and volumes derived from them for both proteins at pH 8 to pH 10 (Table 2.3). This effect was greater for IgG which matches its larger increase in surface charge (-4e at pH 8 to -103e at pH 10) compared to Ovalbumin (-14e at pH 8 to -34e at pH 10). Table 2.3 also contains volume estimated for Myoglobin at pH 10, which is also larger than the value obtained from DLS at pH 7.4. Myoglobin surface charge changes from -1e at pH 8 to -13e at pH 10. The significant increase in Myoglobin surface charge results in structural change and larger hydrodynamic radius,[47] with complete unfolding at pH 11.[48] An enhanced hydration shell and partial denaturing of Myoglobin may explain the larger volume at pH 10 compared to DLS measurement made at pH 7.4.

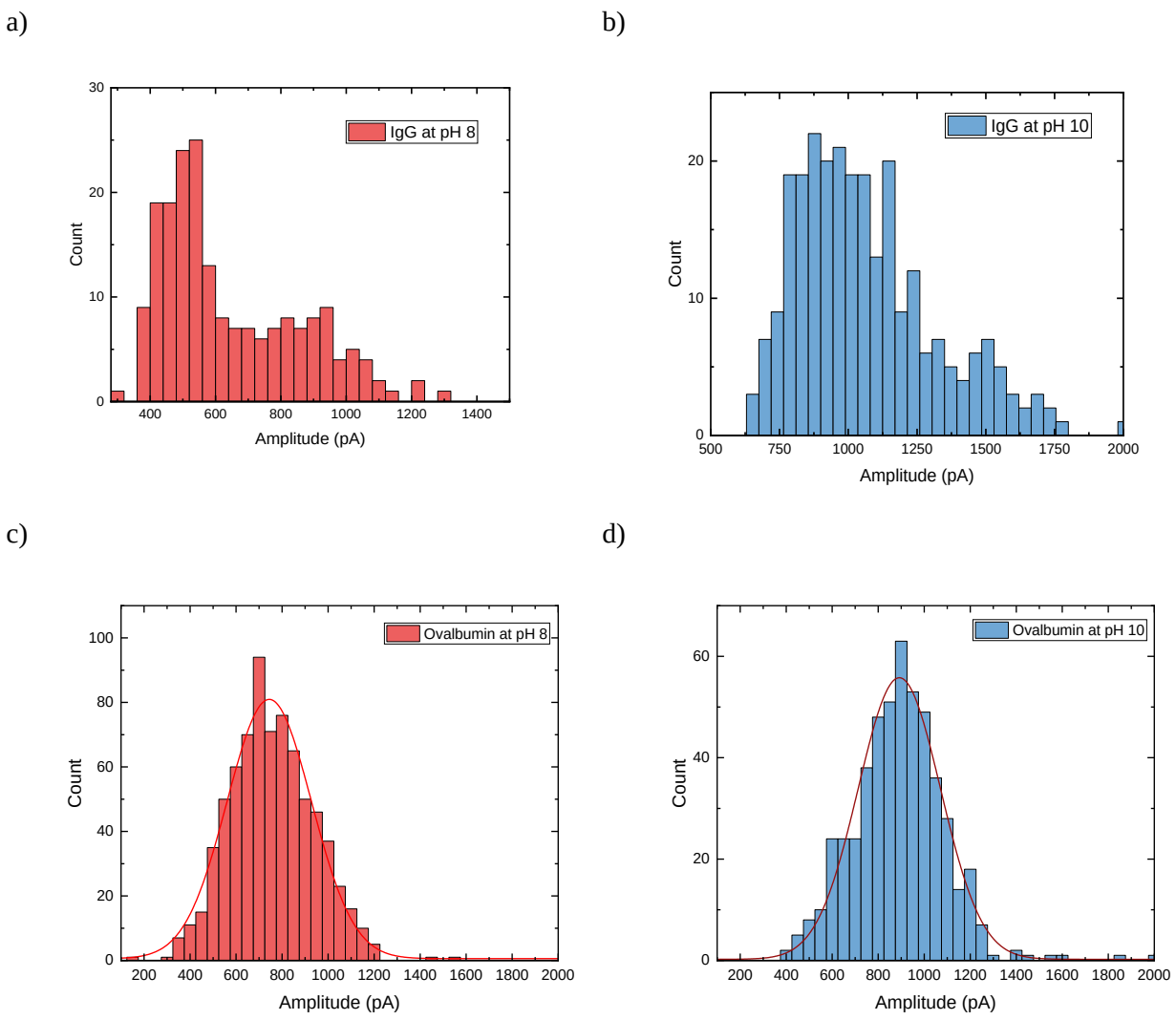

Figure 2.9. IgG measured at -70 mV applied voltage using a hydrogel-backed 21 nm diameter nanopore in 2M KCl buffered to (a) pH = 8 and (b) pH = 10 ; Ovalbumin measured at -70 mV applied voltage using a hydrogel-backed 12 nm diameter nanopore in 2 M KCl buffered to (c) pH =8 and (d) pH = 10;

2.2.4. Detection of Small Proteins

We also explored the effective lower limits in protein size detectable by hydrogel-backed nanopores. As the neutral PEG-DMA hydrogel has an antifouling property and sterically interacts with translocation proteins, the size of protein relative with respect to the mesh size of the hydrogel is an important factor to determine the efficiency of the hydrogel in facilitating protein detection. We measured 400 pM poly-L-glutamic acid sodium salt ($\leq$ 5.5 kD), which has a hydrodynamic

radius of 1.35 nm, smaller than 3.1 nm average mesh size of the PEG-DMA hydrogel. In the absence of hydrogel, no events were detected over 45 minutes at -100 mV applied voltage. With hydrogel present on the *trans* side of the nanopore, events appeared at frequency of around 0.05 Hz within 10 minutes following addition of the protein, much less than 1.83 Hz theoretically expected. Although the hydrogel did enable detection of protein below the hydrogel mesh size, the observed frequency was much lower than the expected frequency. We compared the ratio of observed versus theoretically expected event rates for 5.5 kD poly-L-glutamic acid sodium salt (R_H = 1.3 nm), IgG (R_H = 5.6 nm)[49], Ovalbumin (R_H = 3.3 nm)[50], and Myoglobin (R_H = 2.4 nm)[46] (Figure 2.10), finding that the ratio of observed to predicted capture rates for IgG, Ovalbumin, and Myoglobin are all approximately the same, but drops by over an order of magnitude for poly-L-glutamic acid sodium salt.

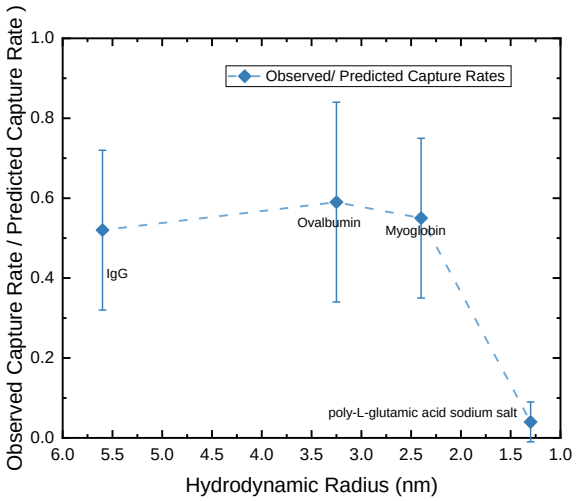

Figure 2.10. The ratio of observed to estimated capture rates for IgG (R_H =5.6 nm), ovalbumin (R_H =3.3 nm), and myoglobin (R_H =2.4 nm) at -50 mV applied voltage using hydrogel-backed 17-23 nm diameter nanopores. The ratio of observed to estimated capture rate for poly-L-glutamic sodium salt (R_H = 1.3 nm) was measured at -90 and -100 mV applied voltage using a hydrogel-backed 10 nm diameter nanopore.

2.3. Conclusion

We have found that hydrogel-backed nanopores can detect a wide range of sizes and concentrations of unlabeled proteins, down to 5.5 kD or smaller, and 10 fM or lower, respectively. Detection of smaller proteins could be enhanced through the use of a hydrogel with smaller mesh size, and detection of lower protein concentration enhanced with longer measurement times. Unknown protein concentrations may be determined following nanopore calibration. We found that a gap between the nanopore chip and the hydrogel may affect the system's sensitivity, with smaller gaps resulting in larger sensitivity. We also found evidence that some proteins escape the pore by diffusing against the electric field to the *cis* chamber. We showed that a single hydrogel-backed nanopore can detect and distinguish unlabeled 18 kD, 44 kD, and 160 kD proteins, indicating the promising potential of this system in quantitative study of unknown protein mixtures. We used an iterative algorithm to determine the volume of an unknown protein more precisely from blockage current measurements. Measured protein volumes showed pH-dependent effects indicating larger hydration shells at higher pH, with this effect increasing with increasing protein charge.

2.4. Materials and Methods

Materials: All chemicals were purchased from Sigma-Aldrich at reagent grade and used as received. Immunoglobulin gamma (IgG), ovalbumin, and poly-L-glutamic acid sodium were purchased from Sigma-Aldrich. Purified myoglobin was generously provided by the Steven Jacobsen lab at UCLA. IgG, ovalbumin, and myoglobin were chosen as the common protein standards for biological studies.

Nanopore fabrication and hydrogel polymerization: 15 nm thick silicon nitride membranes were commercially purchased from Ted Pella Inc.; membranes were PDMS coated and cured for several hours at 120°C before use. Silicon nitride membranes were plasma treated for 30 sec, mounted in a Teflon fluidic cell, and degassed. Nanopores were formed using dielectric breakdown in 2 M KCl, pH 10 at the desired size as previously reported[1]. PEG-DMA hydrogel solution was prepared by mixing 10% (w/v) PEG-1000 Dimethylacrylamide in 2 M KCl, 100 mM Tris-HCl at pH 10 (adjusted by HCl and NaOH), 10% (w/v) ammonium persulfide (APS), and 20% (w/v) tetramethylethylenediamine (TEMED). Nanopore diameters were determined immediately after formation as described previously.[2] After formation of a nanopore, electrolyte in the compartment on the TEM window side was replaced with PEG-DMA hydrogel solution, and polymerized in-situ for 10 minutes before nanopore measurement.

Nanopore measurements: All nanopore measurements were carried out using an Axopatch 200B amplifier and Digidata 1440B or 1322A data acquisition at 100 kHz with a 10 kHz hardware low pass filter. Nanopore measurements were performed in 2 M KCl, 100 mM Tris-HCl, pH 8-10. At least 5 minutes of control measurements were run before protein injection. In all experiments, the hydrogel side (*trans*) of the nanopore chip was grounded, and protein was injected into the other side (*cis*) to make a final concentration of 1 fM – 2 µM; the *cis* solution was briefly stirred before measurements began with -50 to -100 mV applied (V_{cis}-V_{trans}).

Data analysis: All captured data were analyzed using a MATLAB script as previously reported[1].

2.5. References:

(1) Mikheyev, A. S.; Tin, M. M. Y. A First Look at the Oxford Nanopore MinION Sequencer. *Mol. Ecol. Resour.* **2014**, *14* (6), 1097–1102. https://doi.org/10.1111/1755-0998.12324.

(2) Kasianowicz, J. J.; Balijepalli, A. K.; Ettedgui, J.; Forstater, J. H.; Wang, H.; Zhang, H.; Robertson, J. W. F. Analytical Applications for Pore-Forming Proteins. *Biochim. Biophys. Acta* **2016**, *1858*, 593–606. https://doi.org/10.1016/j.bbamem.2015.09.023.

(3) Howorka, S.; Siwy, Z. Nanopore Analytics: Sensing of Single Molecules. *Chem. Soc. Rev.* **2009**, *38* (8), 2360–2384. https://doi.org/10.1039/b813796j.

(4) Ananth, A.; Genua, M.; Aissaoui, N.; Díaz, L.; Eisele, N. B.; Frey, S.; Dekker, C.; Richter, R. P.; Görlich, D. Reversible Immobilization of Proteins in Sensors and Solid-State Nanopores. *Small* **2018**, *14* (18), 1–11. https://doi.org/10.1002/smll.201703357.

(5) Han, A.; Schürmann, G.; Mondin, G.; Bitterli, R. A.; Hegelbach, N. G.; De Rooij, N. F.; Staufer, U. Sensing Protein Molecules Using Nanofabricated Pores. *Appl. Phys. Lett.* **2006**, *88* (9), 28–31. https://doi.org/10.1063/1.2180868.

(6) Yusko, E. C.; Prangkio, P.; Sept, D.; Rollings, R. C.; Li, J.; Mayer, M. Single-Particle Characterization of Aβ Oligomers in Solution. *ACS Nano* **2012**, *6* (7), 5909–5919. https://doi.org/10.1021/nn300542q.

(7) Freedman, K. J.; Jürgens, M.; Prabhu, A.; Ahn, C. W.; Jemth, P.; Edel, J. B.; Kim, M. J. Chemical, Thermal, and Electric Field Induced Unfolding of Single Protein Molecules Studied Using Nanopores. *Anal. Chem.* **2011**, *83* (13), 5137–5144. https://doi.org/10.1021/ac2001725.

(8) Soni, G. V.; Dekker, C. Detection of Nucleosomal Substructures Using Solid-State Nanopores. *Nano Lett.* **2012**, *12* (6), 3180–3186. https://doi.org/10.1021/nl301163m.

(9) Hu, R.; Rodrigues, J. V.; Waduge, P.; Yamazaki, H.; Cressiot, B.; Chishti, Y.; Makowski, L.; Yu, D.; Shakhnovich, E.; Zhao, Q.; Wanunu, M. Differential Enzyme Flexibility Probed Using Solid-State Nanopores. *ACS Nano* **2018**, *12* (5), 4494–4502. https://doi.org/10.1021/acsnano.8b00734.

(10) Oukhaled, A.; Cressiot, B.; Bacri, L.; Pastoriza-Gallego, M.; Betton, J. M.; Bourhis, E.; Jede, R.; Gierak, J.; Auvray, L.; Pelta, J. Dynamics of Completely Unfolded and Native Proteins through Solid-State Nanopores as a Function of Electric Driving Force. *ACS Nano* **2011**, *5* (5), 3628–3638. https://doi.org/10.1021/nn1034795.

(11) Ivankin, A.; Carson, S.; Kinney, S. R. M.; Wanunu, M. Fast, Label-Free Force

Spectroscopy of Histone-DNA Interactions in Individual Nucleosomes Using Nanopores. *J. Am. Chem. Soc.* **2013**, *135* (41), 15350–15352. https://doi.org/10.1021/ja408354s.

(12) Rivas, F.; Zahid, O. K.; Reesink, H. L.; Peal, B. T.; Nixon, A. J.; DeAngelis, P. L.; Skardal, A.; Rahbar, E.; Hall, A. R. Label-Free Analysis of Physiological Hyaluronan Size Distribution with a Solid-State Nanopore Sensor. *Nat. Commun.* **2018**, *9* (1), 1–9. https://doi.org/10.1038/s41467-018-03439-x.

(13) Wloka, C.; Van Meervelt, V.; Van Gelder, D.; Danda, N.; Jager, N.; Williams, C. P.; Maglia, G. Label-Free and Real-Time Detection of Protein Ubiquitination with a Biological Nanopore. *ACS Nano* **2017**, *11* (5), 4387–4394. https://doi.org/10.1021/acsnano.6b07760.

(14) Martyushenko, N.; Bell, N. A. W.; Lamboll, R. D.; Keyser, U. F. Nanopore Analysis of Amyloid Fibrils Formed by Lysozyme Aggregation. *Analyst* **2015**, *140* (14), 4882–4886. https://doi.org/10.1039/c5an00530b.

(15) Plesa, C.; Kowalczyk, S. W.; Zinsmeester, R.; Grosberg, A. Y.; Rabin, Y.; Dekker, C. Fast Translocation of Proteins through Solid State Nanopores-Supporting Information. *Nano Lett.* **2013**, *13* (2), 658–663. https://doi.org/10.1021/nl3042678.

(16) Uram, J. D.; Ke, K.; Mayer, M. Noise and Bandwidth of Current Recordings from Submicrometer Pores and Nanopores. *ACS Nano* **2008**, *2* (5), 857–872. https://doi.org/10.1021/nn700322m.

(17) Larkin, J.; Henley, R. Y.; Muthukumar, M.; Rosenstein, J. K.; Wanunu, M. High-Bandwidth Protein Analysis Using Solid-State Nanopores. *Biophys. J.* **2014**, *106* (3), 696–704. https://doi.org/10.1016/j.bpj.2013.12.025.

(18) Li, W.; Bell, N. A. W.; Hernández-Ainsa, S.; Thacker, V. V.; Thackray, A. M.; Bujdoso, R.; Keyser, U. F. Single Protein Molecule Detection by Glass Nanopores. *ACS Nano* **2013**, *7* (5), 4129–4134. https://doi.org/10.1021/nn4004567.

(19) Steinbock, L. J.; Krishnan, S.; Bulushev, R. D.; Borgeaud, S.; Blokesch, M.; Feletti, L.; Radenovic, A. Probing the Size of Proteins with Glass Nanopores. *Nanoscale* **2014**, *6* (23), 14380–14387. https://doi.org/10.1039/c4nr05001k.

(20) Nir, I.; Huttner, D.; Meller, A. Direct Sensing and Discrimination among Ubiquitin and Ubiquitin Chains Using Solid-State Nanopores. *Biophys. J.* **2015**, *108* (9), 2340–2349. https://doi.org/10.1016/j.bpj.2015.03.025.

(21) Chuah, K.; Wu, Y.; Vivekchand, S. R. C.; Gaus, K.; Reece, P. J.; Micolich, A. P.; Gooding, J. J. Nanopore Blockade Sensors for Ultrasensitive Detection of Proteins in

Complex Biological Samples. *Nat. Commun.* **2019**, *10* (1), 1–9. https://doi.org/10.1038/s41467-019-10147-7.

(22) Yusko, E. C.; Johnson, J. M.; Majd, S.; Prangkio, P.; Rollings, R. C.; Li, J.; Yang, J.; Mayer, M. Controlling Protein Translocation through Nanopores with Bio-Inspired Fluid Walls. *Nat. Nanotechnol.* **2011**, *6* (253–260). https://doi.org/10.1038/nnano.2011.12.

(23) Kong, J.; Bell, N. A. W.; Keyser, U. F. Quantifying Nanomolar Protein Concentrations Using Designed DNA Carriers and Solid-State Nanopores. *Nano Lett.* **2016**, *16* (6), 3557–3562. https://doi.org/10.1021/acs.nanolett.6b00627.

(24) Acharya, S.; Jiang, A.; Kuo, C.; Nazarian, R.; Li, K.; Ma, A.; Siegal, B.; Toh, C.; Schmidt, J. J. Improved Measurement of Proteins Using a Solid-State Nanopore Coupled with a Hydrogel. *ACS Sensors* **2020**, *5*, 370–376. https://doi.org/10.1021/acssensors.9b01928.

(25) Charron, M.; Briggs, K.; King, S.; Waugh, M.; Tabard-cossa, V. Precise DNA Concentration Measurements with Nanopores by Controlled Counting. *Anal. Chem.* **2019**, *91*, 12228–12237. https://doi.org/10.1021/acs.analchem.9b01900.

(26) Freedman, K. J.; Edel, J. B.; Haq, S. R.; Jemth, P.; Fletcher, M. R.; Foley, J. P.; Kim, M. J. Nonequilibrium Capture Rates Induce Protein Accumulation and Enhanced Adsorption to Solid-State Nanopores. *ACS Nano* **2014**, *8* (12), 12238–12249. https://doi.org/10.1021/nn5062645.

(27) Grosberg, A. Y.; Rabin, Y. DNA Capture into a Nanopore: Interplay of Diffusion and Electrohydrodynamics. *J. Chem. Phys.* **2010**, *133* (16). https://doi.org/10.1063/1.3495481.

(28) Muthukumar, M. Theory of Capture Rate in Polymer Translocation. *J. Chem. Phys.* **2010**, *132* (19), 195101–195110. https://doi.org/10.1063/1.3429882.

(29) Muthukumar, M. Communication: Charge, Diffusion, and Mobility of Proteins through Nanopores. *J. Chem. Phys.* **2014**, *141* (8). https://doi.org/10.1063/1.4894401.

(30) Wanunu, M.; Morrison, W.; Rabin, Y.; Grosberg, A. Y.; Meller, A. Electrostatic Focusing of Unlabelled DNA into Nanoscale Pores Using a Salt Gradient. *Nat. Nanotechnol.* **2010**, *5* (2), 160–165. https://doi.org/10.1038/nnano.2009.379.

(31) Howard, J. Mechanics of Motor Proteins and the Cytoskeleton; Sinauer Associates: Sunderland, MA, 2001; p 62.

(32) Wanunu, M.; Morrison, W.; Rabin, Y.; Grosberg, A. Y.; Meller, A. Electrostatic Focusing

of Unlabelled DNA into Nanoscale Pores Using a Salt Gradient. *Nat. Nanotechnol.* **2010**, *5* (2), 160–165. https://doi.org/10.1038/nnano.2009.379.

(33) Chou, T. Enhancement of Charged Macromolecule Capture by Nanopores in a Salt Gradient. *J. Chem. Phys.* **2009**, *131* (3). https://doi.org/10.1063/1.3170952.

(34) Yusko, E. C.; Bruhn, B. R.; Eggenberger, O. M.; Houghtaling, J.; Rollings, R. C.; Walsh, N. C.; Nandivada, S.; Pindrus, M.; Hall, A. R.; Sept, D.; Li, J.; Kalonia, D. S.; Mayer, M. Real-Time Shape Approximation and Fingerprinting of Single Proteins Using a Nanopore. *Nat. Nanotechnol.* **2017**, *12* (4), 360–367. https://doi.org/10.1038/nnano.2016.267.

(35) Golibersuch, D. C. Observation of Aspherical Particle Rotation in Poiseuille Flow via the Resistance Pulse Technique: I. Application to Human Erythrocytes. *Biophys. J.* **1973**, *13* (3), 265–280. https://doi.org/10.1016/S0006-3495(73)85984-3.

(36) Stoner, E. C. The Demagnetizing Factors for Ellipsoids. *London, Edinburgh, Dublin Philos. Mag. J. Sci.* **1945**, *36* (263), 803–821. https://doi.org/10.1080/14786444508521510.

(37) DeBlois, R. W.; Bean, C. P.; Wesley, R. K. A. Electrokinetic Measurements with Submicron Particles and Pores by the Resistive Pulse Technique. *J. Colloid Interface Sci.* **1977**, *61* (2), 323–335. https://doi.org/10.1016/0021-9797(77)90395-2.

(38) DeBlois, R. W.; Bean, C. P. Counting and Sizing of Submicron Particles by the Resistive Pulse Technique. *Rev. Sci. Instrum.* **1970**, *41* (7), 909–916. https://doi.org/10.1063/1.1684724.

(39) Gregg, E. C.; Steidley, K. D. Electrical Counting and Sizing of Mammalian Cells in Suspension. *Biophys. J.* **1965**, *5* (4), 393–405. https://doi.org/10.1016/S0006-3495(65)86724-8.

(40) Han, A.; Schürmann, G.; Linder, V.; De Rooij, N. F.; Staufer, U.; Creus, M.; Ward, T. R. Label-Free Detection of Single Protein Molecules and Protein-Protein Interactions Using Synthetic Nanopores. *Anal. Chem.* **2008**, *80* (12), 4651–4658. https://doi.org/10.1021/ac7025207.

(41) Fologea, D.; Ledden, B.; McNabb, D. S.; Li, J. Electrical Characterization of Protein Molecules by a Solid-State Nanopore. *Appl. Phys. Lett.* **2007**, *91* (5), 1–4. https://doi.org/10.1063/1.2767206.

(42) Smythe, W. R. Flow around a Sphere in a Circular Tube. *Phys. Fluids* **1961**, *4* (6), 756–759. https://doi.org/10.1063/1.1706394.

(43) Smythe, W. R. Flow around a Spheroid in a Circular Tube. *Phys. Fluids* **1964**, *7* (5), 633–638. https://doi.org/10.1063/1.1711260.

(44) Karow, A. R.; Götzl, J.; Garidel, P. Resolving Power of Dynamic Light Scattering for Protein and Polystyrene Nanoparticles. *Pharm. Dev. Technol.* **2015**, *20* (1), 84–89. https://doi.org/10.3109/10837450.2014.910808.

(45) Malvern Application Note-Measurement and Molecular Weight Estimation of Globins. *Malvern Instruments Worldw.* **2009**, 1–4.

(46) Lorber, B. Analytical Light Scattering Methods in Molecular and Structural Biology: Experimental Aspects and Results. **2018**, *ffhal-0166*, 1–41.

(47) Ahmed, U.; Saunders, G. Effect of PH on Protein Size Exclusion Chromatography. *Www.Agilent.Com/Chem* **2012**, 4–5.

(48) Sogbein, O. O.; Simmons, D. A.; Konermann, L. Effects of PH on the Kinetic Reaction Mechanism of Myoglobin Unfolding Studied by Time-Resolved Electrospray Ionization Mass Spectrometry. *J. Am. Soc. Mass Spectrom.* **2000**, *11* (4), 312–319. https://doi.org/10.1016/S1044-0305(99)00149-X.

(49) Zhao, H.; Graf, O.; Milovic, N.; Luan, X.; Bluemel, M.; Smolny, M.; Forrer, K. Formulation Development of Antibodies Using Robotic System and High-Throughput Laboratory (HTL). *J. Pharm. Sci.* **2010**, *99* (5), 2279–2294. https://doi.org/10.1002/jps.22008.

(50) Plesa, C.; Kowalczyk, S. W.; Zinsmeester, R.; Grosberg, A. Y.; Rabin, Y.; Dekker, C. Fast Translocation of Proteins through Solid State Nanopores. *Nano Lett.* **2013**, *13* (2), 658–663. https://doi.org/10.1021/nl3042678.

Chapter 3: Hydrogel-Backed Nanopore as an Ultra-Sensitive Protein Detector for Liquid Chromatography

3.1. Introduction

Studying a complex mixture of native proteins is essential to biology. A simple, reproducible, and powerful approach to studying such mixtures begins with separating various groups of proteins from one another by passing a mixture through a liquid chromatographic column. When passing through a column, proteins can be separated into more simplified groups based on their size and shape, charge, the hydrophobic groups presented on their surfaces, or their binding capacity with a target phase.[1–9]

Introduced by Pharmacia (Sweden) in 1982, protein liquid chromatography (FPLC) became a conventional technique to purify or separate fractions of native proteins in a mixture by passing the sample through a chromatographic column.[2] Chromatographic protein separation is followed by the detection and characterization of each fraction of proteins. Among the typical FPLC instruments, UV-Visible detectors (UV-Vis detectors) are the most common detectors used to analyze the fractions of proteins that emerge from a column.[10] Proteins with the aromatic amino acids, tyrosine and tryptophan, in their primary structures can be detected at 280 nm wavelength.[11] Also, amide peptide bonds have strong absorbance at 214 or 220 nm wavelength, enabling protein detection at a lower wavelength. UV-Vis detectors are convenient to use; they are robust, reliable, reproducible, and non-destructive in identifying protein fractions.

However, a typical UV-Vis detector does not have adequate sensitivity and selectivity in detecting and identifying fractions of proteins for advanced proteomic studies. These detectors cannot resolve low concentrations of proteins or differentiate the target proteins in a sample. To improve the sensitivity and selectivity for studying the chromatographic fractions, fluorescence and electrochemical detectors are some alternatives; however, they are destructive to protein samples, requiring additional sample preparation steps and prior knowledge of the target

proteins.[12,13] In addition, the acquisition of additional information of the physical properties of fractionated proteins is only possible by coupling a UV-Vis detector with more advanced instrumentations. For example, a UV-Vis detector can be coupled with the multi-light scattering (ALS) system[9,14] or mass spectrometer[15,16] to obtain information on the shapes and the molecular weight to charge ratios of detected purified fractions of proteins. However, integrating additional techniques with a UV-Vis detector is expensive, not commonly accessible, and technically challenging. Also, UV-Vis, fluorescence, and electrochemical detectors, as well as mass spectrometers and multi-light scattering systems, are examples of bulk property protein characterization tools; they measure the mean response of protein molecules, and their applications are restricted due to their lack of sensitivity to study low abundance proteins, their lack of selectivity in identifying co-existing proteins or impurities in one fraction, and their limited capability in the comprehensive characterization of protein fractions.

A single-molecule analysis of fractions can used as a complementary approach to precisely detect, accurately identify, and comprehensively analyze the fractionated proteins being eluted off from a chromatographic column. Among single-molecule measurement techniques, electrical nanopore detection has attracted much attention for the real-time identification of native proteins in a solution and the characterization of their physical properties.[17–32]

This work demonstrates that a nanopore backed with the PEG-DMA hydrogel can be an effective, reliable, ultra-sensitive, non-destructive, and easy-to-operate alternative detection platform to analyze chromatographic protein fractions, capable of being integrated with a chromatographic column. Using hydrogel-backed nanopores, we resolved and characterized FPLC fractionated proteins and compared our findings with the readouts of a standard UV-Vis detector. Our findings exhibited that the hydrogel-backed nanopores have a higher sensitivity and

selectivity in protein detection than traditional UV-Vis detectors. The hydrogel-backed nanopores identified proteins at very low concentrations, 100 to 1000 times below the minimum concentration detectable by a UV-Vis detector, accurately characterized FPLC fractions, and selectively discriminated co-existing species in the same fraction. In addition, the proposed application motivated us to integrate the solid-state nanopores with PDMS microchannels to make a fluidic circuit to ease the sample exchange, facilitate fluid manipulation, reduce the dead volumes around a nanopore, and make real-time measurements of the column effluents.

3.2. Results and Discussion

3.2.1. The Hydrogel-Backed Nanopore as an Ultra-Sensitive platform for Characterization of Chromatographic Fractionated Proteins

3.2.1.1. Detection of the Chromatographic Fractions by a Hydrogel-Backed Nanopore

A mixture of proteins that run through a chromatographic column can be separated into simpler fractions. Each fraction can be specified as the fraction of protein, impurity, or pure buffer. We evaluated whether a hydrogel-backed solid-state nanopore can resolve chromatographic fractions of proteins, differentiating between multiple fractions of distinct proteins, and also the buffer fraction. We ran a mixture model of T7 RNA polymerase and polypyrimidine tract binding protein (PTBP1) solution through an affinity column, collected fractions of effluents, measured them with hydrogel-backed nanopores, and compared our results with the UV-Vis readout.

PTBP1 is a 60 kD globular RNA-binding protein[36], with two main domains connected via a flexible linker.[37] T7 RNAP is a 100 kD bacteriophage RNA polymerase and cannot interact with PTBP1. Table 3.1 summarizes the properties of these two proteins. The mixture model was prepared by adding the same volume of purified T7 RNA polymerase and PTBP1 with

concentrations of 100 and 50 µl / ml, respectively. Then the solution was run through an affinity column to separate individual protein fractions. A FPLC-UV chromatogram of fractions can be seen in Figure 1a. The solid blue line exhibits UV-absorbance at 280 nm. The first peak included the first six fractions containing T7 RNA polymerase, and the second peak, after elution, included four fractions of PTBP1.

Table 3.1. Physical properties of T7 RNAP and PTBP1

Protein	Molecular Weight (kD)	Dimension (nm x nm x nm)	Hydrodynamic Diameter (nm)	PI	Charge at pH 9
T7 RNAP	100	7.5 x 7.5 x 6.5[34]	8.1 (pH=8) [35]	7	-17 e
PTBP1	60	7.4 x 6.0 x 6.1[38]	7.4 (pH =7.4) [39]	8.67	-3 e

Following the chromatographic separation, nanopore experiments were conducted using a hydrogel-backed 22 nm diameter nanopore in 2 M KCl pH 9 buffer at an applied voltage of -60 mV. Three fractions of 3B4, 3C5, and 3C10 containing T7 RNA polymerase, elution buffer, and PTBP1, respectively, were diluted 100 times and were separately measured with the exchange of buffer solution between experiments. Following the addition of diluted samples of 3B4 and 3C10, events appeared within 20 minutes, and no events were observed after adding a diluted solution of fraction 3C5 for more than one hour. As expected, our hydrogel-backed nanopore was able to discriminate protein fractions from the buffer fraction. Figure 1b shows short current traces of elution buffer, T7 RNA polymerase, and PTBP1 nanopore measurements. Gaussian histograms of event amplitudes are shown in Figure 1c for both proteins, confirming the globular shape of both proteins.

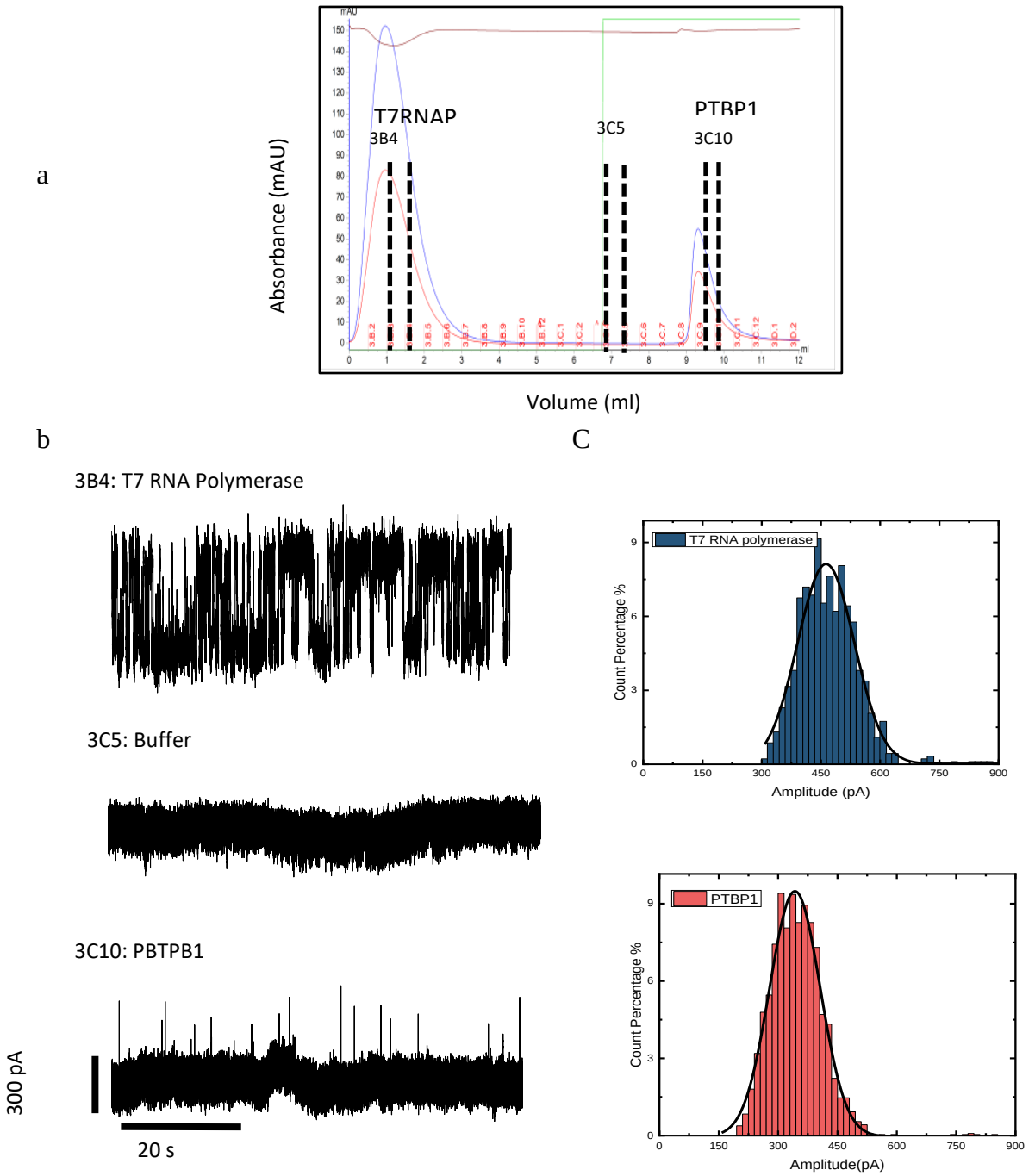

Figure 3.1. Affinity chromatography to separate T7RNA polymerase and PTBP1 in a binary mixture solution a) The UV-Vis detector readout. b) Examples of measured ionic current traces of 3B4, 3C5, and 3C10 fractions using a hydrogel-backed 22 nm diameter nanopore in 2 M KCl, pH 9 buffer at -60 mV applied voltage. c) Amplitude histograms of resolved events for T7 RNA polymerase and PBTP1.

Fitting PTBP1 and T7 RNA polymerase histograms to the Gaussian distributions yield a most probable amplitude of 462.85±2.62 for T7 RNA polymerase and 345.41±1.36 for PTBP1. With the best-fit values of the most probable amplitudes, the excluded volumes of T7 RNAP and PTBP1 were estimated to be 228 nm^3 and 306 nm^3 using the previously described method.[33] The ratio of estimated volumes is 1.34, in full agreement with the ratio of the reported crystallographic dimensions of the two proteins (= 1.34). These results indicate that hydrogel-backed nanopores can resolve protein fractions as the UV-Vis detector does and also provides more structural information about the separated proteins.

Further, we measured all fractions of T7 RNA polymerase and PTBP1 using two different hydrogel-backed nanopores, and we noticed a lag between UV-Vis chromatogram and the amount of proteins in the collected fractions. Our nanopore measurement indicated the peak maxima at 3B4 for T7 RNA polymerase (in contrast with 3B3 in the chromatogram), and at 3C10 for PTBP1 (in contrast with 3C9 in the chromatogram). Data have not been shown.

3.2.1.2. Higher Sensitivity of a Hydrogel-Backed Nanopore to Detect Proteins at Extremely Low Concentrations

Previously, we have shown that we were able to measure diluted concentrations of proteins as low as 10 fM by using a hydrogel-backed nanopore. Knowing this fact, we compared the detectable concentration limits achievable by a hydrogel-backed nanopore and a UV-Vis detector. In the first experiment, a high-concentrated mixture of Myoglobin, Ovalbumin, IgG, and Thyroglobulin was passed through a size exclusion column, and fractions were collected with a fixed volume of 1 ml. Figure 3.2a is the FPLC-UV chromatogram (Figure 3.2a) which illustrates four individual peaks corresponding to the fractionated proteins. The peak before the Thyroglobulin peak contains all of the denatured and aggregated proteins larger in size than

Thyroglobulin. Using a hydrogel-backed 30 nm diameter nanopore, we could not detect considerable number of events, as expected. When the sizes of the particles are bigger that the diameter of the nanopore, they cannot pass through the nanopore to be detected.

We used the FPLC-UV chromatogram as a reference to determine the fractions of proteins. Samples from purified fractions of Myoglobin, Ovalbumin, IgG, and Thyroglobulin were collected and measured separately. After each measurement, the solution was exchanged. Using a hydrogel-backed 18 nm diameter nanopore, we separately measured purified fractions of Myoglobin, Ovalbumin, and IgG, and using a hydrogel-backed 30 nm diameter nanopore, we separately measured IgG and Thyroglobulin fractions. Event amplitude histograms for each measurement are presented in Figures 3.2b and 3.2c.

a

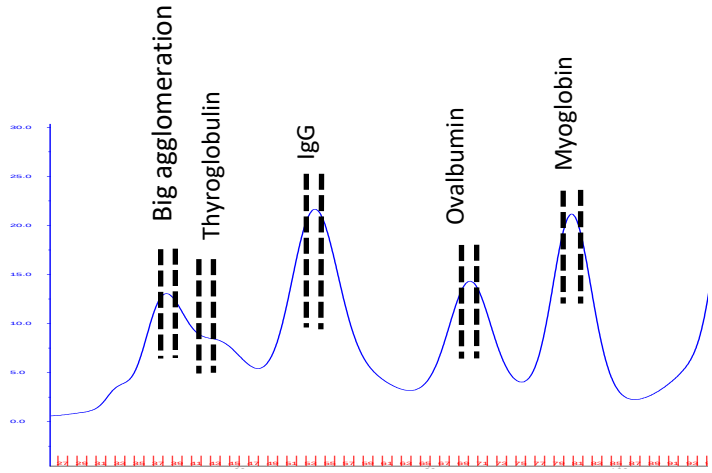

b

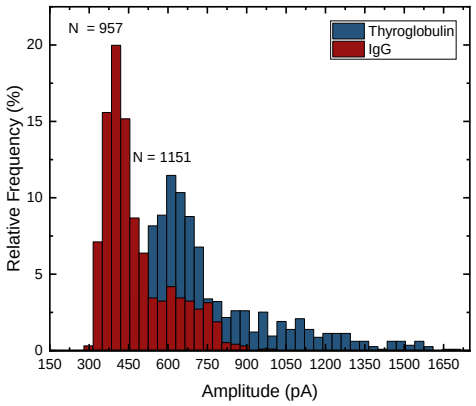

c

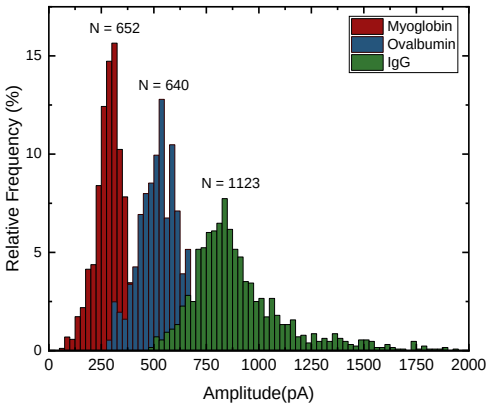

Figure 3.2. Size-exclusion chromatography to separate Myoglobin (18 kD), Ovalbumin (44 kD), IgG (160 kD), and Thyroglobulin (660 kD) from a highly concentrated mixture solution a) The UV-Vis detector readout. b) Nanopore measurement of IgG and Thyroglobulin, using a hydrogel-backed 30 nm diameter nanopore in 2M KCl, pH 10 buffer at -40 mV applied voltage. c) Nanopore measurement of Myoglobin, Ovalbumin, and IgG, using a hydrogel-backed 18 nm diameter nanopore in 2M KCl, pH 10 buffer at -60 mV applied voltage.

Following up on this experiment, we diluted the protein mixture (the highly concentrated mixture solution of Myoglobin, Ovalbumin, IgG, and Thyroglobulin) used in the first experiments

100 times more and ran it through the same column; again, fractions were collected with a fixed volume of 1 ml. However, this time the UV-Vis detector failed to identify fractions of proteins (Figure 3.3a). We explored the collected fractions using hydrogel-backed nanopore biosensors. We used the FPLC-UV chromatogram from the first experiment as a reference to pinpoint the peaks of fractions of individual proteins for the second experiment. Then, samples from the corresponding protein fractions were collected, and nanopore experiments were conducted to measure them. Before each nanopore measurement, the collected samples were diluted 10 times more. Using a hydrogel-backed 15 nm diameter nanopore, we measured corresponding samples from Myoglobin and Ovalbumin fractions, and using a hydrogel-backed 30 nm diameter nanopore, we sensed corresponding samples from IgG and Thyroglobulin fractions. Figures 3.3b and 3.3c illustrate the amplitude histograms of detected proteins from Myoglobin, Ovalbumin, IgG, and Thyroglobulin fractions, in agreement with the findings of the first measurement.

a

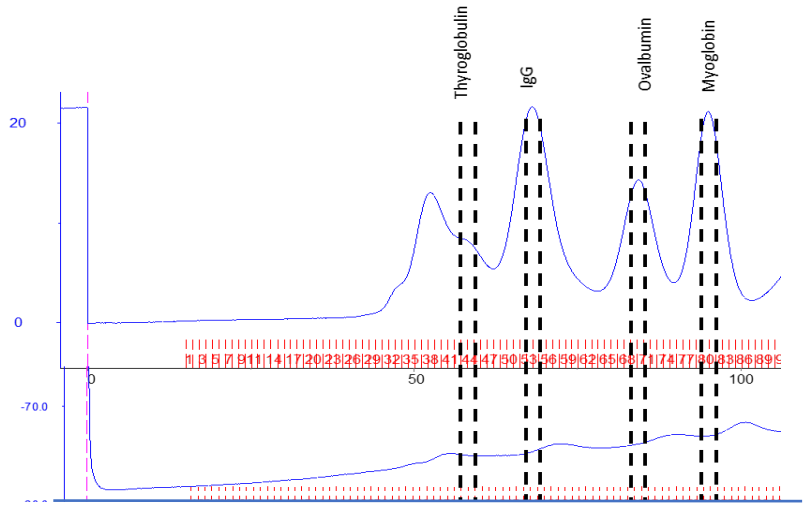

b

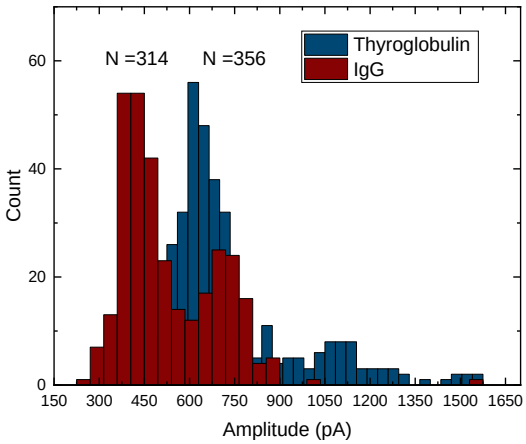

c

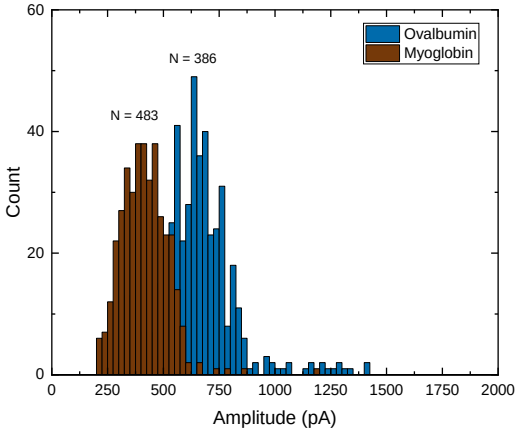

Figure 3.3. Size-exclusion chromatography to separate Myoglobin, Ovalbumin, IgG, and Thyroglobulin from a diluted mixture solution a) The UV-Vis detector read-out of fractions of the diluted mixture compared to the UV-Vis detector read-out of fractions of the original mixture solution. b) Nanopore measurement of purified fractions of Thyroglobulin and IgG, using a hydrogel-backed 30 nm nanopore in 2 M KCl , pH 10 buffer at -40 mV applied voltage. c) Nanopore measurement of purified fractions of Myoglobin and Ovalbumin using a hydrogel-backed 15 nm diameter nanopore 2 M KCl, pH 10 buffer at -60 mV applied voltage.

Hydrogel-backed nanopores sensed the existing proteins in the selected fractions; however, UV-Vis detector could not detect the fractionated proteins. We suspected that the protein concentrations in the diluted mixture for the second experiment were below the detection limit of our UV-Vis detector. To support our hypothesis, we estimated the minimum concentrations of proteins that can be resolved by our FPLC using Beer's law (Equation 3.1):

$$A = \log\left(\frac{I}{I_0}\right) = \epsilon\, l\, c \tag{3.1}$$

where A is the absorbance, I_0 and I are the intensity of incident and transmitted lights, respectively. ε is the molar extinction coefficient of the protein sample, l is the path length of the flow-cell, and c is the molar protein concentration.

Further, to make the approximation, the path length of the flow-cell was assumed to be 2 mm (a default value for AKTA FPLC) and the minimum distinguishable absorbance signal (from baseline noise) was set to be 5 mAu (absorption unit). The molar extinction coefficient for proteins were calculated from their amino acid sequences using Scripps Institute's online protein calculator v3.4 (http://protcalc.sourceforge.net/). The obtained concentration value for each protein indicates the minimum abundance of the protein that should exist in one fraction to be detected. However, the given concentration of an injected protein into the column was divided among tens of fractions, so to find the minimum detectable concentration for each protein that should be injected into the column, in our approximation, the obtained minimum detectable concentrations for one fraction were multiplied by the number of fractions containing the same protein. Table 3.2 shows the minimum concentrations of our measured proteins that should be injected into the column so the UV-Vis detector can sense them. The bigger the proteins are, the higher the extinction coefficients are, and consequently, the lower their minimum detectable concentrations are, as can be seen by a

comparison between the minimum concentrations that are detectable for our measured proteins. Table 3.2 also summarizes the concentrations of the measured proteins in both experiments.

As shown in Table 3.2, in our first experiment involving the high-concentrated mixture of proteins, all protein concentrations were high above the minimum detectable concentrations by the UV-Vis spectrometer. However, in the second experiment with the diluted mixture of proteins, the protein concentrations were much lower than the minimum detectable concentration limits for a UV-Vis detector, explaining why the detector fails to detect the fractionated proteins. Also, it should be noticed that our nanopore measurements were run on samples with 10 times more dilution from the collected fractions of Experiment 2. These findings demonstrated the superior sensitivity of the hydrogel-backed nanopores to study the diluted fractions of proteins over a range of pM to nM concentrations.

Table 3.2. Minimum detectable concentrations of measured proteins using UV-Vis detector, and protein concentrations in a low and high concentrated mixture

Protein	Minimum Detectable Concentrations (μM)			Injected Concentrations to the Column. (μM)	
	In One Fraction	# of Fractions (Fig. 3.2 a)	to be Injected	Exp. 1	Exp. 2
Myoglobin	1.75	11	19.25	294	2.94
Ovalbumin	0.8	13	10.4	227	2.27
IgG	0.1	16	1.6	63	0.63
Thyroglobulin	0.07	7	0.49	14	0.14

3.2.1.3. Higher Selectivity of a Hydrogel-Backed Nanopore to Detect Co-Existing Proteins in One Fraction

Based on affinities between discrete proteins in a mixture and a stationary phase of a chromatographic column, proteins can separate as individuals or as a group of multiple proteins into distinct fractions. Inherently, the UV-Vis detector is not able to specify various species in one fraction. For example, using an FPLC ion-exchange column, we attempted to separate a mixture of IgG (30 μM) and Ovalbumin (20 μM) from each other. At a low ionic strength of 100 mM KCl at pH 8, a mixture of negatively charged IgG and Ovalbumin was loaded into a column to bind electrostatically to the surface cationic groups of the medium. The bound proteins can be separately washed out in order from the medium by a gradual increase in the salt concentration of the running buffer. As the ionic strength of the running buffer increases, salt ions compete with bound proteins for the medium surface charge and displace the proteins to elute and move down from the column. Proteins with less electric charge and less affinity toward the column are the first fractions to leave the column, and proteins with a higher surface electric charge that strongly bind to the medium desorb from the column at the higher ionic strengths. To elute IgG and Ovalbumin from the column, we increased the salt concentration of the running buffer over 12 column volumes to the final concentration of 1M KCl. However, we could not separate IgG and Ovalbumin in two distinguishable peaks, and the UV-Vis detector identified only one peak of proteins (Figure 3.4a). A sample from the resolved peak was collected, diluted 100 times, and run through a hydrogel-backed 20 nm diameter nanopore. A histogram of event amplitudes (Figure 3.4 c) revealed two prominent peaks, indicating the existence of two distinct species within the sample. Using the same nanopore, we measured purified IgG. The precise overlap of the amplitude histogram of IgG (shown in red in Figure 4.4 c) with the second peak of the histogram

of the FPLC sample (blue histogram in Figure 4.4 c) verified the existence of IgG in the resolved FPLC fraction. Therefore, we assumed that the first peak in the blue histogram was the Ovalbumin peak. Also, both the shape of the peak and the ratio of its most probable amplitude in comparison to the IgG peak maximum might reconfirm our assumption. Further, in another experiment, we separated a mixture of IgG and Ovalbumin with a higher degree of separation by slowing down the replacement rate of ions and applying the salt gradient across 60 column volumes. Figure 3.4 b shows the obtained FPLC-UV chromatogram with the main peak containing mostly IgG (-4e at pH 8), and the shoulder mainly including Ovalbumin (-14e at pH 8).

In our first experiment, IgG and Ovalbumin emerged from a column in one fraction, and the UV-Vis detector did not distinguish them. However, the hydrogel-backed nanopore measurement enabled the simultaneous detection and discrimination between IgG and Ovalbumin in the same fraction. The highly selective detection of the hydrogel-facilitated nanopore measurements can expand its application to identify possible impurities in the collected fractions. This capability is especially pronounced for identifying co-existing impurities that may not have UV absorbance at the measured wavelengths.

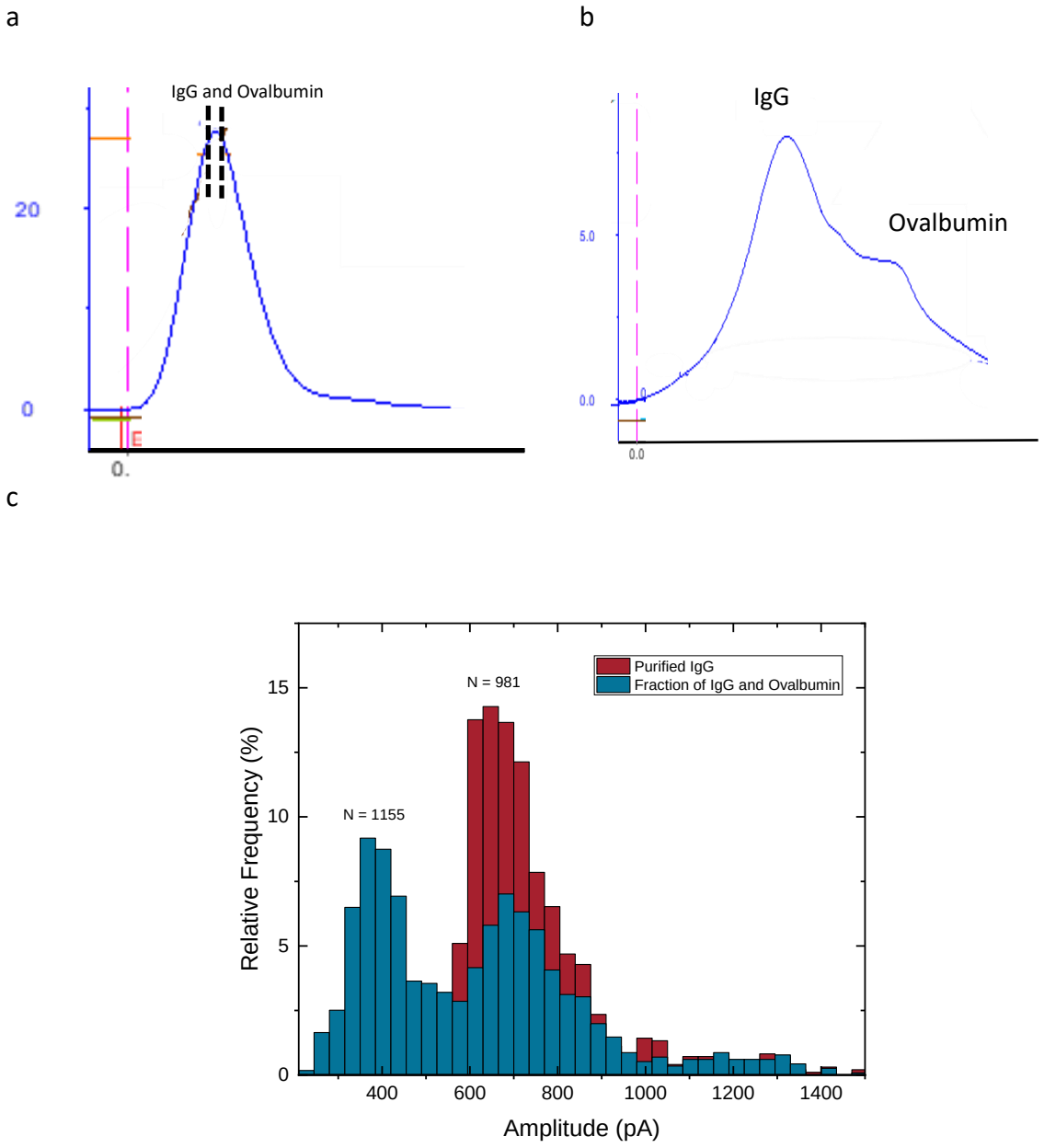

Figure 3.4. Ion exchange chromatography to separate IgG and Ovalbumin a) The UV-Vis detector read-out of fractions over 12 column volumes b) The UV-Vis detector read-out of fractions over 60 column volumes. c) Nanopore measurement of the fraction shown in part a, using a hydrogel-backed 20 nm diameter nanopore in 2 M KCl, pH 10 buffer at -70 mV applied voltage.

3.2.2. Integrating a Hydrogel-Backed Nanopore with Microchannels

So far, we have explored the potential application of the hydrogel-backed nanopore as an ultra-sensitive protein detector for liquid chromatography. Our primary findings indicate that a hydrogel-backed nanopore can be an effective substitute for a typical UV-Vis detector with other promising applications in proteomic studies. A much lower concentration detection limit, a higher precision in measurement, and a more informative analysis of protein fractions are the main features that make the hydrogel-backed nanopore a powerful protein detector to be integrated with liquid chromatographic columns. However, a typical flow-cell utilized in nanopore measurements is not applicable for the live and continuous measurement of the huge number of fractions emerging from a chromatographic column.

A typical flow cell consists of two isolated compartments filled with electrolytes and separated by a nanopore. In these systems, continuously transporting, managing, and manipulating fluids to the compartments is impossible, and changing the sample is done manually by an operator. Each time, the operator swaps the previous sample, cleans and rinses the flow cell several times, and adds a new sample. Also, the existence of dead volumes around a nanopore in a typical flow cell is another problem. Dead volumes around the nanopore are not easily reachable, so the previous sample cannot be thoroughly cleaned and replaced by a new sample. As a result, cross-contaminations between different runs are inevitable.

In addition, previously, we have shown that the proximity of the hydrogel to the pore mouth is an indicating factor in determining the hydrogel's performance in slowing down the proteins; smaller gaps lead to a longer dwell time and more effective protein detection. Elimination of the dead volumes around a nanopore enables the hydrogel precursor solution to be replaced entirely with the electrolyte around the nanopore, prompting the hydrogel to touch the membrane with a

smaller gap after polymerization, improving the detection sensitivity. Therefore, the improved efficacy rendered the Teflon flow cell unnecessary, so we stopped using it.

We adjusted the measurement setting for the newly proposed application and integrated the nanopores with microchannels. We mounted the solid-state nanopores between microfluidic channels to facilitate the rapid and efficient sample replacement through channels to improve the measurement. Further, through a connecting tube, the outlet valve of a chromatographic column can be coupled with the inlet of the top microchannel, making a fluidic circuit to transport samples of eluates to the nanopore, enabling real-time and continuous measurements of protein fractions. Figure 3.5a schematically illustrates the fluidic circuit between the FPLC and the designed microfluidic device.

Our PDMS multilayer microfluidic device (Figure 3.5) is made from two identical layers corresponding to the *cis* and the *trans* compartments at two sides of the membrane, similar to other designs of nanopore-based microfluidic devices.[40,41] Each layer consisted of a 3 mm PDMS slab with a patterned 300 μm wide channel (1 mm height); A 100 μm thin film of PDMS covered each microchannel. Nanopore fluid access to the channels was punched on the PDMS thin film. We used our device exclusively for nanopore measurements and not the nanopore fabrication due to the possibility of generating air bubbles at higher voltages inside the channels.[42,43] To run hydrogel-nanopore measurements, following the insertion of a pre-fabricated dielectric breakdown nanopore between the channels, we chemically polymerized the PEG-DMA hydrogel precursor solution in the *cis* channel at the bottom side of the chip.

a

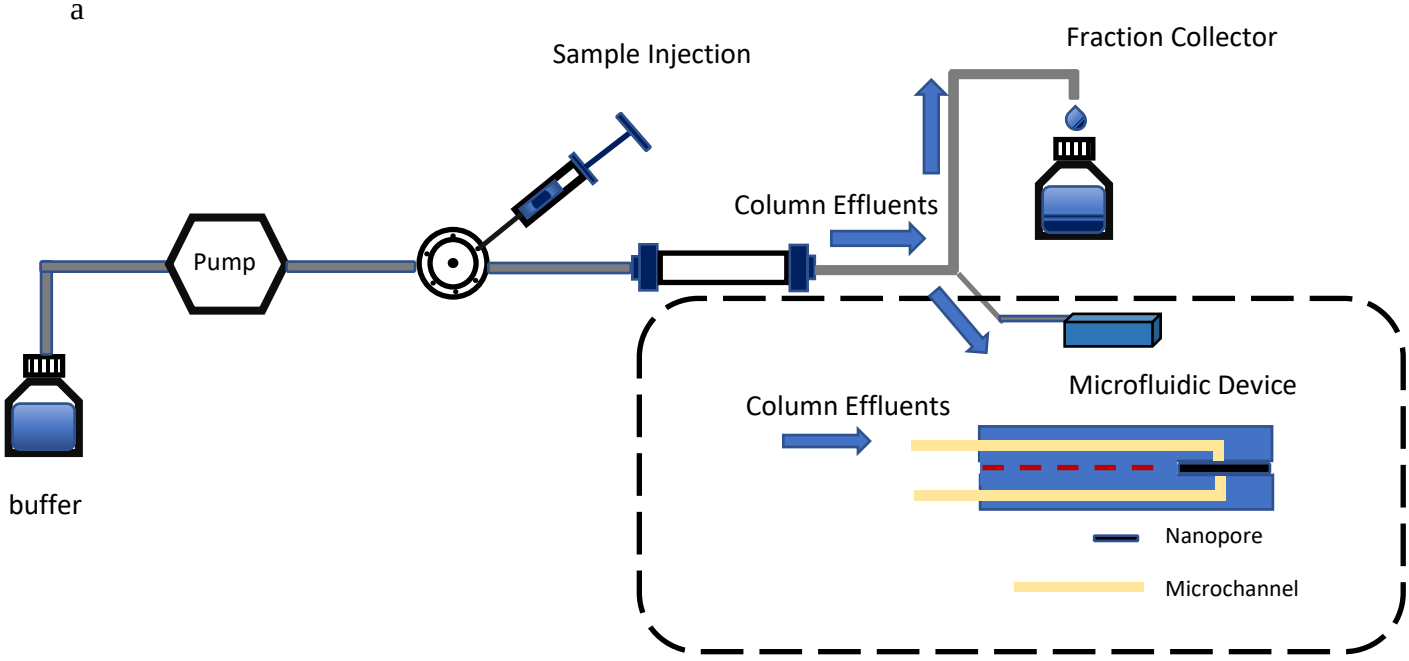

b

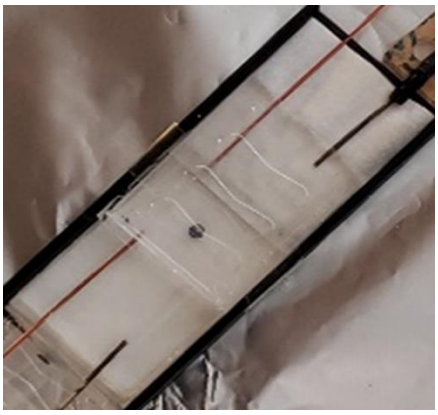

Figure 3.5. a) Schematic illustration of interfacing the microfluidic device with a chromatographic column for live measurement of effluents. b) A solid-state nanopore is mounted between two layers of microchannels.

We measured IgG protein molecules at 100 pM concentration with a 20 nm diameter nanopore backed with a hydrogel-filled channel in 2 M KCl, pH 8 buffer at -70 mV applied voltage. The observed events were long in contrast with the IgG translocation events measured using our traditional Teflon flow cell, and the dwell time exponentially increased with increasing applied voltages. Figure 3.6 shows a short trace of IgG measurement. The extended dwell time of IgG events that we measured using the microfluidic device may confirm that eliminating the dead volume around a nanopore helps the hydrogel gets closer to the membrane, blocking the exit opening of the nanopore to the *trans* side and forcing the protein molecules to diffuse back through the nanopore.

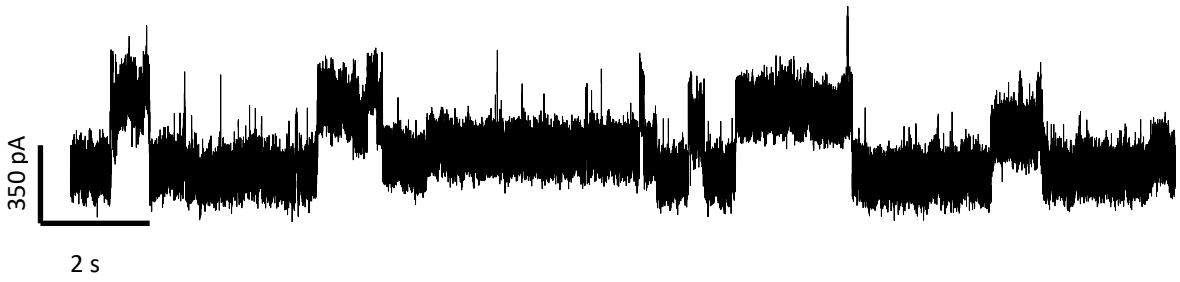

Figure 3.6. Example of the measured ionic current trace of IgG using a 20 nm diameter nanopore interfaced with a hydrogel-filled microchannel in 2M KCl, pH 8 at -70 mV applied voltage

3.3. Summary and Conclusion

We demonstrated that a hydrogel-backed nanopore might be an effective substitute for the standard UV-Vis detectors used to identify fractions of proteins eluted from a liquid chromatographic column for advanced proteomic studies. We exhibited that hydrogel-backed nanopore detectors have higher sensitivity and selectivity in protein detection than the UV-Vis detectors traditionally used. Hydrogel-backed nanopore detectors can resolve proteins at ultra-low

concentrations in the pM range (100-1000 times lower than a minimum detectable concentration by a standard UV-Vis detector) and discriminate between different species that co-exist in one fraction.

Further, we altered the conventional nanopore measurement design to make it compatible to serve as an FPLC detector. We coupled solid-state nanopores with microchannels to create a fluidic circuit from a chromatographic column to a nanopore, facilitating the transport of eluate samples to the nanopore for continuous and real-time measurements of fractions being eluted off from the column. We aim to continue this work by incorporating the hydrogel-backed nanopore-based microfluidic detector with an FPLC instrument and complete our design by live measurement of column effluents.

3.4. Materials and Methods

Materials: All chemicals were purchased from Sigma-Aldrich at reagent grade and used as received. Gel filtration standard solution (containing a mixture of Thyroglobulin, IgG, Ovalbumin, and Myoglobin) was purchased from Bio-Rad. The Black lab generously provided T7 RNA polymerase and polypyrimidine tract binding protein (PTBP1) at UCLA.

Nanopore fabrication and hydrogel polymerization inside the conventional Teflon flow-cell: 15 nm thick silicon nitride membranes were commercially purchased from Ted Pella Inc.; membranes were PDMS coated and cured for several hours at 120°C before use. Silicon nitride membranes were plasma treated for 30 sec, mounted in a Teflon fluidic cell, and degassed. Nanopores were formed using dielectric breakdown in 2 M KCl, pH 10 at the desired size as previously reported[25]. PEG-DMA hydrogel solution was prepared by mixing 10% (w/v) PEG-1000 Dimethylacrylamide in 2 M KCl, 100 mM Tris-HCl at pH 8-10 (adjusted by HCl and NaOH), 10% (w/v) ammonium persulfide (APS), and 20% (w/v) tetramethylethylenediamine (TEMED). Nanopore diameters were determined immediately after formation as described previously.[44] After the formation of a nanopore, the electrolyte in the compartment on the TEM window side was replaced with PEG-DMA hydrogel solution and polymerized in-situ for 10 minutes before nanopore measurement.

Nanopore measurements: All nanopore measurements were carried out using an Axopatch 200B amplifier and Digidata 1440B or 1322A data acquisition at 100 kHz with a 10 kHz hardware low pass filter. Nanopore measurements were performed in 2 M KCl, 100 mM Tris-HCl, pH 8-10. At least 5 minutes of control measurements were run before protein injection. In all Teflon flow-cell experiments, the hydrogel side (*trans*) of the nanopore chip was grounded, and protein was injected

into the other side (*cis*) to make a final concentration of 100 pM – 10 nM; measurements were run at -50 to -70 mV applied voltages (V_{cis}-V_{trans}).

In all microfluidic experiments, the hydrogel side (*cis*) of the nanopore chip was grounded, and protein was injected into the other side (*trans*).

Integrated nanopore-microfluidic device and hydrogel formation inside the microchannel:

Each 3 mm layer of PDMS (with a patterned microchannel) was fabricated by casting degassed PDMS (Sylgard 184 kit, Dow Corning, mixed with 10:1 base to curing agent ratio) on a 3D-printed acrylate-based master mold. The STL file of the master mold was designed on the 3D graphical environment of Tinkercad (https://www.tinkercad.com, Autodesk, USA). Master molds were 3D printed by a stereolithography 3D printer (Formlabs Inc.) without any additional setting on the program. A 3D-printed device holder was made to carry and assemble the layers of the device. 100 μm thin films of PDMS were formed using the floating-on-water fabrication technique as previously described.[45] Briefly, to fabricate a PDMS thin film, a 20 cm diameter Petri dish was filled with 50 mL of pure water, and around 320 mg of PDMS solution was poured onto the water surface on a hot plate at 80 ^{o}C left for a couple of hours. Each PDMS layer was permanently bonded to a PDMS thin film using air plasma. To provide nanopore access to fluidic microchannels, pores were punched on the thin film surfaces on each assembled layer using a biopsy puncher. The designed microfluidic device is reusable and the support nanopore membrane was mounted between assembled layers. The layers and a membrane were stacked and assembled using an external device holder.

To fill the microchannel with the PEG-DMA hydrogel, following the insertion of a prefabricated dielectric breakdown nanopore between the top and bottom layers, the *cis* channel was filled with the hydrogel precursor solution (10% (w/v) PEG-1000 Dimethylacrylamide in 2 M KCl, 100 mM

Tris-HCl at pH 8 HCl + 10% (w/v) ammonium persulfide (APS)+ 20% (w/v) tetramethylethylenediamine (TEMED)) to be chemically polymerized.

Data analysis: All captured data were analyzed using a MATLAB script as previously reported[25].

3.5. References:

(1) Haleem, I. J.; Conrads, T. P.; Janini, G. M.; Veenstra, T. D.; Nci-frederick, S. F. Review Methods for Fractionation , Separation and Profiling of Proteins and Peptides. *Electrophoresis* **2002**, *23* (17), 3048–3061.

(2) Hong, P.; Koza, S.; Bouvier, E. S. P. A Review Size-Exclusion Chromatography for the Analysis of Protein Biotherapeutics and Their Aggregates. *J. Liq. Chromatogr. Relat. Technol.* **2012**, *35* (20), 2923–2950. https://doi.org/10.1080/10826076.2012.743724.

(3) Yaguchi, M.; Rose, D. Chromatographic Separation of Milk Proteins: A Review. *J. Dairy Sci.* **1971**, *54* (12), 1725–1743. https://doi.org/10.3168/jds.S0022-0302(71)86106-4.

(4) Bond, M. D.; Panek, M. E.; Zhang, Z.; Wang, D.; Mehndiratta, P.; Zhao, H.; Gunton, K.; Ni, A.; Nedved, M. L.; Sudhir, B.; Volkin, D. B. Evaluation of a Dual-Wavelength Size Exclusion HPLC Method with Improved Sensitivity to Detect Protein Aggregates and Its Use to Better Characterize Degradation Pathways of an IgG1 Monoclonal Antibody. *J. Pharm. Sci.* **2010**, *99* (6), 2582–2597. https://doi.org/10.1002/jps.22034.

(5) Coskun, O. Separation Tecniques: CHROMATOGRAPHY. *North. Clin. Istanbul* **2016**, *3* (2), 156–160. https://doi.org/10.14744/nci.2016.32757.

(6) Madadlou, A.; O'Sullivan, S.; Sheehan, D. Fast Protein Liquid Chromatography. *Methods Mol. Biol.* **2017**, *1485*, 365–373. https://doi.org/10.1007/978-1-4939-6412-3_19.

(7) Snyder, L. R.; Kirkland, J. J.; Dolan, J. W. *Introduction to Modern Liquid Chromatography*; John Wiley and Sons: New York, 2010.

(8) Scott, R. P. W. Liquid Chromatography Detectors. *Liq. Chromatogr. Anal.* **2020**, 173–210. https://doi.org/10.1201/9781482277593-13.

(9) Some, D.; Amartely, H.; Tsadok, A.; Lebendiker, M. Characterization of Proteins by Size-Exclusion Chromatography Coupled to Multi-Angle Light Scattering (Sec-Mals). *J. Vis. Exp.* **2019**, *2019* (148), 1–9. https://doi.org/10.3791/59615.

(10) Swartz, M. HPLC Detectors: A Brief Review. *J. Liq. Chromatogr. Relat. Technol.* **2010**, *33* (9–12), 1130–1150. https://doi.org/10.1080/10826076.2010.484356.

(11) Stepanchenko, N. S.; Novikova, G. V.; Moshkov, I. E. Protein Quantification. *Russ. J. Plant Physiol.* **2011**, *58* (4), 737–742. https://doi.org/10.1134/S1021443711040182.

(12) Chan, K. C.; Veenstra, T. D.; Issaq, H. J. Comparison of Fluorescence, Laser-Induced Fluorescence, and Ultraviolet Absorbance Detection for Measuring HPLC Fractionated Protein/Peptide Mixtures. *Anal. Chem.* **2011**, *83* (6), 2394–2396. https://doi.org/10.1021/ac1032462.

(13) Chou, C. C.; Lin, S. P.; Lee, K. M.; Hsu, C. T.; Vickroy, T. W.; Zen, J. M. Fast Differentiation of Meats from Fifteen Animal Species by Liquid Chromatography with Electrochemical Detection Using Copper Nanoparticle Plated Electrodes. *J. Chromatogr. B Anal. Technol. Biomed. Life Sci.* **2007**, *846* (1–2), 230–239. https://doi.org/10.1016/j.jchromb.2006.09.006.

(14) Amartely, H.; Avraham, O.; Friedler, A.; Livnah, O.; Lebendiker, M. Coupling Multi Angle Light Scattering to Ion Exchange Chromatography (IEX-MALS) for Protein Characterization. *Sci. Rep.* **2018**, *8* (1), 1–9. https://doi.org/10.1038/s41598-018-25246-6.

(15) Ben M'Barek, S.; Cordewener, J. H. G.; Tabib Ghaffary, S. M.; van der Lee, T. A. J.; Liu, Z.; Mirzadi Gohari, A.; Mehrabi, R.; America, A. H. P.; Robert, O.; Friesen, T. L.; Hamza, S.; Stergiopoulos, I.; de Wit, P. J. G. M.; Kema, G. H. J. FPLC and Liquid-Chromatography Mass Spectrometry Identify Candidate Necrosis-Inducing Proteins from Culture Filtrates of the Fungal Wheat Pathogen Zymoseptoria Tritici. *Fungal Genet. Biol.* **2015**, *79*, 54–62. https://doi.org/10.1016/j.fgb.2015.03.015.

(16) Collins, L. A.; Mirza, S. P.; Kissebah, A. H.; Olivier, M. Integrated Approach for the Comprehensive Characterization of Lipoproteins from Human Plasma Using FPLC and Nano-HPLC-Tandem Mass Spectrometry. *Physiol. Genomics* **2010**, *40* (3), 208–215. https://doi.org/10.1152/physiolgenomics.00136.2009.

(17) Plesa, C.; Ruitenberg, J. W.; Witteveen, M. J.; Dekker, C. Detection of Individual Proteins Bound along DNA Using Solid-State Nanopores. *Nano Lett.* **2015**, *15* (5). https://doi.org/10.1021/acs.nanolett.5b00249.

(18) Freedman, K. J.; Haq, S. R.; Fletcher, M. R.; Foley, J. P.; Jemth, P.; Edel, J. B.; Kim, M. J. Nonequilibrium Capture Rates Induce Protein Accumulation and Enhanced Adsorption to Solid-State Nanopores. *ACS Nano* **2014**, *8* (12), 12238–12249. https://doi.org/10.1021/nn5062645.

(19) Zhang, Y.; Zhao, J.; Si, W.; Kan, Y.; Xu, Z.; Sha, J.; Chen, Y. Electroosmotic Facilitated Protein Capture and Transport through Solid-State Nanopores with Diameter Larger than Length. *Small Methods* **2020**, *4* (11), 1–8. https://doi.org/10.1002/smtd.201900893.

(20) Ananth, A.; Genua, M.; Aissaoui, N.; Díaz, L.; Eisele, N. B.; Frey, S.; Dekker, C.; Richter, R. P.; Görlich, D. Reversible Immobilization of Proteins in Sensors and Solid-State Nanopores. *Small* **2018**, *14* (18), 1–11. https://doi.org/10.1002/smll.201703357.

(21) Li, W.; Bell, N. A. W.; Hernández-Ainsa, S.; Thacker, V. V.; Thackray, A. M.; Bujdoso, R.; Keyser, U. F. Single Protein Molecule Detection by Glass Nanopores. *ACS Nano* **2013**, *7* (5), 4129–4134. https://doi.org/10.1021/nn4004567.

(22) Cressiot, B.; Oukhaled, A.; Patriarche, G.; Pastoriza-Gallego, M.; Betton, J. M.; Auvray, L.; Muthukumar, M.; Bacri, L.; Pelta, J. Protein Transport through a Narrow Solid-State Nanopore at High Voltage: Experiments and Theory. *ACS Nano* **2012**, *6* (7), 6236–6243. https://doi.org/10.1021/nn301672g.

(23) LIU, Y.; YAO, X. F.; WANG, H. Y. Protein Detection Through Single Molecule Nanopore. *Chinese J. Anal. Chem.* **2018**, *46* (6), e1838–e1846. https://doi.org/10.1016/S1872-2040(18)61093-X.

(24) Kong, J.; Bell, N. A. W.; Keyser, U. F. Quantifying Nanomolar Protein Concentrations Using Designed DNA Carriers and Solid-State Nanopores. *Nano Lett.* **2016**, *16* (6), 3557–3562. https://doi.org/10.1021/acs.nanolett.6b00627.

(25) Acharya, S.; Jiang, A.; Kuo, C.; Nazarian, R.; Li, K.; Ma, A.; Siegal, B.; Toh, C.;

Schmidt, J. J. Improved Measurement of Proteins Using a Solid-State Nanopore Coupled with a Hydrogel. *ACS Sensors* **2020**, *5*, 370–376. https://doi.org/10.1021/acssensors.9b01928.

(26) Soni, G. V.; Dekker, C. Detection of Nucleosomal Substructures Using Solid-State Nanopores. *Nano Lett.* **2012**, *12* (6), 3180–3186. https://doi.org/10.1021/nl301163m.

(27) Ananth, A.; Genua, M.; Aissaoui, N.; Díaz, L.; Eisele, N. B.; Frey, S.; Dekker, C.; Richter, R. P.; Görlich, D. Reversible Immobilization of Proteins in Sensors and Solid-State Nanopores. *Small* **2018**, *14* (18). https://doi.org/10.1002/smll.201703357.

(28) Freedman, K. J.; Haq, S. R.; Edel, J. B.; Jemth, P.; Kim, M. J. Single Molecule Unfolding and Stretching of Protein Domains inside a Solid-State Nanopore by Electric Field. *Sci. Rep.* **2013**, *3*, 1–8. https://doi.org/10.1038/srep01638.

(29) Oukhaled, A.; Cressiot, B.; Bacri, L.; Pastoriza-Gallego, M.; Betton, J. M.; Bourhis, E.; Jede, R.; Gierak, J.; Auvray, L.; Pelta, J. Dynamics of Completely Unfolded and Native Proteins through Solid-State Nanopores as a Function of Electric Driving Force. *ACS Nano* **2011**, *5* (5), 3628–3638. https://doi.org/10.1021/nn1034795.

(30) Larkin, J.; Henley, R. Y.; Muthukumar, M.; Rosenstein, J. K.; Wanunu, M. High-Bandwidth Protein Analysis Using Solid-State Nanopores. *Biophys. J.* **2014**, *106* (3), 696–704. https://doi.org/10.1016/j.bpj.2013.12.025.

(31) Hu, R.; Rodrigues, J. V.; Waduge, P.; Yamazaki, H.; Cressiot, B.; Chishti, Y.; Makowski, L.; Yu, D.; Shakhnovich, E.; Zhao, Q.; Wanunu, M. Differential Enzyme Flexibility Probed Using Solid-State Nanopores. *ACS Nano* **2018**, *12* (5), 4494–4502. https://doi.org/10.1021/acsnano.8b00734.

(32) Freedman, K. J.; Bastian, A. R.; Chaiken, I.; Kim, M. J. Solid-State Nanopore Detection of Protein Complexes: Applications in Healthcare and Protein Kinetics. *Small* **2013**, *9* (5), 750–759. https://doi.org/10.1002/smll.201201423.

(33) Nazarian, R.; Lee, E.; Siegel, B.; Kuo, C.; Acharya, S.; Schmidt, J. Quantitative Measurements of Protein Volume and Concentration Using Hydrogel-Backed Nanopores. *ACS Sensors* **2021**. https://doi.org/10.1021/acssensors.1c00284.

(34) Sousa, R.; Chung, Y. J.; Rose, J. P.; Wang, B. C. Crystal Structure of Bacteriophage T7 RNA Polymerase at 3.3 Å Resolution. *Nature* **1993**, *364* (6438), 593–599. https://doi.org/10.1038/364593a0.

(35) Tong, X.; Hu, R.; Li, X.; Zhao, Q. Probing Conformational Change of T7 RNA Polymerase and DNA Complex by Solid-State Nanopores. *Chinese Phys. B* **2018**, *27* (11). https://doi.org/10.1088/1674-1056/27/11/118705.

(36) Monie, T. P.; Hernandez, H.; Robinson, C. V.; Simpson, P.; Matthews, S.; Curry, S. The Polypyrimidine Tract Binding Protein Is a Monomer. *Rna* **2005**, *11* (12), 1803–1808. https://doi.org/10.1261/rna.2214405.

(37) Domains, T. H. E.; Polypyrimidine, O. F.; Binding, T.; Distinct, H.; Structural, R. N. a. The Domains of Polypyrimidine Tract Binding Protein. *Biochemistry* **2010**, *48* (10), 2063–2074. https://doi.org/10.1021/bi8016872.THE.

(38) Joshi, A.; Coelho, M. B.; Kotik-Kogan, O.; Simpson, P. J.; Matthews, S. J.; Smith, C. W. J.; Curry, S. Crystallographic Analysis of Polypyrimidine Tract-Binding Protein-Raver1 Interactions Involved in Regulation of Alternative Splicing. *Structure* **2011**, *19* (12), 1816–1825. https://doi.org/10.1016/j.str.2011.09.020.

(39) Rees, M.; Gorba, C.; Chiara, C. De; Bui, T. T. T.; Garcia-maya, M.; Drake, A. F.; Okazawa, H.; Pastore, A.; Svergun, D.; Chen, Y. W. Solution Model of the Intrinsically Disordered Polyglutamine Tract-Binding. *Biophysj* **2012**, *102* (7), 1608–1616. https://doi.org/10.1016/j.bpj.2012.02.047.

(40) Roman, J.; Jarroux, N.; Patriarche, G.; Franc, O.; Pelta, J.; Le, B.; Bacri, L.; Nanosciences, C. De; Nanotechnologies, D.; Paris-sud, U.; Paris-saclay, U.; Marcoussis, C. N. Functionalized Solid-State Nanopore Integrated in a Reusable Micro Fl Uidic Device for a Better Stability and Nanoparticle Detection. **2017**. https://doi.org/10.1021/acsami.7b14717.

(41) Roman, J.; Franc, O.; Jarroux, N.; Patriarche, G.; Pelta, J.; Bacri, L.; Le, B. Solid-State Nanopore Easy Chip Integration in a Cheap and Reusable Micro Fl Uidic Device for Ion Transport and Polymer Conformation Sensing. **2018**. https://doi.org/10.1021/acssensors.8b00700.

(42) Dong, M.; Tang, Z.; He, X.; Guan, W. Direct Observation of Redox-Induced Bubble Generation and Nanopore Formation Dynamics in Controlled Dielectric Breakdown. *ACS Appl. Electron. Mater.* **2020**, *2* (9), 2954–2960. https://doi.org/10.1021/acsaelm.0c00576.

(43) Turner, I. S.; Us, W. A.; Flusberg, B.; Us, G. A. (12) United States Patent. **2017**, *2* (12).

(44) Kowalczyk, S. W.; Grosberg, A. Y.; Rabin, Y.; Dekker, C. Modeling the Conductance and DNA Blockade of Solid-State Nanopores. *Nanotechnology* **2011**, *22* (31), 1–5. https://doi.org/10.1088/0957-4484/22/31/315101.

(45) Kim, D.; Kim, S. H.; Park, J. Y. Floating-on-Water Fabrication Method for Thin Polydimethylsiloxane Membranes. *Polymers (Basel).* **2019**, *11* (8). https://doi.org/10.3390/polym11081264.

Chapter 4: Hydrogel-backed Lipid Coated Nanopores

4.1. Introduction

Chapter 2 and chapter 3 of this dissertation have mainly focused on the promising capabilities of a hydrogel-backed nanopore to serve as an ultra-sensitive protein detector. We demonstrated that using hydrogel-backed nanopores, we could identify low-concentrated proteins and quantify protein shapes, volumes, and concentrations by statistical analysis of hundreds to thousands of protein translocation events. In this approach, the maximum value of the ionic current blockades from each translocation event is determined, and the distribution of maximum amplitudes is used to estimate protein shapes and volumes, as discussed in Chapter 2.

In addition to a population of translocation events, a single protein translocation event can be decoded to extract enriched information on the shape, volume, charge, dipole moment, and rotational diffusion constant of a protein. Upon application of an external electric field across a nanopore, a translocating spheroid protein inside the pore can rotate and distort the electric field to various extents, depending on its orientation relative to the electric field, resulting in fluctuations in the measured ionic current blockades.[1] The current blockade is at its maximum when the protein is in its extreme crosswise orientation and is at its minimum when the protein is in its extreme lengthwise direction. A non-charged spheroid protein can freely rotate, randomize different directions, and almost equally sample extreme lengthwise and extreme crosswise orientations. In this case, the probability distribution of protein orientations is a symmetrical bimodal distribution with two maxima corresponding to the extreme lengthwise and crosswise orientations.

However, in the uniform electric field inside a nanopore, a charged spheroid protein with a permanent dipole moment experiences a torque that tends to align it in the direction of the electric field. As a result, the protein cannot randomize different orientations anymore, and the likelihood of sampling different directions gets biased by the potential energy of protein dipole moment in

the uniform electric field inside a nanopore. In the case of a protein with an electrical dipole moment, the probability distribution of orientations is an asymmetric skewed bimodal distribution due to the competition between the Brownian diffusional rotation and electrical torque that tends to align the protein in a particular orientation.

Therefore, the distribution of the ionic current modulations of a translocating protein reflects its size, extreme orientations, and dipole moment and can be very informative. The peak minimum and the peak maximum of the ionic current distribution determine the protein shape and volume.[1–3] Also, the skewness and kurtosis of the ionic current distribution determine the protein charge and dipole moment.[1] The protein rotational diffusion coefficient can be determined by monitoring the time-dependence of the current modulation of a single translocation event.

However, the intra-event ionic current analysis is challenging mainly due to the short residence time of a protein inside a nanopore and finite resolution of the amplifiers to resolve ionic current modulations of a rotating protein. To sample all orientation-dependent current distribution values, a protein molecule should stay sufficiently long inside a nanopore. However, only a small fraction of the total number of events (<< 1%) are long enough to be selected for intra-event analysis due to the fast translocation of proteins through the nanopore.[4] Also, conventional recording systems with a resolution of 20 μs do not have enough resolution to resolve all orientation-dependent current modulations of a rotating protein. Typically, proteins rotate at a rate of $10^5 – 10^6$ rad^2/s in the confined space of a nanopore[2], equivalent to a less than 10 μs transition from the extreme lengthwise to the extreme crosswise direction, much below the temporal resolution of the conventional amplifiers. As a result, the accuracy in intra-event ionic current blockade analysis strongly relies on the number, duration, and bandwidth of individual pulses; [2]

the greater number of events with sufficiently long dwell times and low signal-to-noise ratios enables a more precise approximation of the physical parameters of the proteins.

Another challenge in precisely analyzing intra-event ionic current modulation arises from non-specific surface interactions between proteins and nanopores. The non-specific interactions in nanopore systems can prevent electric-field-induced rotation and translocation of proteins inside the nanopore and interfere with the obtained results.[5,6] To control the nanopore surface charge and physicochemical properties, various chemical and physical surface modification techniques have been investigated extensively, including atomic layer deposition of metal oxides,[7–10] surfactant coatings,[5,11] modifications with anti-fouling polymers and polyethylene glycol (PEG),[12–14] salinization,[15–18] monolayer self-assembly of thiol on gold,[19,20] and fluid lipid bilayer coating.[1,6,21] Among coating methods, fluid lipid-bilayer coating has been shown to be the most efficient approach to prevent non-specific adsorption and interaction of proteins to the pore wall, allowing artifact-free translational and rotational motion of proteins inside a nanopore.

Intra-event ionic current blockade analysis is complex, but in a few research works, intra-event ionic current analysis of individual translocation events has been used to study protein properties. Yusko and coworkers[1,6] used the bio-inspired technique for coating a nanopore with a fluidic lipid bilayer and tethered the target proteins to the bilayer. They have shown that the translocation velocity of the tethered proteins is dominated by the in-plane diffusion constant of the lipids and reduced by two order magnitudes, which results in long and time-dependent blockade currents, and enables a quantitative determination of the shape, volume, dipole moment, charge, and rotational diffusion constant of proteins. However, in this technique, a target protein had to be attached to a lipid anchor ligand embedded in the bilayer, which required prior knowledge about a target protein. Later, Houghtaling and coworkers[2] utilized the high bandwidth

amplifier at 500 kHz combined with the low noise lipid-bilayer coated nanopores to determine the volume, shape, and dipole moment of native and label-free proteins (larger in size than 40 kD) in a solution at high μM ranges of concentrations. Still, they observed considerable uncertainty in the estimated parameters.

Here, we demonstrated that integrating lipid-bilayer coated nanopores with a hydrogel is a suitable platform for acquiring artifact-free and long protein translocation events for the accurate intra-event ionic current analysis and extraction of enriched information on biased Brownian translational and rotational dynamics of proteins in the uniform electric field inside a nanopore. The presence of the hydrogel extends the residence time of proteins inside a nanopore, enabling accurate and ultra-sensitive protein detection.[22] The surface lipid-bilayer coating of a nanopore minimizes edge effects and non-specific interactions between a nanopore and proteins, allowing artifact-free electric-field-induced rotation of protein molecules. In addition, we introduced a straightforward protocol to lipid-coat the nanopores without pretreatment of nanopore surfaces due to the unique surface chemistry of dielectric breakdown nanopores.[23] Using hydrogel-backed lipid-bilayer coated nanopores, we measured IgG, Ovalbumin, and gold nanoparticles (5 nm diameter) and determined their volumes from single translocation events with lower uncertainty compared to previous studies. Further, we observed higher applied voltages increased the probability of IgG alignment. We determined the volume and the length-to-diameter ratio of IgG molecules at different applied voltages and noticed an expansion in the conformation of IgG molecules with an increase in the voltage.

4.2.Results and Discussion

4.2.1. Lipid-Bilayer Coating of Dielectric Break-down Nanopores

To create a lipid-bilayer coating on the pore surface, immediately after dielectric breakdown nanopore formation, we added a solution of suspension of 1-palmitoyl-2-oleoyl-glycerol-3-phosphocholine (POPC) unilamellar liposomes at 10 mM concentration to the *cis* side of the membrane as described by other studies.[1,2,6,21] The fusion of liposomes on the surface of a nanopore forms a lipid-bilayer coating, changing the dimension of the nanopore; the nanopore diameter reduces, and its length increases by the thickness of the bilayer and the thickness of the interstitial water layer between the fluidic bilayer and the wall of the pore[1,6,14,24,25]. Figure 4.1a schematically represents the change in the nanopore dimensions, and Equations 4.1 and 4.2 express the shift in the nanopore conductance before and after lipid coating[6,26]:

$$G_{before} = \sigma\left(\frac{l_p}{\pi r_p^2} + \frac{1}{2 r_p}\right)^{-1} \tag{4.1}$$

$$G_{after} = \sigma\left(\frac{l_p + 2d + 2W_L}{\pi \left(r_p - d - W_L\right)^2} + \frac{1}{2\left(r_p - d - W_L\right)}\right)^{-1} \tag{4.2}$$

where σ is the conductance of the buffer, l_p and $r_p$are the length and diameter of the nanopore, d is the thickness of the lipid bilayer, and $W_L$is the thickness of the interstitial water layer between the bilayer and the wall of the pore.

As an example, we measured the ionic current of the nanopores before and after the lipid coating procedure for four nanopores. As expected, we have observed a significant reduction in nanopore conductance after lipid coating. We plotted the nanopore conductance after lipid coating as a function of the conductance before coating (blue diamonds in Figure 4.1b). We also analytically calculated the expected change in the nanopore conductance

before and after lipid coating based on Equations 4.1 and 4.2, shown by a dashed red line in Figure 4.2b.

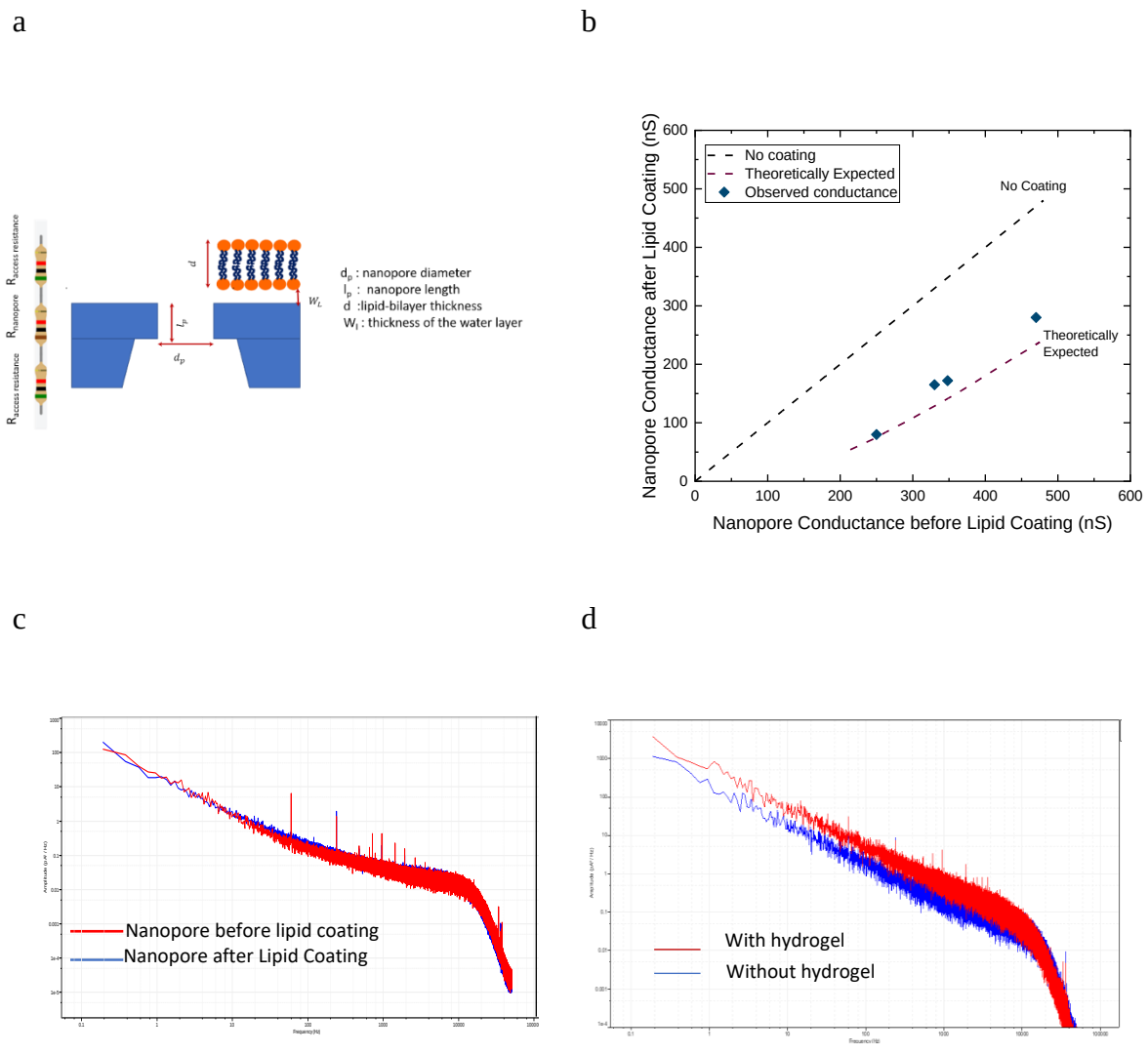

Figure 4.1. Lipid coated nanopore a) Schematic illustration of changes in nanopore diameter and length after lipid-bilayer coating. b) Analysis of 4 used nanopore properties before and after lipid coating modification: nanopore conductivities after lipid coating as a function of conductivities before coating. c) nanopore noise power spectrum before and after lipid coating. d) lipid-coated nanopore power spectrum before and after interfacing with the PEG-DMA hydrogel.

We compared our experimental observations with analytical expectations; we found a deviation of less than 25% from the theoretically expected values, which is in fair agreement with previous studies on the observed reduction in the nanopore conductance by a stable lipid bilayer coating.[25]

In addition, we have not noticed any significant changes in the baseline noise of the nanopore after lipid coating, consistent with previously reported studies.[6,24] The power spectrum analysis of a nanopore before and after lipid coating is shown in Figure 4.1 c.

4.2.2. Interfacing a Lipid-Bilayer Coated Nanopore with The PEG-DMA Hydrogel

We interfaced a lipid-coated nanopore with the hydrogel by polymerizing the PEG-DMA hydrogel precursor solution on the *trans* side of the membrane. Typically, after hydrogel polymerization, we have observed an increase in the baseline noise of the ionic current (Figure 4.1d); the increase level varies between different experiments.

We evaluated if the presence of the hydrogel at the *trans* side of a lipid-coated nanopore would slow down the proteins. We measured IgG at 100 pM concentration using a 21 nm diameter lipid-coated nanopore in 2 M KCl, pH 10 buffer at -50 mV applied voltage with and without the presence of the hydrogel. Without the hydrogel, we did not observe any translocation events over 30 minutes. We swapped the sample, cleaned and rinsed the flow cell, and repeated the experiment using the same lipid-coated nanopore but with the presence of the hydrogel at the *trans* side of the membrane. Following the control experiment, IgG was added to the *cis* chamber at 100 pM concentration, and translocation events appeared at the frequency of 0.16 Hz. Figure 4.2 shows a short trace of current measurements with and without the presence of the hydrogel at an applied voltage of -50 mV.

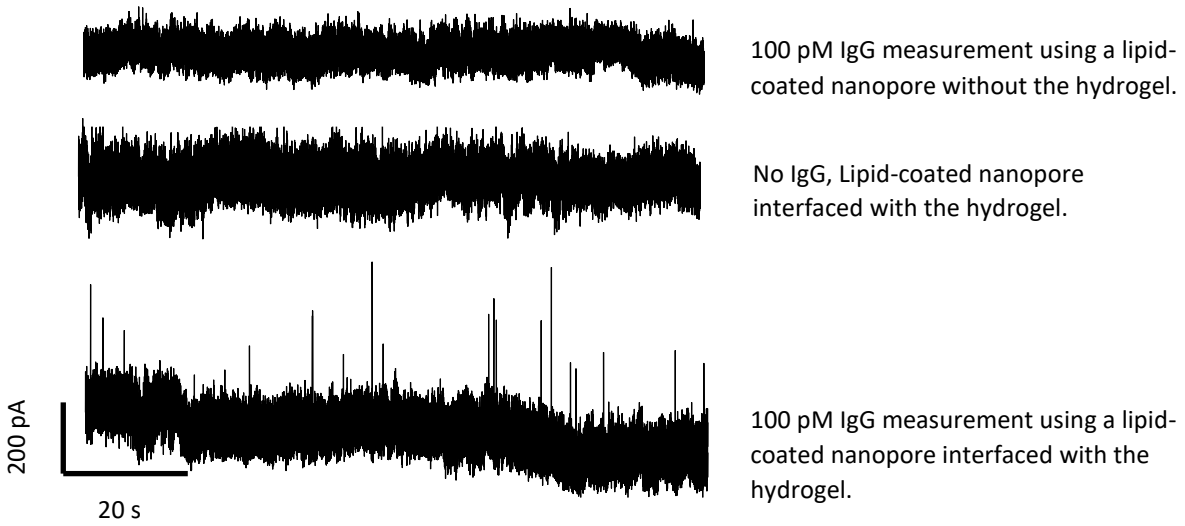

Figure 4.2. IgG measurement using a 21 nm diameter lipid-coated nanopore in 2 M KCl, pH 10 buffer at -50 mV applied voltage. a) the ionic current trace of 100 pM IgG measurement using the lipid-coated nanopore without the hydrogel b) the ionic current trace of the lipid-coated nanopore interfaced with the hydrogel as a control experiment. c) the ionic current trace of 100 pM IgG measurement using the same lipid-coated nanopore interfaced with the hydrogel.

4.2.3. Analysis of Single Translocation Events

As we discussed earlier, the protein shape and volume can be estimated by analyzing the intra-event ionic current modulations. We interfaced the hydrogel with a lipid-coated nanopore to enhance the resolvability of various protein orientations. Having the hydrogel at the distal side of a membrane slows down the proteins and increases their residence time inside the nanopore to repeat the rotation cycles more and more, which may increase the chance of detecting missed orientations. Using hydrogel-backed bilayer-lipid coated nanopores, we sensed 0.1-1 nM purified IgG, Ovalbumin, and 5nm diameter gold nanoparticles at 2M KCl, pH 8 buffer. Figure 4.3 represents examples of measured ionic current traces of single translocation events of IgG, Ovalbumin, and spherical gold nanoparticles. Also, from each trace, an event was selected to

make a histogram of the current distribution. Alongside each trace, the concatenated histogram from individually analyzed intra-event ionic current distributions was illustrated. The concatenated histograms of all analyzed single translocation events were used to show the mean behavior of the single translocation events statistically.

Example of an ionic current trace	Histogram of the selected event	Concatenated histogram (Mean behavior)
a) IgG, $d_{\text{lipid-coated nanopore}}$= 21 nm, applied voltage = -70 mV		
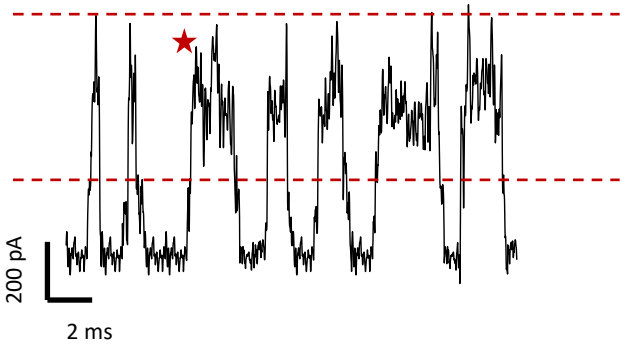	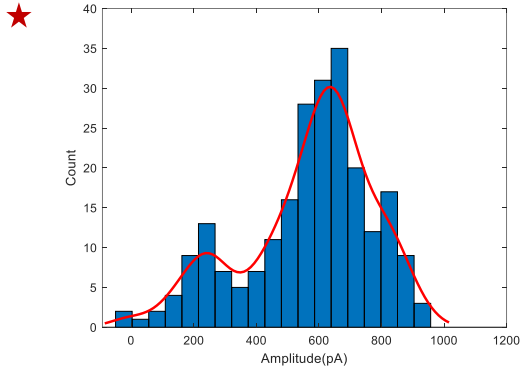	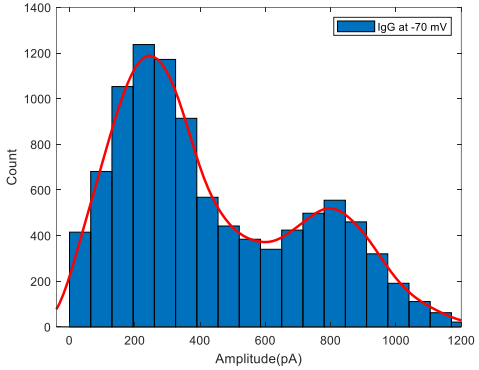
b) Ovalbumin, $d_{\text{lipid-coated nanopore}}$= 12 nm, applied voltage = -100 mV		
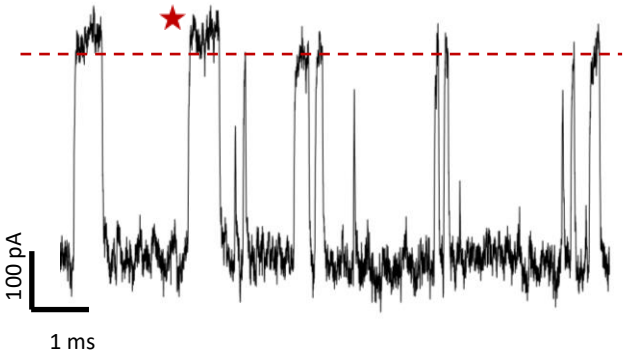	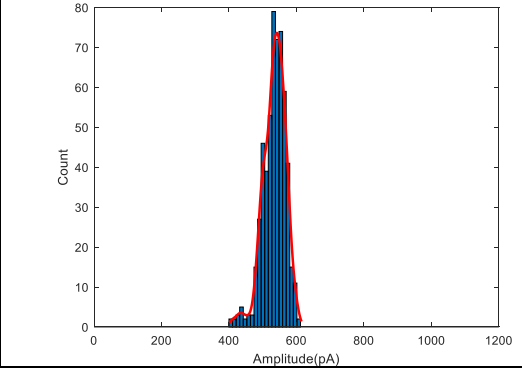	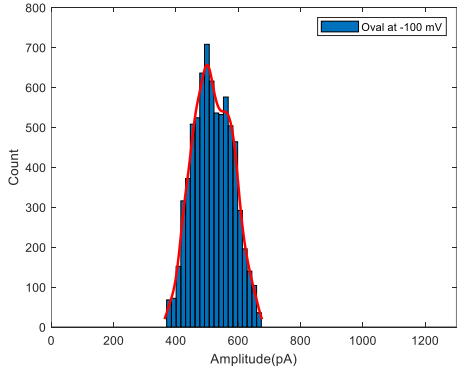

c) 5nm Diameter Gold Nanoparticles, $d_{\text{lipid-coated nanopore}}$= 13 nm, applied voltage = -100 mV

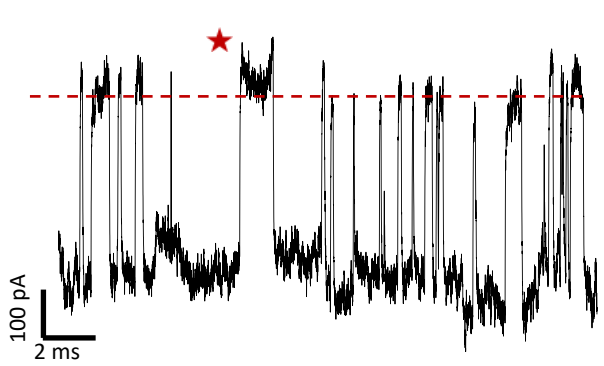

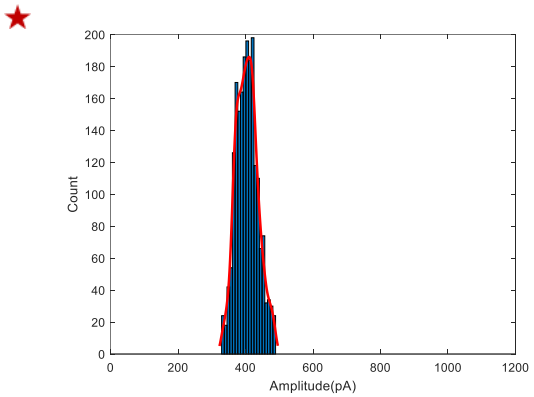

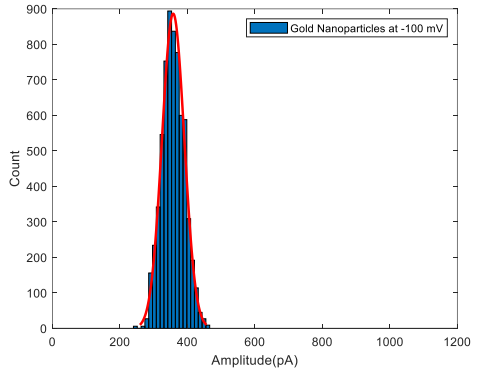

Figure 4.3. Short ionic current traces of measured nanoparticles using hydrogel-backed lipid-coated nanopores at 2M KCl, pH 8; alongside each short trace, the ionic current amplitude histogram of the selected event and the mean histogram from concatenation of 20 single event histograms were illustrated: a) measured IgG current trace using 21 nm lipid-coated nanopore at -70 mV applied voltage, b) measured Ovalbumin current trace using 12 nm lipid-coated nanopore at -100 mV applied voltage, c) measured gold nanoparticle current trace using 13 nm lipid-coated nanopore at -100 mV applied voltage. The red curve is the best-fit Gaussian distribution to determine the peak maxima of ionic current histograms.

4.2.3.1 Volume Estimation from Single Translocation Events

The scatter plot in Figure 4.4 represents the estimated volumes of IgG, Ovalbumin, and gold nanoparticles from individual translocation events from the measurements shown in Figure 4.3. The median volume for each cluster of data was calculated from the concatenated histogram of all the corresponding single translocation events. The calculated volumes of IgG (~ 270 nm^3), Ovalbumin (~ 172 nm^3), and gold nanoparticles (~ 127 nm^3) are within reasonable agreement compared to previously reported values.[3] The volumes estimated based on Dynamic Light Scattering (DLS) measurements are to be 258 nm^3 for IgG, 150 nm^3 for Ovalbumin, and 110 nm^3 for gold nanoparticles at physiological pH.

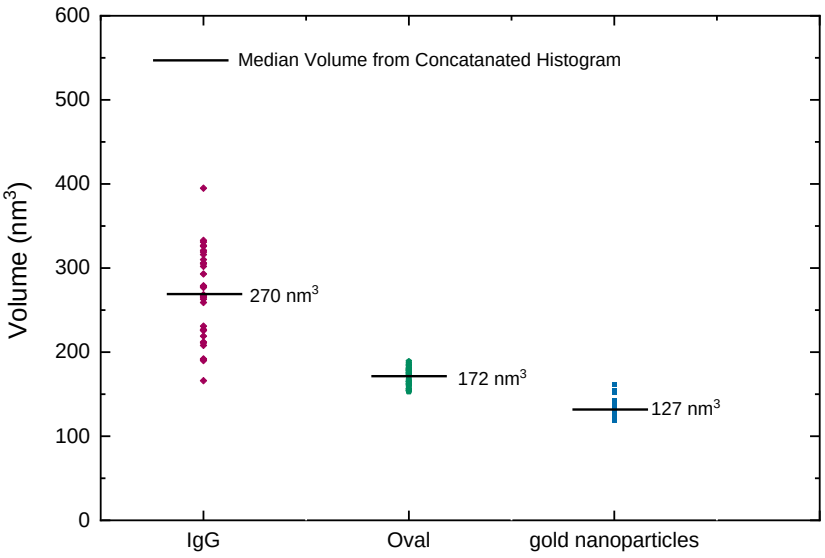

Figure 4.4. Estimated volumes of IgG ($d_{lipid\text{-}coated\ naopore}$ = 21 nm, $V_{applied}$ = -70 mV), Ovalbumin ($d_{lipid\text{-}coated\ naopore}$ = 12 nm, $V_{applied}$ = -100 mV), and gold nanoparticles ($d_{lipid\text{-}coated\ naopore}$ = 13 nm, $V_{applied}$ = -100 mV) from individual translocation events using lipid-coated nanopores interfaced with the hydrogel in 2M KCl, pH 8 buffer.

4.2.3.2. IgG Alignment in The Direction of The Electric Field

The electric force inside a nanopore applies a torque that tends to align the dipole moment of a protein in the direction of the electric field. On the other hand, Brownian diffusional forces tend to randomize the orientation of a protein. The competing effect between these forces determines the orientation distribution of a protein inside a nanopore. At higher applied electrical potentials, the electric force dominates, and the alignment probability of a protein in a particular direction of the electric field goes up.

To observe the protein alignment in the direction of the electric field, we measured IgG at various voltages. IgG has a dipole moment parallel to its symmetry axis.[1] The IgG molecule fully aligned with the electric field is directed to the orientation that corresponds to its extreme lengthwise. It is expected that increasing the external electric field increases the probability of the extreme lengthwise orientation and decreases the probability of being in the extreme crosswise direction. We analyzed individual intra-event ionic current blockades and concatenated the individual histograms to compare the mean alignment probability of IgG in the electric field direction at different voltages. To quantify the effect of the electric field, at each voltage we estimated the ratio of the orientation probability at the extreme lengthwise to the extreme crosswise. Figure 4.5 illustrates the orientation-dependent ionic current distribution of the concatenated histograms of single events at different applied voltages of -40, -60, and -80 mV with the estimated alignment probability at each voltage. We fitted the obtained distributions to the convolution model developed by Yusko and coworkers[1] based on the rotation of non-spherical proteins in the uniform electric field and estimated the dipole moment to be 325±25 D. There are no reported values of dipole moment for the sample of IgG we measured in our experiment by other approaches. The dipole moment of proteins varies in a broad range from tens to thousands

Debye, and the average dipole moment is 550 D. It should be noticed that our calculated IgG dipole moment was estimated from IgG measurements at a relatively high ionic strength provided by the 2 M KCL buffer. For a buffer with a high salt concentration, the protein dipole moment is effectively screened, resulting in an inaccurate estimation.[27,28] Usually, the dipole moments of proteins are measured using very diluted buffers with low ionic strength to avoid ion interference. However, using the same method, Yusko and coworkers calculated the dipole moment of monoclonal anti-biotin IgG to be 816±80 D in 2 M KCL, in full agreement with their measurement at very diluted buffer using dielectric impedance spectroscopy.[1]

Alignment Probability

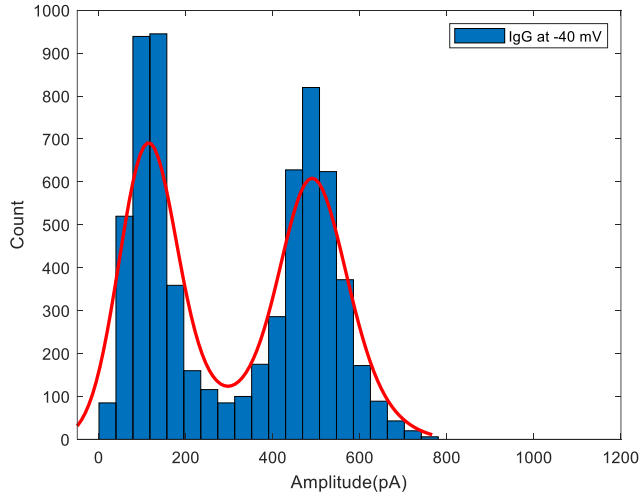

$P(I_{max})/P(I_{min})=1.13$

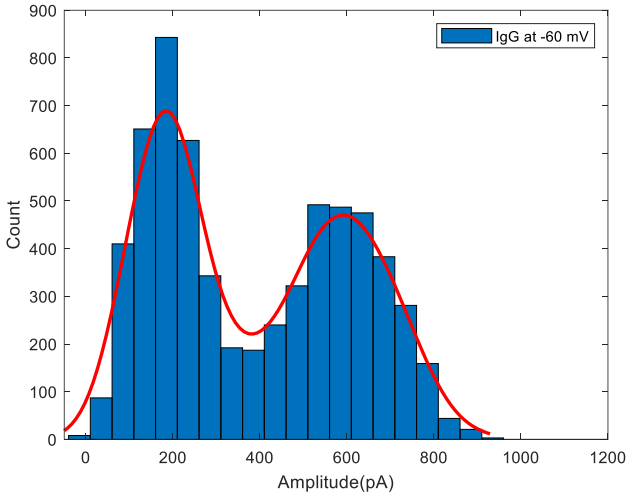

$P(I_{max})/P(I_{min})=1.45$

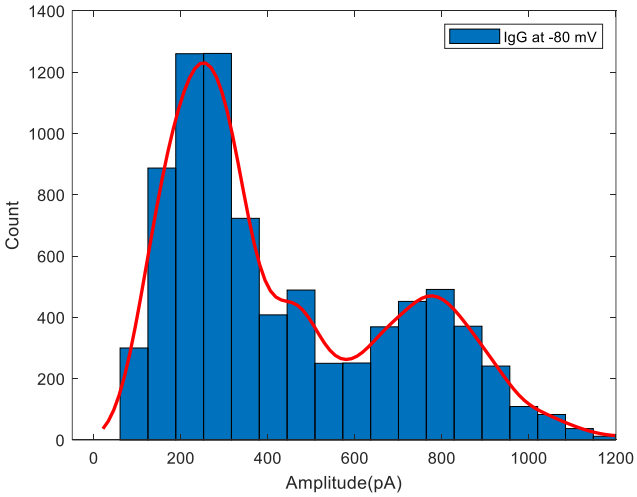

$P(I_{max})/P(I_{min})=2.56$

Figure 4.5. IgG orientation-dependent ionic current blockade distributions alongside with the alignment probability at the concentration of 5 nM in 2 M KCl, pH 8 buffer at the applied voltages of -40, -60, and -80 mV. Red curves are the best bimodal Gaussian fit to determine the peak maximum and the minimum.

4.2.3.3. The Shape and Volume Determination of IgG as a Function of Applied Voltage

Further, we determined the volume and the diameter-to-length ratio of IgG from single translocation events longer than 500 μs at -40, -60, and -80 mV. Figure 4.6a and b illustrate the estimated volumes and length-to-diameter ratios of IgG at different voltages. As shown in the figure, the estimated volume and length-to-diameter increased by increasing the applied voltage, suggesting that the protein was getting rounder. We can think of several possibilities that may explain the slight change in IgG volume: (1) the unfolding of IgG molecules (2) deformation of the hydration shell surrounding IgG molecules (3) IgG conformational change induced by the stronger electric field intensity.

To further investigate which scenario occurred in our experimental setup, we explored whether we could observe the same effect for other nanoparticles by increasing the voltage. We repeated the experiment and measured gold nanoparticles and Ovalbumin at different electric potentials; however, we have not observed significant changes in their estimated volumes measured at different voltages (Figure 4.6 a and b). At pH 8, Ovalbumin (-14 e) has a higher surface negative charge than IgG (-4e), and at more intense electric fields, it feels a stronger electrophoretic force; however, at the higher voltages of -80 and -100 mV, we did not observe any evidence of unfolding the protein or a deformation of the surrounding hydration shell. Therefore, we ruled out unfolding possibilities of IgG molecules and the deformation of the surrounding hydration shell.

a

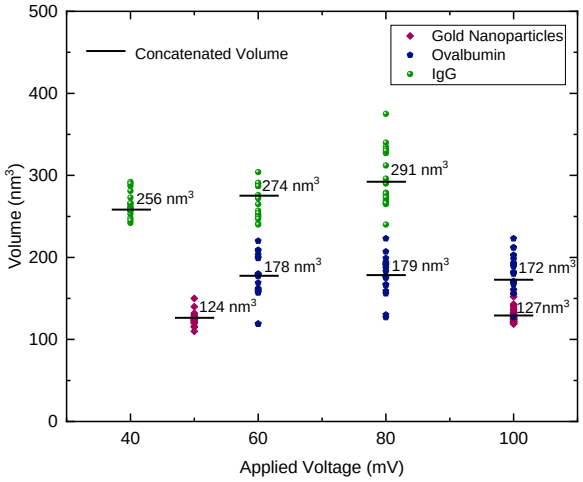

b

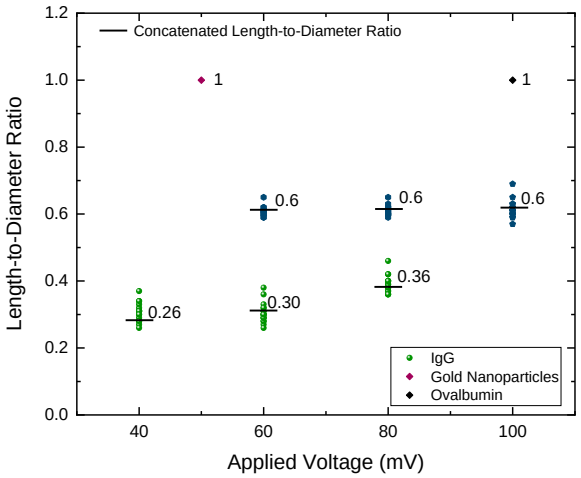

Figure 4.6. Estimated parameters a) volumes, and b) the length-to-diameter ratio from individual single translocation events of: IgG using a hydrogel-backed 26 nm diameter lipid-coated nanopore at -40, -60, and -80 applied voltages, Ovalbumin using a hydrogel-backed 12 nm diameter lipid-coated nanopore at -60, -80, and -100 mV applied voltages, and 5nm diameter gold nanoparticles using a hydrogel-backed 13 nm diameter lipid-coated nanopore at -50 and -100 mV applied voltages. All measurements were performed in 2M KCl, pH 8.

Alternatively, the electric field induced the expansion of IgG molecules. IgG is a very flexible protein, and its flexibility is correlated to its antigen-binding activity. In IgG molecules, two flexible hinges connect two Fab parts to the central F_c region, adjusting the accessibility of binding sites of Fab regions to antigens.[29] IgG hinges can expand in an external electric field. For example, Ghisellini and coworkers[29] exhibited that the external electric field (100-200 mV applied voltage at 5 mM buffer concentration) could manipulate the two flexible hinges in IgG molecular structure (push and pull toward the charged electrode) and influence its binding affinity. We think increasing the strength of the electric field in our system caused the hinges to expand more from each other, making the molecule rounder and bulkier. The expansion of IgG molecules was also observed in higher pH solutions when each IgG hinge becomes negatively charged and they repel each other.[3]

4.3. Summary and Conclusion

We showed that the integration of hydrogel with a lipid-coated nanopore significantly enhances the dwell time of a single protein translocation event, enabling us to resolve time-dependent current fluctuations corresponding to the biased rotation of a protein inside the uniform electric field of a nanopore without the interfering artifacts of pore-protein interactions. Using this approach, we measured IgG, Ovalbumin, and gold nanoparticles, and we determined the shape and volume of the proteins and the nanoparticle from single translocation events. Our estimates for volumes and shapes by this approach were consistent and in agreement with reference values. We observed an increase in IgG alignment in the direction of the electric field with increasing the voltage. Further, we noticed a slight expansion in the volume and shape of IgG molecules at higher

voltages; this is likely due to IgG's flexibility and an intense electric field's ability to expand the hinges from one another.

4.4. Materials and Methods

Materials: All chemicals were purchased from Sigma-Aldrich at reagent grade and used as received. Immunoglobulin gamma (IgG), Ovalbumin, and poly-L-glutamic acid sodium were purchased from Sigma-Aldrich. 1-palmitoyl-2-oleoyl-glycerol-3-phosphocholine (POPC) was purchased from Avanti Polar Lipids.

Nanopore fabrication: 15 nm thick silicon nitride membranes were commercially purchased from Ted Pella Inc.; membranes were PDMS coated and cured for several hours at 120°C before use. Silicon nitride membranes were plasma treated for 30 seconds, mounted in a Teflon fluidic cell, and degassed. Nanopores were formed using dielectric breakdown in 2 M KCl, pH 10 at the desired size as previously reported[22].

Formation of lipid bilayer and preparation of lipid liposomes: Lipid bilayers were formed on the surface of silicon nitride membranes by fusion of small unilamellar liposomes of POPC as previously reported.[6] To prepare liposomes of POPC, 1 ml of a solution of 5 mg/ml lipid in chloroform was evaporated under pure argon gas for around 20 minutes until the lipid film clearly appeared at the bottom of the vial. Then the lipid film was re-hydrated in 150 mM KCl and 10 mM HEPES at pH 7.5 to the final lipid concentration of 2 mM. The lipid solution in KCl was sonicated for 10 to 20 minutes, following by extensive extrusion through polycarbonate membrane using the Avanti mini extruder.

To lipid coat the nanopore, immediately after nanopore fabrication, the buffer solution on one side of the membrane was replaced by a solution of unilamellar liposomes of POPC. After 20 minutes, the POPC solution was swapped. To remove the excess liposomes, the box compartment was rinsed with ultra-pure water for a couple of minutes. Lipid-coated nanopore diameters were determined using Equation 4.2.

Hydrogel polymerization:

PEG-DMA hydrogel solution was prepared by mixing 10% (w/v) PEG-1000 Dimethylacrylamide in 2 M KCl, 100 mM Tris-HCl at the desired pH (adjusted by HCl and NaOH), 10% (w/v) ammonium persulfide (APS), and 20% (w/v) tetramethylethylenediamine (TEMED). After lipid-

coating a nanopore, the electrolyte in the compartment on the TEM window side was replaced with PEG-DMA hydrogel solution and polymerized in-situ for 10 minutes before nanopore measurement.

Nanopore measurements: All nanopore measurements were carried out using an Axopatch 200B amplifier and Digidata 1440B or 1322A data acquisition at 100 kHz with a 10 kHz hardware low pass filter. Nanopore measurements were performed in 2 M KCl, 100 mM Tris-HCl, pH 8-10. At least 5 minutes of control measurements were run before protein injection. In all experiments, the hydrogel side (*trans*) of the nanopore chip was grounded, and protein was injected into the other side (*cis*) to make a final concentration of 0.1 – 1 nM; the *cis* solution was briefly stirred before measurements began with -40 to -100 mV applied (V_{cis}-V_{trans}).

Data analysis: All captured data were analyzed using a MATLAB script as previously reported[22].

4.5. References:

(1) Yusko, E. C.; Bruhn, B. R.; Eggenberger, O. M.; Houghtaling, J.; Rollings, R. C.; Walsh, N. C.; Nandivada, S.; Pindrus, M.; Hall, A. R.; Sept, D.; Li, J.; Kalonia, D. S.; Mayer, M. Real-Time Shape Approximation and Fingerprinting of Single Proteins Using a Nanopore. *Nat. Nanotechnol.* **2017**, *12* (4), 360–367. https://doi.org/10.1038/nnano.2016.267.

(2) Houghtaling, J.; Ying, C.; Eggenberger, O. M.; Fennouri, A.; Nandivada, S.; Acharjee, M.; Li, J.; Hall, A. R.; Mayer, M. Estimation of Shape, Volume, and Dipole Moment of Individual Proteins Freely Transiting a Synthetic Nanopore. *ACS Nano* **2019**, *13* (5), 5231–5242. https://doi.org/10.1021/acsnano.8b09555.

(3) Nazarian, R.; Lee, E.; Siegel, B.; Kuo, C.; Acharya, S.; Schmidt, J. Quantitative Measurements of Protein Volume and Concentration Using Hydrogel-Backed Nanopores. *ACS Sensors* **2021**. https://doi.org/10.1021/acssensors.1c00284.

(4) Plesa, C.; Kowalczyk, S. W.; Zinsmeester, R.; Grosberg, A. Y.; Rabin, Y.; Dekker, C. Fast Translocation of Proteins through Solid State Nanopores. *Nano Lett.* **2013**, *13* (2), 658–663. https://doi.org/10.1021/nl3042678.

(5) Li, X.; Hu, R.; Li, J.; Tong, X.; Diao, J. J.; Yu, D.; Zhao, Q. Non-Sticky Translocation of Bio-Molecules through Tween 20-Coated Solid-State Nanopores in a Wide PH Range. *Appl. Phys. Lett.* **2016**, *109* (14). https://doi.org/10.1063/1.4964117.

(6) Yusko, E. C.; Johnson, J. M.; Majd, S.; Prangkio, P.; Rollings, R. C.; Li, J.; Yang, J.; Mayer, M. Controlling Protein Translocation through Nanopores with Bio-Inspired Fluid Walls. *Nat. Nanotechnol.* **2011**, *6* (253–260). https://doi.org/10.1038/nnano.2011.12.

(7) Chen, P.; Mitsui, T.; Farmer, D. B.; Golovchenko, J.; Gordon, R. G.; Branton, D. Atomic Layer Deposition to Fine-Tune the Surface Properties and Diameters of Fabricated Nanopores. *Nano Lett.* **2004**, *4* (7), 1333–1337. https://doi.org/10.1021/nl0494001.

(8) Elam, J. W.; Routkevitch, D.; Mardilovich, P. P.; George, S. M. Conformal Coating on Ultrahigh-Aspect-Ratio Nanopores of Anodic Alumina by Atomic Layer Deposition. *Chem. Mater.* **2003**, *15* (18), 3507–3517. https://doi.org/10.1021/cm0303080.

(9) Thangaraj, V.; Lepoitevin, M.; Smietana, M.; Balanzat, E.; Bechelany, M.; Janot, J. M.; Vasseur, J. J.; Subramanian, S.; Balme, S. Detection of Short SsDNA and DsDNA by Current-Voltage Measurements Using Conical Nanopores Coated with Al2O3 by Atomic Layer Deposition. *Microchim. Acta* **2016**, *183* (3), 1011–1017. https://doi.org/10.1007/s00604-015-1706-2.

(10) Waduge, P.; Bilgin, I.; Larkin, J.; Henley, R. Y.; Goodfellow, K.; Graham, A. C.; Bell, D. C.; Vamivakas, N.; Kar, S.; Wanunu, M. Direct and Scalable Deposition of Atomically Thin Low-Noise MoS2 Membranes on Apertures. *ACS Nano* **2015**, *9* (7), 7352–7359. https://doi.org/10.1021/acsnano.5b02369.

(11) Xie, Y.; Xue, J.; Wang, L.; Wang, X.; Jin, K.; Chen, L.; Wang, Y. Surface Modification of Single Track-Etched Nanopores with Surfactant CTAB. *Langmuir* **2009**, *25* (16), 8870–8874. https://doi.org/10.1021/la9017213.

(12) Emilsson, G.; Sakiyama, Y.; Malekian, B.; Xiong, K.; Adali-kaya, Z.; Lim, R. Y. H.; Dahlin, A. B. Gating Protein Transport in Solid State Nanopores by Single Molecule Recognition. **2018**. https://doi.org/10.1021/acscentsci.8b00268.

(13) Roman, J.; Jarroux, N.; Patriarche, G.; Français, O.; Pelta, J.; Le Pioufle, B.; Bacri, L. Functionalized Solid-State Nanopore Integrated in a Reusable Microfluidic Device for a Better Stability and Nanoparticle Detection. *ACS Appl. Mater. Interfaces* **2017**, *9* (48), 41634–41640. https://doi.org/10.1021/acsami.7b14717.

(14) Awasthi, S.; Sriboonpeng, P.; Ying, C.; Houghtaling, J.; Shorubalko, I.; Marion, S.; Davis, S. J.; Sola, L.; Chiari, M.; Radenovic, A.; Mayer, M. Polymer Coatings to Minimize Protein Adsorption in Solid-State Nanopores. *Small Methods* **2020**, *4* (11), 1–10. https://doi.org/10.1002/smtd.202000177.

(15) Anderson, B. N.; Muthukumar, M.; Meller, A. PH Tuning of DNA Translocation Time through Organically Functionalized Nanopores. *ACS Nano* **2013**, *7* (2), 1408–1414. https://doi.org/10.1021/nn3051677.

(16) Ananth, A.; Genua, M.; Aissaoui, N.; Díaz, L.; Eisele, N. B.; Frey, S.; Dekker, C.; Richter, R. P.; Görlich, D. Reversible Immobilization of Proteins in Sensors and Solid-State Nanopores. *Small* **2018**, *14* (18). https://doi.org/10.1002/smll.201703357.

(17) Wanunu, M.; Meller, A. Chemically Modified Solid-State Nanopores. **2007**. https://doi.org/10.1021/nl070462b.

(18) Giamblanco, N.; Coglitore, D.; Janot, J. M.; Coulon, P. E.; Charlot, B.; Balme, S. Detection of Protein Aggregate Morphology through Single Antifouling Nanopore. *Sensors Actuators, B Chem.* **2018**, *260*, 736–745. https://doi.org/10.1016/j.snb.2018.01.094.

(19) Siwy, Z.; Trofin, L.; Kohli, P.; Baker, L. A.; Trautmann, C.; Martin, C. R. Protein Biosensors ’based on Biofunctionalized Conical Gold Nanotubes. *J. Am. Chem. Soc.* **2005**, *127* (14), 5000–5001. https://doi.org/10.1021/ja043910f.

(20) Sexton, L. T.; Horne, L. P.; Sherrill, S. A.; Bishop, G. W.; Baker, L. A.; Martin, C. R. Resistive-Pulse Studies of Proteins and Protein/Antibody Complexes Using a Conical Nanotube Sensor. *J. Am. Chem. Soc.* **2007**, *129* (43), 13144–13152. https://doi.org/10.1021/ja0739943.

(21) Yusko, E. C.; Prangkio, P.; Sept, D.; Rollings, R. C.; Li, J.; Mayer, M. Single-Particle Characterization of Aβ Oligomers in Solution. *ACS Nano* **2012**, *6* (7), 5909–5919. https://doi.org/10.1021/nn300542q.

(22) Acharya, S.; Jiang, A.; Kuo, C.; Nazarian, R.; Li, K.; Ma, A.; Siegal, B.; Toh, C.; Schmidt, J. J. Improved Measurement of Proteins Using a Solid-State Nanopore Coupled with a Hydrogel. *ACS Sensors* **2020**, *5*, 370–376. https://doi.org/10.1021/acssensors.9b01928.

(23) Bandara, Y. M. N. D. Y.; Karawdeniya, B. I.; Hagan, J. T.; Chevalier, R. B.; Dwyer, J. R. Chemically Functionalizing Controlled Dielectric Breakdown Silicon Nitride Nanopores by Direct Photohydrosilylation. *ACS Appl. Mater. Interfaces* **2019**, *11*, 30411–30420.

https://doi.org/10.1021/acsami.9b08004.

(24) Eggenberger, O. M.; Ying, C.; Mayer, M. Surface Coatings for Solid-State Nanopores. *Nanoscale* **2019**, *11* (42), 19636–19657. https://doi.org/10.1039/c9nr05367k.

(25) Ying, C.; Houghtaling, J.; Eggenberger, O. M.; Guha, A.; Nirmalraj, P.; Awasthi, S.; Tian, J.; Mayer, M. Formation of Single Nanopores with Diameters of 20-50 Nm in Silicon Nitride Membranes Using Laser-Assisted Controlled Breakdown. *ACS Nano* **2018**, *12* (11), 11458–11470. https://doi.org/10.1021/acsnano.8b06489.

(26) Ying, C.; Houghtaling, J.; Eggenberger, O. M.; Guha, A.; Nirmalraj, P.; Awasthi, S.; Tian, J.; Mayer, M. Formation of Single Nanopores with Diameters of 20-50 Nm in Silicon Nitride Membranes Using Laser-Assisted Controlled Breakdown. *ACS Nano* **2018**, *12* (11), 11458–11470. https://doi.org/10.1021/acsnano.8b06489.

(27) Petro, M. G.; Garcia, E. A.; Herrera-alonso, M.; Bevan, M. A. Ionic Strength-Dependent Interactions and Dimensions of Adsorbed Zwitterionic Copolymers. **2019**. https://doi.org/10.1021/acs.langmuir.9b00218.

(28) Porschke, D.; Creminon, C.; Cousin, X.; Bon, C. Electrooptical Measurments Demonstrate a Large Permanent Dipole Moment Associated with Acetylcholinesterase. *Biophys. J.* **1996**, *70* (April 1995).

(29) Ghisellini, P.; Caiazzo, M.; Alessandrini, A.; Eggenhöffner, R.; Vassalli, M.; Facci, P. Direct Electrical Control of IgG Conformation and Functional Activity at Surfaces. *Sci. Rep.* **2016**, *6*, 3–10. https://doi.org/10.1038/srep37779.

Chapter 5: Summary and Conclusion

5.1. Summary

Much progress has been made recently in label-free protein identification using nanopores.[1–4] However, accurate detection and characterization of proteins in solution using nanopores is difficult because of the large fraction of missed translocation events due to short event time and limited resolution of conventional current amplifiers. Recently, our group[4] has shown that introducing hydrogel on the *trans* side of silicon nitride nanopore effectively improves protein detection by sterically hindering the passage of proteins from *cis* side, leading to significantly enhanced protein residence time within the nanopore sensing zone, and resulting in a great reduction in missed translocation events.

5.1.1. Measurement Limits and Quantitative Characterization of Proteins Using Hydrogel-Backed Nanopores

Our initial findings indicated that hydrogel interfaced with a nanopore enhanced protein detection; however, the protein size and concentration limits that could be studied with this approach were unknown. Also, it was unclear how much characterization information could be extracted from our nanopore measurements. So, in the first part of this work, we explored the sensitivity, measurement limits, and characterization capabilities of our hydrogel-facilitated nanopore system. We demonstrated the ability of the hydrogel-backed nanopores to sense unlabeled proteins as small as 5.5 kD in size and 10 fM in concentration, without a major restriction on the nanopore size. To our knowledge, these measurement limits in size and concentration are the lowest size and concentration recorded for single-molecule detection of unlabeled proteins using a standard amplifier and without the extra adjustment on the experimental setup.

Also, using hydrogel-backed nanopores, we precisely determined the shapes and volumes of various proteins. We showed that the hydrodynamic radius of proteins strongly depends on the

solution pH; larger hydration shells surround proteins at higher pH when the proteins are highly negatively charged. Using hydrogel-backed nanopores further, we quantified the unknown concentrations of proteins. We showed that the frequency of protein translocation events linearly scales with bulk concentrations over a wide range of concentrations, and an unknown protein concentration can be determined from an interpolation of the frequency-concentration calibration curve with less than 10% error.

Also, we proposed several competing mechanisms for the detection enhancement enabled by the presence of the hydrogel. We found that a gap between the nanopore chip and the hydrogel affects the system sensitivity, with smaller gaps resulting in increased sensitivity. When the hydrogel is in full contact with the nanopore, proteins can escape the pore by diffusing back against the electric field. The proteins measured with this system had longer dwell time and a much higher event rate.

5.1.2. Integrating the Hydrogel-Facilitating Nanopore Platform with a Chromatographic Column to Study a Mixture Solution of Proteins

We found that our hydrogel-backed nanopores were powerful detectors in the analysis of purified proteins. For the next step, we wondered whether we could identify and characterize a mixture solution of proteins using hydrogel-backed nanopore detectors. We started our investigation with the first and most trivial approach, fractionating a mixture solution of proteins into more simple chromatographic fractions. Then, each fraction was studied with a hydrogel-backed nanopore. We found that a nanopore backed with the hydrogel can be an effective, reliable, ultra-sensitive, non-destructive, and easy-to-operate detection platform to analyze chromatographic protein fractions.

Additionally, we adjusted the measurement setting for the newly proposed application and integrated the nanopores with the microchannels. We mounted the solid-state nanopore between microfluidic channels to facilitate the rapid and efficient sample replacement through channels. Further, we connected the outlet valve of a chromatographic column to the inlet of the top microchannel to make a fluidic circuit to transport samples of eluates to the nanopore for real-time and continuous measurements of protein fractions.

5.1.3. Lipid-Coating a Nanopore Backed with the Hydrogel for Intra-Event Ionic Current Analysis of Single Translocation Events

In chapter 2 and 3, we characterized the resolved proteins by analyzing a population of hundreds of events. However, we can extract interesting physical information about proteins by analyzing individual single translocation events. As a matter of fact, this approach is even more attractive because it allows real-time protein characterization and also enables us to study a mixture solution of proteins without additional simplification steps. Further, we thought and investigated whether we could use our platform for individual intra-event ionic current analysis.

Therefore, in the third part of this dissertation, we demonstrated that integrating lipid-bilayer coated nanopores with the hydrogel is a suitable platform for acquiring artifact-free and long protein translocation events for the accurate intra-event ionic current analysis. Using hydrogel-backed lipid-bilayer coated nanopores, we measured IgG, Ovalbumin, and gold nanoparticles (5 nm diameter) and determined their volumes from single translocation events. Further, we observed that higher applied voltages increased the probability of IgG alignment, as theoretically expected, but it was never experimentally observed to our knowledge. We determined the volume and the

length-to-diameter ratio of IgG molecules at different applied voltages and noticed an expansion in the conformation of IgG molecules with an increase in the voltage.

5.2. Conclusion and Suggestions for Future Work

Through this work, we learned a lot about hydrogel-backed nanopores, their measurement limits, and their capabilities in protein detection and identification. We also learned how to adjust our system and adopt new settings which enhance and gear this technology towards other desired applications. To put it shortly, we built all the necessary infrastructures to use this platform for relevant medical and biological studies.

For instance, our hydrogel-facilitating nanopore measurement can be utilized to study the molecular mechanism of the cellular process. Here is an example: studying disease pathogenesis of Hypertriglyceridemia at the molecular level: Hypertriglyceridemia is an elevated triglyceride level in the blood which may lead to coronary heart disease and heart attack. It was found that dysregulation in lipoprotein lipase (LPL) activity leads to mislocalization of this protein inside the cells and prevents the processing of triglyceride-rich lipoproteins to keep the normal blood level of triglyceride. In previous studies it was hypothesized that ANGPTL4 protein can interact with LPL proteins, promoting the unfolding of LPL proteins, and making the LPL proteins inactive. However, this process has not been experimentally investigated. Using hydrogel-backed nanopores, we can investigate the possibility of the inactivation mechanism and unfolding of LPL proteins in the presence of ANGPTL4 protein and shed light on this mechanism at the molecular level. Fully understanding this mechanism helps with the development of new medicines to prevent Hypertriglyceridemia.

Also, our hydrogel-facilitating nanopore can be utilized for single-cell studies. In Chapter 3, we integrated our hydrogel-facilitated nanopore biosensor with a conventional Fast Protein Liquid Chromatography (FPLC) instrument to study a mixture solution of proteins. We can make this system much more efficient by miniaturizing the different types of liquid chromatographic systems (LC) on a micro-chip and integrate them with the hydrogel-backed nanopores. The integrated on-chip LC-nanopore backed with a hydrogel system can be used for single-cell studies and biomarker discoveries. The cells can be lysed in the microchannel, the proteins can be extracted, then separated into smaller groups by passing them through a micro-column and be analyzed with hydrogel-backed nanopores.

5.3. References:

(1) Yusko, E. C.; Johnson, J. M.; Majd, S.; Prangkio, P.; Rollings, R. C.; Li, J.; Yang, J.; Mayer, M. Controlling Protein Translocation through Nanopores with Bio-Inspired Fluid Walls. *Nat. Nanotechnol.* **2011**, *6* (253–260). https://doi.org/10.1038/nnano.2011.12.

(2) Yusko, E. C.; Bruhn, B. R.; Eggenberger, O. M.; Houghtaling, J.; Rollings, R. C.; Walsh, N. C.; Nandivada, S.; Pindrus, M.; Hall, A. R.; Sept, D.; Li, J.; Kalonia, D. S.; Mayer, M. Real-Time Shape Approximation and Fingerprinting of Single Proteins Using a Nanopore. *Nat. Nanotechnol.* **2017**, *12* (4), 360–367. https://doi.org/10.1038/nnano.2016.267.

(3) Houghtaling, J.; Ying, C.; Eggenberger, O. M.; Fennouri, A.; Nandivada, S.; Acharjee, M.; Li, J.; Hall, A. R.; Mayer, M. Estimation of Shape, Volume, and Dipole Moment of Individual Proteins Freely Transiting a Synthetic Nanopore. *ACS Nano* **2019**, *13* (5), 5231–5242. https://doi.org/10.1021/acsnano.8b09555.

(4) Acharya, S.; Jiang, A.; Kuo, C.; Nazarian, R.; Li, K.; Ma, A.; Siegal, B.; Toh, C.; Schmidt, J. J. Improved Measurement of Proteins Using a Solid-State Nanopore Coupled with a Hydrogel. *ACS Sensors* **2020**, *5*, 370–376. https://doi.org/10.1021/acssensors.9b01928.